International Journal of Solids and Structures 202 (2020) 854–880

Contents lists available at ScienceDirect

International Journal of Solids and Structures

journal homepage: www.elsevier.com/locate/ijsolstr

The mathematical theory of a higher-order geometrically-exact beam with a deforming cross-section

Mayank Chadha *, Michael D. Todd

Department of Structural Engineering, University of California San Diego, 9500 Gilman Drive, La Jolla, CA 92093-0085, USA

ARTICLE INFO

Article history:
Received 11 January 2020
Received in revised form 17 April 2020
Accepted 3 June 2020
Available online 4 July 2020

Keywords:
Coupled Poisson's and warping effect
Variational formulation
Geometrically-exact beam
Large deformations
Finite element formulation

ABSTRACT

This paper investigates the variational formulation and numerical solution of a higher-order, geometrically exact Cosserat type beam with deforming cross-section, instigated from generalized kinematics presented in earlier works. The generalizations include the effects of a fully-coupled Poisson's and warping deformations in addition to other deformation modes from Simo-Reissner beam kinematics.

The kinematics at hand renders the deformation map to be a function of not only the configuration of the beam but also elements of the tangent space of the beam's configuration (axial strain vector, curvature, warping amplitude, and their derivatives). While this complicates the process of deriving the balance laws and exploring the variational formulation of the beam, the completeness of the result makes it worthwhile. The weak and strong form are derived for the dynamic case considering a general boundary.

We restrict ourselves to a linear small-strain elastic constitutive law and the static case for numerical implementation. The finite element modeling of this beam has higher regularity requirements. The matrix (discretized) form of the equation of motion is derived. Finally, numerical simulations comparing various beam models are presented.

1. Introduction

The development of the beam/rod theories idealized by a space curve goes back to two and half centuries ago and was instrumental in accelerating the second industrial revolution (Euler and Truesdell, 1960). Interestingly, further development of beam theory continues to date. The advanced and versatile applications of beam theory to numerous areas such as the deformation of biopolymers (Travers and Thompson, 2004; Manning et al., 1996), biological structures (Klapper, 1996), shape-sensing (Todd et al., 2013; Chadha and Todd, 2016, 2017b,c), robotics, multi-body dynamics (Lang et al., 2011), composite structures (Hodges, 2006), contact problems (Meier et al., 2018), thermal problems (Green and Naghdi, 1979; Altenbach et al., 2012), micro and nanostructures used in MEMS and NEMS etc., necessitates further development and refinement of this theory. We first perform a relevant literature review in the next few paragraphs.

Duhem (1893) and Darboux (1894) investigated a kinematic idea that provided a sense of rotation to any material point, such that a point in the object not only has a position vector associated with it but also has an attached triad that assigns a sense of rotation to these material points. It was Cosserat and Cosserat (1909) who conceived the idea of moving frames to capture geometrically exact non-linear deformation of the beams (and shells) using framed space curve. Ericksen and Truesdell Ericksen and Truesdell (1957) generalized the Cosserat brother's work to develop a non-linear theory of rods and shells for finite strain. Some of the prominent investigations and research on theory of rods include (Hay, 1942; Cohen, 1966; Whitman and DeSilva, 1969; Green et al., 1974a,b; Antman, 1974; Antman and Jordan, 1975; Argyris, 1982; Argyris and Symeonidis, 1980a; Argyris and Symeonidis, 1980b; Reissner, 1972, 1973; Simo, 1985). The developments in the beam theory in the last century are summarized in Ericksen and Truesdell (1957), Yang et al. (2003) and Chadha and Todd (2017a).

Among these seminal contributions, the work by Reissner was the first major leap forward towards the *geometrically-exact beam theory*, when he extended *Kirchhoff–Love beam theory* (Love, 2013) to also capture shear deformation in addition to bending and torsion in 2D (Reissner, 1972) and 3D (Reissner, 1981). The prominent work by Simo, 1985 extended Reissner's beam to 3D (with geometric-exactness preserved) in the setting of differential

* Corresponding author.
E-mail addresses: machadha@eng.ucsd.edu (M. Chadha), mdtodd@eng.ucsd.edu (M.D. Todd).

https://doi.org/10.1016/j.ijsolstr.2020.06.002
0020-7683/

geometry (now called *Simo-Reissner beam theory*). Many papers were published in the same time period concerning finite element formulation of geometrically-exact beams, the primary contributors being: Simo et al. (Simo, 1985; Simo and Hughes, 1986; Simo and Vu-Quoc, 1986, 1988); Iura et al. (Iura and Atluri, 1988a,b); Cardona et al. (Cardona and Géradin, 1988); Ibrahimbegovic (Ibrahimbegović, 1995). These papers considered linearly elastic material and addressed both static and dynamic cases, but they presented different approaches to time-stepping schemes and updating rotation vector: Eulerian (Simo and Hughes, 1986; Simo and Vu-Quoc, 1988), updated Lagrangian (Cardona and Géradin, 1988), and total Lagrangian (Ibrahimbegović, 1995; Iura and Atluri, 1988b). Since these papers got published, research tackling the theoretical and computational techniques gained momentum and the advanced research in this field continues to occur till date, for examples: problems related to discretization and interpolation approaches (Zupan and Saje, 2003; Zupan and Zupan, 2018; Crisfield and Jelenic, 1983; Borkovic et al., 2018; Chadha and Todd, 2019; Sander, 2010; Sonneville et al., 2014), mixed formulation (Li et al., 2017), non-linear materials and constitutive law (Mata et al., 2007, 2008; Arora et al., 2019; Pimenta et al., 2008), space and time-integration schemes (Simo et al., 1995; Demoures et al., 2014; Romero and Armero, 2002), initially curved configuration (Kapania and Li, 2003; Chadha and Todd, 2017a), higher-order Kirchhoff–love beam (Boyer et al., 2011; Meier et al., 2019; Greco and Cuomo, 2013), and enhanced kinematics (Simo and Hughes, 1986; Sokolov et al., 2015; Yiu, 2005; Chadha and Todd, 2019). Noteworthy contributions to computational formulation of geometrically-exact beam including shear deformation and their applications (e.g., multi-body dynamics of earth orbiting satellites) was made by Vu-Quoc in collaboration with Simo (Vu-Quoc, 1986; Vu-Quoc and Simo, 1987; Simo and Vu-Quoc, 1987). Simo and Vu-Quoc (Simo and Vu-Quoc, 1991) extended their previous work (Simo, 1985; Simo and Vu-Quoc, 1986) to incorporate warping using a Saint–Venant warping function. McRobie and Lasenby (1999) presented an alternative derivation of the Simo Vu-Quoc beam by using Clifford or geometric algebra for both derivation and numerical implementation. A very recent paper by Carrera and Zozulya (2019) gives Carrera Unified Formulation (CUF) for the micropolar beams.

Our recent work Chadha and Todd (2019) investigated and refined the kinematics of Cosserat beams. This development incorporated a fully coupled Poisson's and warping effect along with the classical deformation effects like bending, torsion, shear, and axial deformation for the case of finite displacement and strain; it thus allowed us to capture a three dimensional, multi-axial strain fields using single-manifold kinematics. Numerous works on shear based deformation are founded on Timoshenko's beam theory that assumes a uniform shear strain distribution restricting the cross-section to remain planar. However, the kinematics developed in Chadha and Todd (2019) also considers non-uniform shear deformation due to bending-induced shear. For such beam kinematics, we first focus our attention on performing a step-by-step analysis of the balance laws and the variational formulation of the beam. Unlike the traditional geometrically-exact beam theory where the deformation map is a function of the differential invariants (curvatures) of a framed curve, the work presented in Chadha and Todd (2019) considers a deformation map that also depends on the higher-order derivatives of the curvatures and mid-curve strains due to the inclusion of a *fully coupled Poisson's and warping effect*. This makes the process of obtaining a variation of these quantities challenging. We observe that the theory converges to the one presented in Simo and Vu-Quoc (1991) if we ignore the Poisson's effect and bending induced non-uniform shear. To numerically solve the system, we restrict this paper to static case and utilize a multiaxial linear material constitutive law valid for large deformation but limited to small strains, thus relating the reduced forces to their corresponding finite strain counterpart (in addition to the mid-curve axial strain, curvature, and warping amplitude, we also have their derivatives). Linearization of the weak form is detailed and is followed by matrix formulation of the equation of motion. For simplicity, we assume displacement-prescribed boundary conditions. We update the rotation tensor in an Eulerian sense using an *incremental current rotation vector*. We obtain and update curvature and its derivatives using the results presented in another recent paper (Chadha and Todd, 2019a).

Section 2–5 details the kinematics and variational formulation, whereas, the Sections 6–9 deals with the discussion of constitutive law and numerical formulation. In Section 2, we summarize the kinematics detailed in Chadha and Todd (2019). In Section 3, we obtain the variation of quantities required for derivation of field equations. In Sections 4 and 5, we derive the governing equations. Section 6 discusses the multi-axial linearly elastic constitutive law considering large deformation but small strain. Section 7 describes the finite element formulation for static case, and Section 8 illustrates numerical examples. Finally, Section 9 concludes the paper.

2. Comprehensive kinematics and mathematical tools

We first present some preliminary definitions and notations: the dot product, ordinary vector product, and tensor product of two Euclidean vectors $\boldsymbol{v}_1$ and $\boldsymbol{v}_2$ are defined as $\boldsymbol{v}_1 \cdot \boldsymbol{v}_2 = \boldsymbol{v}_1^T \boldsymbol{v}_2$, $\boldsymbol{v}_1 \times \boldsymbol{v}_2$, and $\boldsymbol{v}_1 \otimes \boldsymbol{v}_2$ respectively. The Euclidean norm is represented by $\|.\|$ or the un-bolded version of the symbol (for example, $\|\boldsymbol{v}\| \equiv v$). The n^{th} order partial derivative with respect to a scalar, ξ_1 for instance, is given by the operator $\partial^n_{\xi_1}$, with $\partial^1_{\xi_1} \equiv \partial_{\xi_1}$. A vector, a tensor or a matrix is represented by bold symbol and their components are given by indexed un-bolded symbols. The action of a tensor $\boldsymbol{A}$ onto the vector $\boldsymbol{v}$ is represented by $\boldsymbol{A}\boldsymbol{v} \equiv \boldsymbol{A}.\boldsymbol{v}$. The contraction between two tensors $\boldsymbol{A}$ and $\boldsymbol{B}$ is given by $\boldsymbol{A} : \boldsymbol{B} = A_{ij}B_{ij} = \text{trace}\left(\boldsymbol{B}^T.\boldsymbol{A}\right)$. We note that the centered dot "·" is meant for dot product between two vectors, whereas the action of a tensor onto the vector, the matrix multiplication or product of a scalar to a matrix (or a vector) is denoted by a lower dot ".". Vectors when expressed in array form are columnar in nature. Vertical concatenation of n vectors (for example, of dimension 3×1) $\boldsymbol{v}_1, \boldsymbol{v}_2, \ldots, \boldsymbol{v}_n$ is represented by the vector $[\boldsymbol{v}_1; \boldsymbol{v}_2; \ldots; \boldsymbol{v}_n]$ (of dimension $3n \times 1$). The n dimensional Euclidean space is represented by $\mathbb{R}^n$, with $\mathbb{R}^1 = \mathbb{R}$, with $\mathbb{R}^+$ denoting the set of positive real numbers (including 0). The diagonal matrix, for example, consisting of the diagonal elements (a, b, c) is denoted by $\text{diagonal}[a, b, c]$. Finally, $\boldsymbol{0}_3, \boldsymbol{I}_3$ represents 3×3 zero matrix and the identity matrix respectively. The zero vector is defined as $\boldsymbol{0}_1 = [0; 0; 0]$.

In this section, we shall briefly review the concepts and kinematics discussed in Chadha and Todd (2019) to establish continuity in the write-up.

2.1. Deformation map and configuration of the beam

Let an open set $\Omega_0 \subset \mathbb{R}^3$ and $\Omega \subset \mathbb{R}^3$ with at least piecewise smooth boundaries Ξ_0 and Ξ represent the undeformed and deformed configuration of the beam respectively. The beam configuration is described by the mid-curve and a family of cross-sections. To lay the kinematic description of a beam, we assume the undeformed configuration Ω_0 to be *straight*.

Let the fixed orthonormal reference basis be represented by $\{\boldsymbol{E}_i\}$ with origin at $(0, 0, 0)$. The regular curve $\boldsymbol{\varphi}_0 : [0, L] \longrightarrow \mathbb{R}^3$ represents the mid-curve associated with Ω_0. It is parameterized by the

arc-length $\xi_1 \in [0, L]$. We assume that the undeformed configuration is made up of continuously varying plane family of cross-sections $B_0(\xi_1)$, such that $\boldsymbol{\varphi}_0 = \xi_1 \boldsymbol{E}_1$ is the locus of geometric centroid of the family of cross-sections $B_0(\xi_1)$. The cross-section $B_0(\xi_1)$ is spanned by the vectors $\boldsymbol{E}_2 - \boldsymbol{E}_3$ originating at $\boldsymbol{\varphi}_0(\xi_1)$ such that $(\xi_2, \xi_3) \in B_0(\xi_1)$. Let $\Gamma_0(\xi_1)$ represent the peripheral boundary of $B_0(\xi_1)$, such that $\mathfrak{S}_0 = B_0(0) \cup B_0(L) \cup_{\forall \xi_1} \Gamma_0(\xi_1)$. Any material point in the beam is defined by its material coordinate (ξ_1, ξ_2, ξ_3) with a position vector $\boldsymbol{R}_0 = \xi_i \boldsymbol{E}_i$.

In order to proceed further, we first define the deformed configuration Ω_1 of the beam restrained by *rigid cross-section* constraint. The configuration Ω_1 is defined by a regular mid-curve $\boldsymbol{\varphi}(\xi_1)$ and a family of plane cross-sections $B_1(\xi_1)$, parameterized by the undeformed arc-length ξ_1. Equivalently, the mid-curve $\boldsymbol{\varphi}(s(\xi_1))$ and a family of plane cross-sections $B_1(s(\xi_1))$ are reparametrized by the deformed arc-length s, such that $\xi_1 = \xi_1(s)$ is at least C^1 continuous and $\partial_s \xi_1 \neq 0$. The director frame field $\{\boldsymbol{d}_i(\xi_1)\}$ defines the orientation of the cross-section $B_1(s(\xi_1))$. We have, $B_1(\xi_1) = \left\{(\xi_2, \xi_3) \in \mathbb{R}^2_{\xi_1}\right\}$, where $\mathbb{R}^2_{\xi_1}$ is 2D Euclidean space spanned by the directors $\boldsymbol{d}_2(\xi_1) - \boldsymbol{d}_3(\xi_1)$, with origin at $\boldsymbol{\varphi}(\xi_1)$. We define the deformation map $\boldsymbol{\phi}_1 : \boldsymbol{R}_0 \in \Omega_0 \mapsto \boldsymbol{R}_1 \in \Omega_1$, such that

$$\boldsymbol{\phi}_1(\boldsymbol{R}_0) = \boldsymbol{R}_1 = \boldsymbol{\varphi}(\xi_1) + \boldsymbol{r}_1; \tag{1a}$$
$$\boldsymbol{r}_1 = \xi_2 \boldsymbol{d}_2 + \xi_3 \boldsymbol{d}_3. \tag{1b}$$

The deformed configuration Ω_2 is defined by the mid-curve $\boldsymbol{\varphi}(\xi_1)$ and non-planar family of warped cross-section $B_2(\xi_1) \subset \mathbb{R}^3_{\xi_1}$, where $\mathbb{R}^3_{\xi_1}$ is the 3D Euclidean space spanned by the director triad $\{\boldsymbol{d}_i(\xi_1)\}$ originating at $\boldsymbol{\varphi}(\xi_1)$. The deformation map $\boldsymbol{\phi}_2 : \boldsymbol{R}_0 \in \Omega_0 \mapsto \boldsymbol{R}_2 \in \Omega_2$ is then defined as

$$\boldsymbol{\phi}_2(\boldsymbol{R}_0) = \boldsymbol{R}_2 = \boldsymbol{\varphi}(\xi_1) + \xi_2 \boldsymbol{d}_2(\xi_1) + \xi_3 \boldsymbol{d}_3(\xi_1) + W(\xi_1, \xi_2, \xi_3) \boldsymbol{d}_1(\xi_1). \tag{2}$$

In the equation above, $W(\xi_1, \xi_2, \xi_3)$ denotes the warping function. Simo and Vu-Quoc (1991) investigated Cosserat beam subjected to Saint–Venant's warping such that $W(\xi_1, \xi_2, \xi_3) = p(\xi_1)\Psi(\xi_2, \xi_3)$, where $p(\xi_1)$ gives warping amplitude and $\Psi(\xi_2, \xi_3)$ is the warping function obtained by solving the corresponding Neumann boundary value problem defined by Eq. [13] of Simo and Vu-Quoc (1991). Chadha and Todd (2019) proposed a modified warping function that includes warping due to bending induced shear and non-uniform torsion in asymmetric cross-section (refer to Section 2.3, 2.4, and the appendix of Chadha and Todd (2019)). It is discussed in Section 2.4.

The final deformed state Ω defined by the mid-curve $\boldsymbol{\varphi}$ and a family of cross-section $B(\xi_1) = \left(W, \hat{\xi}_2, \hat{\xi}_3\right) \in \mathbb{R}^3_{\xi_1}$. It incorporates a fully coupled Poisson's and warping effect. The deformation map for Ω is given by $\boldsymbol{\phi} : \boldsymbol{R}_0 \in \Omega_0 \mapsto \boldsymbol{R} \in \Omega$, such that

$$\begin{aligned} &\boldsymbol{\phi}(\boldsymbol{R}_0) = \boldsymbol{R} = \boldsymbol{\varphi}(\xi_1) + \boldsymbol{r}; \\ &\boldsymbol{r} = \hat{\xi}_2 \boldsymbol{d}_2(\xi_1) + \hat{\xi}_3 \boldsymbol{d}_3(\xi_1) + W \boldsymbol{d}_1(\xi_1). \end{aligned} \tag{3}$$

Here, the vector $\boldsymbol{r}$ gives the position vector of a material point (ξ_2, ξ_3) in the deformed cross-section $B(\xi_1)$ with respect to the point $\boldsymbol{\varphi}(\xi_1)$. Let $\Gamma(\xi_1)$ represent the boundary of cross-section $B(\xi_1)$, such that $\mathfrak{S} = B(0) \cup B(L) \cup_{\forall \xi_1} \Gamma(\xi_1)$. The coordinates $\left(\hat{\xi}_2, \hat{\xi}_3\right)$ are obtained by Poisson's transformation $P_{\xi_1} : (\xi_2, \xi_3) \in B_1 \mapsto \left(\hat{\xi}_2, \hat{\xi}_3\right) \in B_3$, such that

$$\hat{\xi}_i = \left(1 - \nu(\boldsymbol{\lambda}_1^2 \cdot \boldsymbol{d}_1)\right)\xi_i \text{ for } i = 2, 3. \tag{4}$$

In the equation above, ν represents Poisson's ratio and is assumed to be a constant (homogeneous material). The quantity $\boldsymbol{\lambda}_1^2$ is the first strain vector of the deformed configuration Ω_2 defined in Eq. (15). Therefore, $\boldsymbol{\lambda}_1^2 \cdot \boldsymbol{d}_1$ essentially gives the longitudinal strain along $\boldsymbol{d}_1$ at the material point (ξ_1, ξ_2, ξ_3) in the deformed state Ω_2. Fig. 1 illustrates various configurations described so far.

2.2. Rotation and finite strain parameters

2.2.1. Axial strain vector

The midcurve axial strain $e(\xi_1)$, and the three shear angles $\gamma_{11}(\xi_1), \frac{\pi}{2} - \gamma_{12}(\xi_1)$, and $\frac{\pi}{2} - \gamma_{12}(\xi_1)$ subtended by the directors

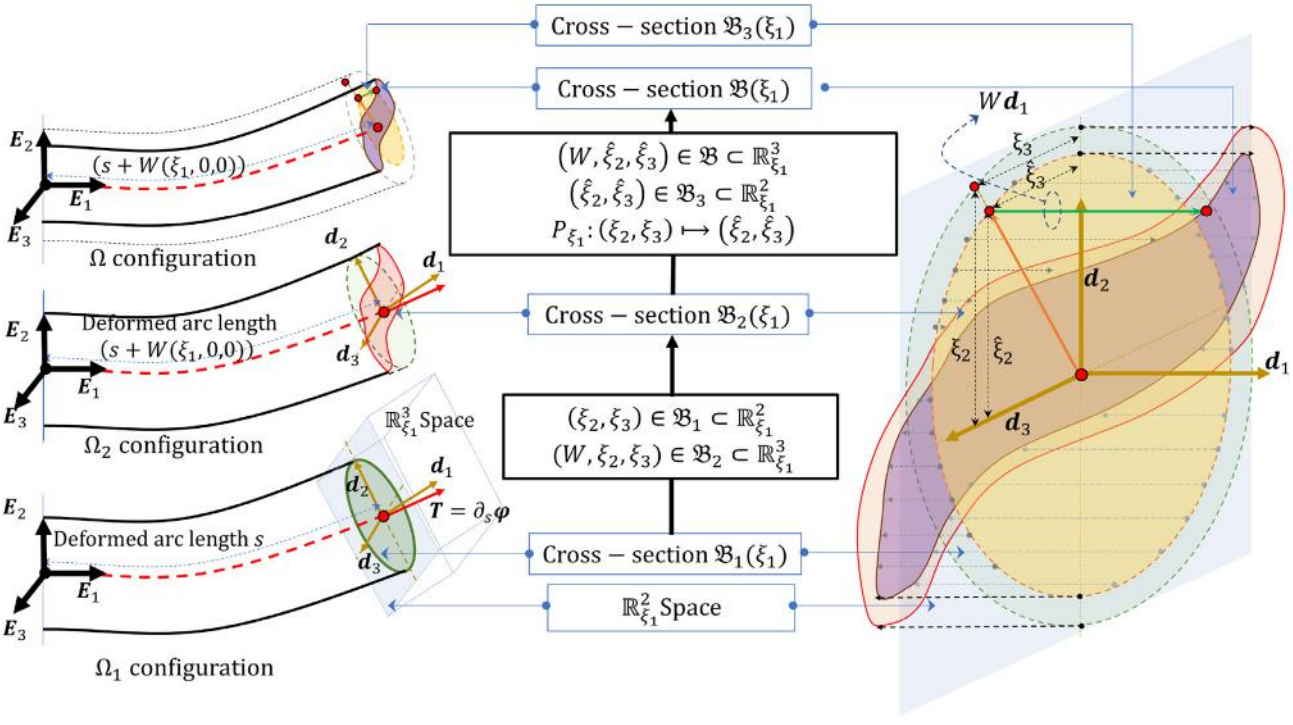

Fig. 1. Schematic diagram illustrating geometric description of various deformed configurations.

$\boldsymbol{d}_1$, $\boldsymbol{d}_2$, and $\boldsymbol{d}_3$ with the tangent vector $\partial_s\boldsymbol{\varphi}$ to the deformed mid-curve $\boldsymbol{\varphi}$ are defined as

$$e = \frac{\mathrm{ds}-\mathrm{d}\xi_1}{\mathrm{d}\xi_1} \Rightarrow \frac{\mathrm{d}\xi_1}{\mathrm{ds}} = \frac{1}{1+e};$$
$$\partial_s\boldsymbol{\varphi}\cdot\boldsymbol{d}_i = \left\{\begin{array}{ll}\cos\gamma_{1i}, & \text{for } i=1\\ \sin\gamma_{1i}, & \text{for } i=2,3\end{array}\right\}. \tag{5}$$

This leads us to the definition of axial strain vector $\boldsymbol{\varepsilon}$ as

$$\boldsymbol{\varepsilon} = \partial_{\xi_1}\boldsymbol{\varphi} - \boldsymbol{d}_1 = \bar{\varepsilon}_i\boldsymbol{d}_i = \varepsilon_i\boldsymbol{E}_i. \tag{6}$$

As in the equation above, the components of a vector $\boldsymbol{v}$ in $\{\boldsymbol{E}_i\}$ and $\{\boldsymbol{d}_i\}$ is denoted as $\boldsymbol{v} = v_i\boldsymbol{E}_i = \overline{v}_i\boldsymbol{d}_i$.

2.2.2. Finite rotation and curvature

The director triad $\{\boldsymbol{d}_i\}$ is related to the fixed reference triad $\{\boldsymbol{E}_i\}$ by means of an orthogonal tensor $\boldsymbol{Q} \in SO(3)$, such that

$$\boldsymbol{d}_i = \boldsymbol{Q}.\boldsymbol{E}_i \Rightarrow \boldsymbol{Q} = \boldsymbol{d}_i \otimes \boldsymbol{E}_i. \tag{7}$$

Finite rotations are represented by an element of a proper orthogonal rotation (Lie) group $SO(3)$ with its Lie algebra $so(3)$ (refer to Chadha and Todd, 2019a). The rotation tensor can be parameterized by a rotation vector $\boldsymbol{\theta} \in \mathbb{R}^3$ by means of exponential map $\exp : so(3) \longrightarrow SO(3)$. The local homeomorphism of exp map in the neighborhood of identity $\boldsymbol{I}_3 \in SO(3)$ for $\theta \in [0, \pi)$, guarantees the existence of a unique inverse of exponential map in the neighborhood of $\boldsymbol{I}_3 \in SO(3)$, called the logarithm map $\log : SO(3) \longrightarrow so(3)$, such that

$$\boldsymbol{Q}(\boldsymbol{\theta}) = \exp\left(\hat{\boldsymbol{\theta}}\right). \tag{8a}$$
$$\log\left(\boldsymbol{Q}(\boldsymbol{\theta})\right) = \log\left(\exp\left(\hat{\boldsymbol{\theta}}\right)\right) = \hat{\boldsymbol{\theta}} \in so(3), \text{ with } \|\log\left(\boldsymbol{Q}(\boldsymbol{\theta})\right)\| = \theta. \tag{8b}$$

From here on, any matrix quantity with a hat on it $(\hat{.})$ represents an anti-symmetric matrix. The equation above allows us to evaluates the deviation between two rotation tensors, say the approximated rotation tensor $\boldsymbol{Q}^h$ and the exact rotation tensor $\boldsymbol{Q}$, by measuring the length of the geodesic between them, such that the error $\boldsymbol{Q}_{\text{error}}$ is quantified as

$$\boldsymbol{Q} = \boldsymbol{Q}_{\text{error}}.\boldsymbol{Q}^h;$$
$$e_{\boldsymbol{Q}} = \|\log\left(\boldsymbol{Q}_{\text{error}}\right)\| \in [0, \pi). \tag{9}$$

For any $\hat{\boldsymbol{a}}, \hat{\boldsymbol{b}} \in so(3)$, we define the Lie-bracket as $[.,.] : so(3) \times so(3) \longrightarrow \mathbb{R}^3$, such that:

$$\left[\hat{\boldsymbol{a}}, \hat{\boldsymbol{b}}\right] = \left(\hat{\boldsymbol{a}}.\hat{\boldsymbol{b}} - \hat{\boldsymbol{b}}.\hat{\boldsymbol{a}}\right). \tag{10}$$

It is important to understand the derivative of director triad as it defines local change of the triad. We have

$$\partial_{\xi_1}\boldsymbol{d}_i = \partial_{\xi_1}\boldsymbol{Q}.\boldsymbol{E}_i = \partial_{\xi_1}\boldsymbol{Q}.\boldsymbol{Q}^T.\boldsymbol{d}_i = \hat{\boldsymbol{\kappa}}.\boldsymbol{d}_i. \tag{11}$$

Here, $\hat{\boldsymbol{\kappa}} = \partial_{\xi_1}\boldsymbol{Q}.\boldsymbol{Q}^T$ represents the curvature tensor. It is an anti-symmetric matrix with the corresponding axial vector $\boldsymbol{\kappa} = \overline{\kappa}_i\boldsymbol{d}_i$, known as curvature vector. We define $T_{\boldsymbol{Q}}SO(3)$ as the tangent plane of non-linear $SO(3)$ manifold, such that $\partial_{\xi_1}\boldsymbol{Q} = \hat{\boldsymbol{\kappa}}.\boldsymbol{Q} \in T_{\boldsymbol{Q}}SO(3)$. We note that $so(3) = T_{\boldsymbol{I}_3}SO(3)$, i.e., the tangent space of $SO(3)$ at the identity. We define the material curvature $\hat{\overline{\boldsymbol{\kappa}}} = \boldsymbol{Q}^T.\hat{\boldsymbol{\kappa}}.\boldsymbol{Q} = \boldsymbol{Q}^T.\partial_{\xi_1}\boldsymbol{Q} \in so(3)$ obtained by parallel transport of $\hat{\boldsymbol{\kappa}}.\boldsymbol{Q}$ from $T_{\boldsymbol{Q}}SO(3) \longrightarrow so(3)$. Let $\boldsymbol{\kappa}$ and $\overline{\boldsymbol{\kappa}}$ represent the axial vector corresponding to the anti-symmetric matrix $\hat{\boldsymbol{\kappa}}$ and $\hat{\overline{\boldsymbol{\kappa}}}$ respectively. It can then be proven that $\overline{\boldsymbol{\kappa}} = \boldsymbol{Q}^T.\boldsymbol{\kappa}$ such that if $\boldsymbol{\kappa} = \overline{\kappa}_i\boldsymbol{d}_i$, then $\overline{\boldsymbol{\kappa}} = \overline{\kappa}_i\boldsymbol{E}_i$. Refer to Section 2.2 of (Chadha and Todd, 2019a) for better understanding of material and spatial curvature; and left-invariant and right-invariant tangent vector fields. We call the quantities $\hat{\overline{\boldsymbol{\kappa}}}$ and $\overline{\boldsymbol{\kappa}}$ as *material representation*; and $\hat{\boldsymbol{\kappa}}$ and $\boldsymbol{\kappa}$ as *spatial representation* of the *curvature tensor* and the *curvature vector* respectively. Like curvature tensor, we can have material form of other quantities like deformation gradient tensor, angular velocity etc. For instance, the material form of axial strain vector and cross-section position vectors ($\boldsymbol{r}_1$ and$\boldsymbol{r}$) isgiven by $\overline{\boldsymbol{\varepsilon}} = \boldsymbol{Q}^T.\boldsymbol{\varepsilon}, \overline{\boldsymbol{r}}_1 = \boldsymbol{Q}^T.\boldsymbol{r}_1$, and $\overline{\boldsymbol{r}} = \boldsymbol{Q}^T.\boldsymbol{r}$ respectively. From here on, we recognize any material vector or tensor with a bar $(\overline{.})$ over it.

Finally, consider a spatial and material vector $\boldsymbol{v} = \overline{v}_i\boldsymbol{d}_i = v_i\boldsymbol{E}_i$ and $\overline{\boldsymbol{v}} = \overline{v}_i\boldsymbol{E}_i$ respectively, such that $\boldsymbol{v} = \boldsymbol{Q}.\overline{\boldsymbol{v}}$. The derivative of these vectors are obtained as

$$\partial_{\xi_1}\boldsymbol{v} = \partial_{\xi_1}\overline{v}_i.\boldsymbol{d}_i + \overline{v}_i.\partial_{\xi_1}\boldsymbol{d}_i = \tilde{\partial}_{\xi_1}\boldsymbol{v} + \boldsymbol{\kappa}\times\boldsymbol{v};$$
$$\partial_{\xi_1}\overline{\boldsymbol{v}} = \partial_{\xi_1}\overline{v}_i.\boldsymbol{E}_i = \boldsymbol{Q}^T.\tilde{\partial}_{\xi_1}\boldsymbol{v}. \tag{12}$$

In the equation above, $\tilde{\partial}_{\xi_1}\boldsymbol{v}$ defines co-rotational derivative of spatial vector $\boldsymbol{v}$. It essentially gives the change in components of the vector $\boldsymbol{v}$, provided the frame of reference is assumed to be fixed. Along similar lines, the co-rotational derivative of the tensor $\boldsymbol{A}$ is defined as $\tilde{\partial}_{\xi_1}\boldsymbol{A} = \boldsymbol{Q}.\partial_{\xi_1}\overline{\boldsymbol{A}}.\boldsymbol{Q}^T$, more detail of which can be found in Section 2.2.4 of Chadha and Todd (2019a). From here on, $\tilde{\partial}_x(.)$ denotes the co-rotational derivative of quantity $(.)$ with respect to x.

2.3. Deformation gradient tensor and strain vectors

The deformation gradient tensor $\boldsymbol{F}$ of the final deformed state Ω referenced to Ω_0 can be defined (refer to Eq. (30) of Chadha and Todd (2019)) as,

$$\boldsymbol{F} = \partial_{\xi_i}\boldsymbol{R}\otimes\boldsymbol{E}_i = (\boldsymbol{\lambda}_i + \boldsymbol{d}_i)\otimes\boldsymbol{E}_i = (\boldsymbol{\lambda}_i\otimes\boldsymbol{E}_i) + \boldsymbol{Q} = \boldsymbol{H} + \boldsymbol{Q}. \tag{13}$$

It consist of two parts: change in infinitesimal tangent vector by virtue of rotation (change in direction) and straining (change in magnitude). Readers are referred to Section 3 of Chadha and Todd (2019) for detailed interpretation of strain vector $\boldsymbol{\lambda}_i$. The expression of strain vector $\boldsymbol{\lambda}_i$ is obtained in Eq. (35) of Chadha and Todd (2019). The material form of strain vectors $\boldsymbol{\lambda}_i$ and the deformation gradient tensor $\boldsymbol{F}$ are given by the following

$$\overline{\boldsymbol{\lambda}}_i = \boldsymbol{Q}^T.\boldsymbol{\lambda}_i = \boldsymbol{Q}^T.\partial_{\xi_1}\boldsymbol{R} - \boldsymbol{E}_i; \tag{14a}$$
$$\overline{\boldsymbol{F}} = \overline{\boldsymbol{\lambda}}_i\otimes\boldsymbol{E}_i + \boldsymbol{I}_3 = \overline{\boldsymbol{H}} + \boldsymbol{I}_3 = \boldsymbol{Q}.\boldsymbol{F}.\boldsymbol{I}_3 = \boldsymbol{Q}.\boldsymbol{F}. \tag{14b}$$

The quantities $\boldsymbol{H} = \boldsymbol{\lambda}_i\otimes\boldsymbol{E}_i$ and $\overline{\boldsymbol{H}} = \overline{\boldsymbol{\lambda}}_i\otimes\boldsymbol{E}_i$ gives spatial and material form of *strain tensor* respectively.

2.4. Revisiting the deformation map $\boldsymbol{\phi}$

The strain vector $\boldsymbol{\lambda}_1^2$ is crucial in defining the Poisson's transformation as seen in Eq. (4). We recall that the quantity $\boldsymbol{\lambda}_1^2$ is the first strain vector of the deformed configuration Ω_2, such that $\boldsymbol{\lambda}_1^2\cdot\boldsymbol{d}_1$ essentially gives the longitudinal strain along $\boldsymbol{d}_1$ at the material point (ξ_1, ξ_2, ξ_3) in the deformed state Ω_2. We can obtain the expression of $\boldsymbol{\lambda}_i^2$ from the expression of $\boldsymbol{\lambda}_i$ as

$$\boldsymbol{\lambda}_1^2 = \boldsymbol{\lambda}_1|_{\xi_j\to\xi_j} = \left(\boldsymbol{\varepsilon} + \xi_3.\partial_{\xi_1}\boldsymbol{d}_3 + \xi_2.\partial_{\xi_1}\boldsymbol{d}_2 + \partial_{\xi_1}W.\boldsymbol{d}_1 + W.\partial_{\xi_1}\boldsymbol{d}_1\right);$$
$$\boldsymbol{\lambda}_1^2.\boldsymbol{d}_1 = \left(\overline{\varepsilon}_1 + \xi_3\overline{\kappa}_2 - \xi_2\overline{\kappa}_3 + \partial_{\xi_1}W\right). \tag{15}$$

To maintain the single-manifold character of Cosserat beams, it is necessary to pre-define the cross-sectional deformation dependences upon the Poisson's and warping effects. We briefly discuss the warping function W. In Chadha and Todd (2019), we arrived at the governing differential equation (Eqs. (68a) and (68b) of Chadha and Todd (2019)) for warping for an asymmetrical beam cross-section subjected to the curvature and axial strains for the linear case the solution of which yielded W in a variable separable form as the following

$$W(\xi_1,\xi_2,\xi_3) = \sum_{n=0}^{\infty} \partial_{\xi_1}^{2n}\overline{\kappa}_1.\Psi_{1(2n)} + \partial_{\xi_1}^{2n+1}\overline{\kappa}_2.\Psi_{2(2n+1)} + \partial_{\xi_1}^{2n+1}\overline{\kappa}_3.\Psi_{3(2n+1)}. \tag{16}$$

Proposing this form of warping function was inspired by the work of Brown and Burgoyne (Brown and Burgoyne, 1994; Burgoyne and Brown, 1994). The cross-section dependent warping functions in Eq. (16) (like $\Psi_{10}, \Psi_{12}, \ldots; \Psi_{21}, \Psi_{23}, \ldots$) can be obtained by solving the set of governing differential equation discussed in appendix 6.1.4 of Chadha and Todd (2019). Higher-order derivatives of $\overline{\kappa}_1$ take care of non-uniform torsion (unlike Saint Venant's warping) whereas higher-order derivatives of $\overline{\kappa}_j$ $(j = 2, 3)$ capture bending-induced non-uniform shear deformation (unlike Timoshenko's uniform shear). We assume that the contribution of higher-order derivative (> 1) of curvatures to warping is negligible. Thus, to facilitate the computation of governing field equations, we consider a simplified warping function for this paper

$$\begin{aligned} W(\xi_1,\xi_2,\xi_3) &= p(\xi_1)\Psi_1(\xi_2,\xi_3) + \partial_{\xi_1}\overline{\kappa}_2.\Psi_2(\xi_2,\xi_3) \\ &\quad + \partial_{\xi_1}\overline{\kappa}_3.\Psi_3(\xi_2,\xi_3) \\ &= p(\xi_1)\Psi_1(\xi_2,\xi_3) + \partial_{\xi_1}\overline{\boldsymbol{\kappa}}\cdot\overline{\boldsymbol{\Psi}}_{23}. \end{aligned} \tag{17}$$

In the equation above, $\overline{\boldsymbol{\Psi}}_{23} = \Psi_2(\xi_2,\xi_3)\boldsymbol{E}_2 + \Psi_3(\xi_2,\xi_3)\boldsymbol{E}_3$ and $\partial_{\xi_1}\overline{\boldsymbol{\kappa}} = \partial_{\xi_1}\overline{\kappa}_i.\boldsymbol{E}_i$. For the sake of computation, the cross-section dependent functions $\Psi_1(\xi_2,\xi_3), \Psi_2(\xi_2,\xi_3)$, and $\Psi_3(\xi_2,\xi_3)$ are assumed to be known. Therefore, all we require in this paper is to know the warping functions beforehand. In this case, we have obtained the warping functions by solving the governing differential equation derived in Chadha and Todd (2019) assuming that the deformation due to warping is small with linear isotropic material. However, it is possible to solve for the warping functions in the non-linear setting as the structure deforms by numerically solving for the warping function at every iteration (refer to Arora et al., 2019).

2.5. Revisiting the material and spatial strain vector $\boldsymbol{\lambda}_i$

In this Section, we elaborate the expressions of strain vectors $\boldsymbol{\lambda}_i$ and $\overline{\boldsymbol{\lambda}}_i$ in a desirable form. Using the definition of $\boldsymbol{R}$ in (3), and the definition of the strain vector as $\boldsymbol{\lambda}_i = \partial_{\xi_i}\boldsymbol{R} - \boldsymbol{d}_i$, we obtain the expressions for material and spatial form of strain vector $\overline{\boldsymbol{\lambda}}_i$ expressed in matrix form as

$$\overline{\boldsymbol{\mathcal{L}}} = \overline{\boldsymbol{L}}.\overline{\boldsymbol{\epsilon}} \text{ and } \boldsymbol{\mathcal{L}} = \boldsymbol{L}.\boldsymbol{\epsilon}. \tag{18}$$

where

$$\begin{aligned} &\overline{\boldsymbol{\mathcal{L}}} = \left[\overline{\boldsymbol{\lambda}}_1; \overline{\boldsymbol{\lambda}}_2; \overline{\boldsymbol{\lambda}}_3\right]; \quad \boldsymbol{\mathcal{L}} = [\boldsymbol{\lambda}_1; \boldsymbol{\lambda}_2; \boldsymbol{\lambda}_3]; \\ &\overline{\boldsymbol{\epsilon}} = \left[\overline{\boldsymbol{\varepsilon}}; \partial_{\xi_1}\overline{\boldsymbol{\varepsilon}}; \overline{\boldsymbol{\kappa}}; \partial_{\xi_1}\overline{\boldsymbol{\kappa}}; \partial_{\xi_1}^2\overline{\boldsymbol{\kappa}}; \partial_{\xi_1}^3\overline{\boldsymbol{\kappa}}; p; \partial_{\xi_1}p; \partial_{\xi_1}^2 p\right], \end{aligned} \tag{19}$$

such that

$$\boldsymbol{\mathcal{L}} = \boldsymbol{Q}_3.\overline{\boldsymbol{\mathcal{L}}} \text{ and } \boldsymbol{\epsilon} = \boldsymbol{\Lambda}.\overline{\boldsymbol{\epsilon}}. \tag{20}$$

Here, $\boldsymbol{\Lambda} = \text{diagonal}[\boldsymbol{Q}, \boldsymbol{Q}, \boldsymbol{Q}, \boldsymbol{Q}, \boldsymbol{Q}, \boldsymbol{Q}, \boldsymbol{I}_3]$ and $\boldsymbol{Q}_3 = \text{diagonal}[\boldsymbol{Q}, \boldsymbol{Q}, \boldsymbol{Q}]$ respectively. We carefully note that for any $n, \boldsymbol{Q}.\partial_{\xi_1}^n\overline{\boldsymbol{\kappa}} = \tilde{\partial}_{\xi_1}^n\boldsymbol{\kappa}$ (refer to *Propositions 1 and 3* in Chadha and Todd (2019a) that also defines the operator $\tilde{\partial}_{\xi_1}^n$). Therefore,

$$\boldsymbol{\epsilon} = \left[\boldsymbol{\varepsilon};\ \tilde{\partial}_{\xi_1}\boldsymbol{\varepsilon};\ \boldsymbol{\kappa};\ \tilde{\partial}_{\xi_1}\boldsymbol{\kappa};\ \tilde{\partial}_{\xi_1}^2\boldsymbol{\kappa};\ \tilde{\partial}_{\xi_1}^3\boldsymbol{\kappa};\ p;\ \partial_{\xi_1}p;\ \partial_{\xi_1}^2 p\right]. \tag{21}$$

The matrices $\overline{\boldsymbol{L}}$ can be expanded as

$$\overline{\boldsymbol{L}} = \begin{bmatrix} \overline{\boldsymbol{L}}_{\boldsymbol{\varepsilon}}^{\boldsymbol{\lambda}_1} & \overline{\boldsymbol{L}}_{\partial_{\xi_1}\boldsymbol{\varepsilon}}^{\boldsymbol{\lambda}_1} & \overline{\boldsymbol{L}}_{\boldsymbol{\kappa}}^{\boldsymbol{\lambda}_1} & \overline{\boldsymbol{L}}_{\partial_{\xi_1}\boldsymbol{\kappa}}^{\boldsymbol{\lambda}_1} & \overline{\boldsymbol{L}}_{\partial_{\xi_1}^2\boldsymbol{\kappa}}^{\boldsymbol{\lambda}_1} & \overline{\boldsymbol{L}}_{\partial_{\xi_1}^3\boldsymbol{\kappa}}^{\boldsymbol{\lambda}_1} & \overline{\boldsymbol{L}}_{p}^{\boldsymbol{\lambda}_1} & \overline{\boldsymbol{L}}_{\partial_{\xi_1}p}^{\boldsymbol{\lambda}_1} & \overline{\boldsymbol{L}}_{\partial_{\xi_1}^2 p}^{\boldsymbol{\lambda}_1} \\ \overline{\boldsymbol{L}}_{\boldsymbol{\varepsilon}}^{\boldsymbol{\lambda}_2} & \overline{\boldsymbol{L}}_{\partial_{\xi_1}\boldsymbol{\varepsilon}}^{\boldsymbol{\lambda}_2} & \overline{\boldsymbol{L}}_{\boldsymbol{\kappa}}^{\boldsymbol{\lambda}_2} & \overline{\boldsymbol{L}}_{\partial_{\xi_1}\boldsymbol{\kappa}}^{\boldsymbol{\lambda}_2} & \overline{\boldsymbol{L}}_{\partial_{\xi_1}^2\boldsymbol{\kappa}}^{\boldsymbol{\lambda}_2} & \overline{\boldsymbol{L}}_{\partial_{\xi_1}^3\boldsymbol{\kappa}}^{\boldsymbol{\lambda}_2} & \overline{\boldsymbol{L}}_{p}^{\boldsymbol{\lambda}_2} & \overline{\boldsymbol{L}}_{\partial_{\xi_1}p}^{\boldsymbol{\lambda}_2} & \overline{\boldsymbol{L}}_{\partial_{\xi_1}^2 p}^{\boldsymbol{\lambda}_2} \\ \overline{\boldsymbol{L}}_{\boldsymbol{\varepsilon}}^{\boldsymbol{\lambda}_3} & \overline{\boldsymbol{L}}_{\partial_{\xi_1}\boldsymbol{\varepsilon}}^{\boldsymbol{\lambda}_3} & \overline{\boldsymbol{L}}_{\boldsymbol{\kappa}}^{\boldsymbol{\lambda}_3} & \overline{\boldsymbol{L}}_{\partial_{\xi_1}\boldsymbol{\kappa}}^{\boldsymbol{\lambda}_3} & \overline{\boldsymbol{L}}_{\partial_{\xi_1}^2\boldsymbol{\kappa}}^{\boldsymbol{\lambda}_3} & \overline{\boldsymbol{L}}_{\partial_{\xi_1}^3\boldsymbol{\kappa}}^{\boldsymbol{\lambda}_3} & \overline{\boldsymbol{L}}_{p}^{\boldsymbol{\lambda}_3} & \overline{\boldsymbol{L}}_{\partial_{\xi_1}p}^{\boldsymbol{\lambda}_3} & \overline{\boldsymbol{L}}_{\partial_{\xi_1}^2 p}^{\boldsymbol{\lambda}_3} \end{bmatrix}. \tag{22}$$

The corresponding spatial form $\boldsymbol{L}$ consisting of the component matrices $\boldsymbol{L}_x^{\lambda_i}$, with $x \in \boldsymbol{\epsilon}$ is obtained as

$$\boldsymbol{L} = \boldsymbol{Q}_3.\overline{\boldsymbol{L}}.\boldsymbol{\Lambda}^T. \tag{23}$$

We call the quantities $\overline{\boldsymbol{L}}_x^{\lambda_i}$ (given in Appendix A.1) and $\boldsymbol{L}_x^{\lambda_i}$ the material and spatial $\boldsymbol{L}$-terms, respectively. The elaborate expression of material and spatial $\boldsymbol{L}$ matrices is contained in the supplementary material.

2.6. Configuration and the state space

Adapting the kinematics discussed above, we find that there are three primary quantities required to defined the configuration $\Omega : \boldsymbol{\varphi} \in \mathbb{R}^3$, $\boldsymbol{Q} \in SO(3)$ and $p \in \mathbb{R}$. For static case, the configuration, tangent, and state space of the beam Ω is given as

$$\mathbb{C} := \left\{\boldsymbol{\Phi} = (\boldsymbol{\varphi}, \boldsymbol{Q}, p) : [0, L] \longrightarrow \mathbb{R}^3 \times SO(3) \times \mathbb{R}\right\}; \tag{24a}$$

$$T_{\boldsymbol{\Phi}}\mathbb{C} := \left\{\tilde{\boldsymbol{\Phi}} = \left(\partial_{\xi_1}\boldsymbol{\varphi}, \partial_{\xi_1}\boldsymbol{Q}, \partial_{\xi_1}p\right) : [0, L] \longrightarrow \mathbb{R}^3 \times T_{\boldsymbol{Q}}SO(3) \times \mathbb{R}\right\}; \tag{24b}$$

$$T\mathbb{C} := \left\{\left(\boldsymbol{\Phi}, \tilde{\boldsymbol{\Phi}}\right) | \boldsymbol{\Phi} \in \mathbb{C}, \tilde{\boldsymbol{\Phi}} \in T_{\boldsymbol{\Phi}}\mathbb{C}\right\}. \tag{24c}$$

It is interesting to interpret the curvature vector $\boldsymbol{\kappa}$ and the derivative of rotation vector $\partial_{\xi_1}\boldsymbol{\theta}$ with a physical viewpoint. At an arc-length ξ_1, the director triad $\{\boldsymbol{d}_i(\xi_1)\}$ rotates about the vector $\boldsymbol{\kappa}(\xi_1).\mathrm{d}\xi_1$ to yield the triad at $\{\boldsymbol{d}_i(\xi_1 + \mathrm{d}\xi_1)\}$. Whereas, the triad $\{\boldsymbol{d}_i(\xi_1)\}$ and $\{\boldsymbol{d}_i(\xi_1 + \mathrm{d}\xi_1)\}$ are obtained by finite rotation of the frame $\{\boldsymbol{E}_i\}$ about the rotation vector $\boldsymbol{\theta}(\xi_1)$ and $\boldsymbol{\theta}(\xi_1 + \mathrm{d}\xi_1) = \boldsymbol{\theta}(\xi_1) + \partial_{\xi_1}\boldsymbol{\theta}(\xi_1).\mathrm{d}\xi_1$ respectively. , the material form of axial strain vector and cross-section Fig. 2(left) illustrates the idea discussed here. In terms of the exponential map,

$$\begin{aligned} \boldsymbol{Q}(\xi_1 + \mathrm{d}\xi_1) &= \exp(\hat{\boldsymbol{\kappa}}(\xi_1).\mathrm{d}\xi_1).\boldsymbol{Q}(\xi_1) \\ &= \exp(\hat{\boldsymbol{\kappa}}(\xi_1).\mathrm{d}\xi_1).\exp\left(\hat{\boldsymbol{\theta}}(\xi_1)\right) \\ &= \exp\left(\hat{\boldsymbol{\theta}}(\xi_1) + \partial_{\xi_1}\hat{\boldsymbol{\theta}}(\xi_1).\mathrm{d}\xi_1\right). \end{aligned} \tag{25}$$

The equation above can be used to obtain the relationship between $\hat{\boldsymbol{\kappa}}$ and $\partial_{\xi_1}\hat{\boldsymbol{\theta}}$ as shown in Eq. (7) of Chadha and Todd (2019a). With slight abuse of notation, we can associate the tangent space with curvature tensor field $\hat{\boldsymbol{\kappa}}(\xi_1)$ (instead of $\partial_{\xi_1}\boldsymbol{Q} = \hat{\boldsymbol{\kappa}}.\boldsymbol{Q}$). The isomorphism between $so(3)$ and $\mathbb{R}^3$ permits one to identify the tensor field $\hat{\boldsymbol{\kappa}}(\xi_1)$ with its corresponding axial vector $\boldsymbol{\kappa}(\xi_1) \in \mathbb{R}^3$. Thus, the state space is defined by the set $(\boldsymbol{\varphi}, \{\boldsymbol{d}_i\}, p; \partial_{\xi_1}\boldsymbol{\varphi}, \boldsymbol{\kappa}, \partial_{\xi_1}p)$. Redefining the tangent space described in Eq. (24b) yields

$$T_{\boldsymbol{\Phi}}\mathbb{C} := \left\{\tilde{\boldsymbol{\Phi}} = \left(\partial_{\xi_1}\boldsymbol{\varphi}, \boldsymbol{\kappa}, \partial_{\xi_1}p\right) : [0, L] \longrightarrow \mathbb{R}^3 \times \mathbb{R}^3 \times \mathbb{R}\right\}. \tag{26}$$

For the dynamic case, we define the configuration space parameterized with arc-length and time (ξ_1, t) as,

$$\mathbb{C} := \left\{\boldsymbol{\Phi} = (\boldsymbol{\varphi}, \boldsymbol{Q}, p) : [0, L] \times \mathbb{R}^+ \longrightarrow \mathbb{R}^3 \times SO(3) \times \mathbb{R}\right\}. \tag{27}$$

However, it is important to look at the configuration of beam Ω_t at a fixed time $t \in \mathbb{R}^+$ to study curvature vector $\boldsymbol{\kappa}$ and consider a point with constant arc-length to understand the evolution of director field with time (given by angular velocity tensor $\hat{\boldsymbol{\omega}} = \partial_t\boldsymbol{Q}.\boldsymbol{Q}^T$). Hence,

$$\begin{aligned} &\boldsymbol{Q}(\xi_1 + \mathrm{d}\xi_1, t) = \exp(\hat{\boldsymbol{\kappa}}(\xi_1, t).\mathrm{d}\xi_1).\boldsymbol{Q}(\xi_1, t); \\ &\boldsymbol{Q}(\xi_1, t + \mathrm{d}t) = \exp(\hat{\boldsymbol{\omega}}(\xi_1, t + \mathrm{d}t).\mathrm{d}t).\boldsymbol{Q}(\xi_1, t). \end{aligned} \tag{28}$$

Fig. 3 illustrates the discussion on $SO(3)$ manifold carried out so far.

Remark 1. We guide the readers on what is to come next by detailing the structure of the following writing. Even though the beam is a 3D structure, we model it as a 1D single-manifold structure. As is clear from the configuration space of the beam in

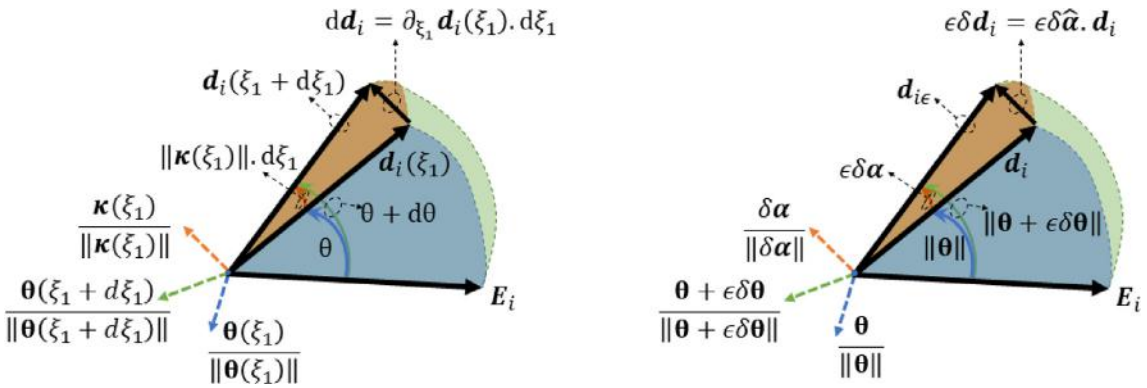

Fig. 2. Physical interpretation of curvature $\boldsymbol{\kappa}$ (left figure) and variation of rotation vector $\delta\boldsymbol{\alpha}$ (right figure) resulting in infinitesimal rotation.

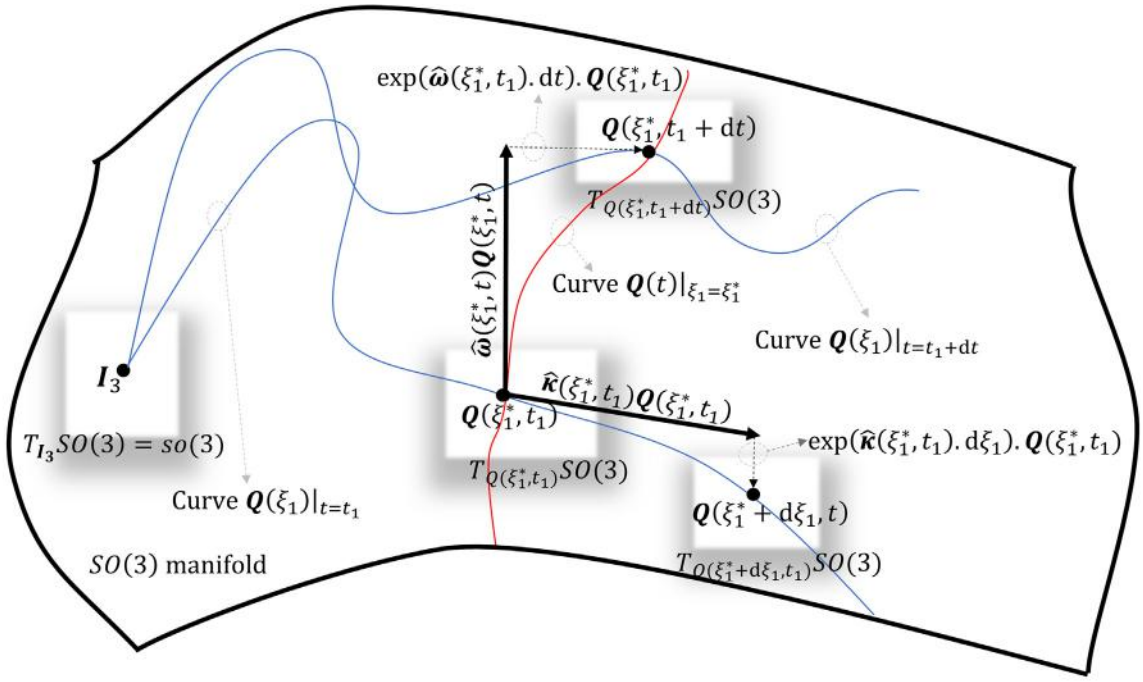

Fig. 3. Geometric representation of $SO(3)$ manifold, exponential map, tangent plane $T_{\boldsymbol{Q}}SO(3)$, curvature tensor $\hat{\boldsymbol{\kappa}}$, and angular velocity tensor $\hat{\boldsymbol{\omega}}$.

Eq. (24a), this reduced 1D beam theory consist of 7 primary degrees of freedom: 3 components of the position vector $\boldsymbol{\varphi}$ defining translation, 3 components of the rotation vector $\boldsymbol{\theta}$ parameterizing $\boldsymbol{Q}$, and the warping amplitude p. Therefore, we expect a single equation describing the weak form and a set of 7 governing differential equations as a strong form. Corresponding to each of these degree of freedom, we have 7 strain terms: axial strain $\boldsymbol{\varepsilon}$, $\boldsymbol{\kappa}$, and $\partial_{\xi_1}p$ that constitutes the tangent space $T_{\boldsymbol{\Phi}}\mathbb{C}$. Unlike, Simo Vu-Quoc beam (Simo and Hughes, 1986), the kinematics of the beam in this paper depends on higher-order derivatives of these strain terms, thus, making the derivation of the variation of these terms challenging. Therefore, Section 3 is dedicated to obtaining the variation of these terms so that they can be used to obtain the weak form in Section 4. The strong form of governing equation is then obtained from the weak form in Section 5. The reduced internal forces and their respective strain conjugates are related by linear constitutive law in Section 6. Finally, Section 7 derives the matrix form of the equation that may be numerically solved.

3. Variation

To obtain the virtual work principle (a weak form of equilibrium equation), we need to obtain admissible variation of the deformed configuration. We also must linearize the weak form for numerically solving the system. This shall be covered in the second part of this paper. However, since both variation and linearization are geometrically similar procedures (that help us operate on the tangent space $T_{\boldsymbol{\Phi}}\mathbb{C}$), we shall carefully describe the variation of deformation map and associated strain quantities here.

3.1. Admissible variation of the deformed configuration Ω

To obtain the virtual deformed configuration of the system, we superimpose an admissible variation or admissible infinitesimal (and instantaneous) displacement field $\delta\boldsymbol{\Phi} = (\delta\boldsymbol{\varphi}, \delta\boldsymbol{Q}, \delta p)$ to the configuration $\boldsymbol{\Phi} = (\boldsymbol{\varphi}, \boldsymbol{Q}(\boldsymbol{\theta}), p)$. The varied configuration is then defined by $\boldsymbol{\Phi}_\epsilon = (\boldsymbol{\varphi}_\epsilon, \boldsymbol{Q}_\epsilon, p_\epsilon)$, such that for $\epsilon > 0$, we have

$$\boldsymbol{\varphi}_\epsilon = \boldsymbol{\varphi} + \epsilon\delta\boldsymbol{\varphi}, \text{ and } \delta\boldsymbol{\varphi} = \partial_\epsilon \boldsymbol{\varphi}_\epsilon|_{\epsilon=0}; \tag{29a}$$

$$\boldsymbol{Q}_\epsilon = \boldsymbol{Q}(\boldsymbol{\theta} + \epsilon\delta\boldsymbol{\theta}) = \boldsymbol{Q}(\epsilon\delta\boldsymbol{\alpha}).\boldsymbol{Q}(\boldsymbol{\theta}), \text{ and } \delta\boldsymbol{Q} = \partial_\epsilon \boldsymbol{Q}_\epsilon|_{\epsilon=0}; \tag{29b}$$

$$p_\epsilon = p + \epsilon\delta p, \text{ and } \delta p = \partial_\epsilon p_\epsilon|_{\epsilon=0}. \tag{29c}$$

Unlike the variation in the mid-curve axial vector, and the warping amplitude, understanding the variation in the rotation tensor needs some detailed investigation. This is because $\boldsymbol{\varphi} \in \mathbb{R}^3$ and $p \in \mathbb{R}$ belong to linear vector spaces, where as $SO(3)$ is a non-linear manifold. It is advantageous to express the virtual rotation tensor by means of *virtual rotation vector in current state* $\delta\boldsymbol{\alpha}$ contrary to the *variation of total rotation vector* $\delta\boldsymbol{\theta}$. Hence, the varied director field is then given by

$$\boldsymbol{d}_{i\epsilon} = \boldsymbol{Q}_\epsilon.\boldsymbol{E}_i = \boldsymbol{Q}(\epsilon\delta\boldsymbol{\alpha}).\boldsymbol{d}_i. \tag{30}$$

Refer to Fig. 2 (right image) for physical interpretation of the virtual current rotation vector $\delta\boldsymbol{\alpha}$. The rotation tensor $\boldsymbol{Q}_\epsilon = \boldsymbol{Q}(\boldsymbol{\theta} + \epsilon\delta\boldsymbol{\theta})$ transforms the vector $\boldsymbol{E}_i$ to $\boldsymbol{d}_{i\epsilon}$ in a single step, whereas, the tensor $\boldsymbol{Q}_\epsilon = \boldsymbol{Q}(\epsilon\delta\boldsymbol{\alpha}).\boldsymbol{Q}(\boldsymbol{\theta})$ performs the same transformation in two steps: $\boldsymbol{E}_i \overset{\boldsymbol{Q}(\boldsymbol{\theta})}{\longrightarrow} \boldsymbol{d}_i \overset{\boldsymbol{Q}(\epsilon\delta\boldsymbol{\alpha})}{\longrightarrow} \boldsymbol{d}_{i\epsilon}$. From Eq. (29b), we arrive at the expression of virtual rotation tensor and director field

$$\delta\boldsymbol{Q} = \partial_\epsilon\left(\exp(\epsilon\delta\hat{\boldsymbol{\alpha}}).\exp\left(\hat{\boldsymbol{\theta}}\right)\right)|_{\epsilon=0} = \left(\delta\hat{\boldsymbol{\alpha}}.\exp(\epsilon\delta\hat{\boldsymbol{\alpha}}).\exp\left(\hat{\boldsymbol{\theta}}\right)\right)|_{\epsilon=0} = \delta\hat{\boldsymbol{\alpha}}.\boldsymbol{Q}(\boldsymbol{\theta}); \tag{31a}$$

$$\delta\boldsymbol{d}_i = \delta\boldsymbol{Q}.\boldsymbol{E}_i = \delta\hat{\boldsymbol{\alpha}}.\boldsymbol{d}_i. \tag{31b}$$

Here, $\delta\hat{\boldsymbol{\alpha}}$ represents the anti-symmetric matrix associated with the vector $\delta\boldsymbol{\alpha}$. We define the material form of incremental rotation $\delta\hat{\overline{\boldsymbol{\alpha}}}$ (with $\delta\overline{\boldsymbol{\alpha}}$ being the associated axial vector) as

$$\delta\hat{\overline{\boldsymbol{\alpha}}} = \boldsymbol{Q}^T.\delta\hat{\boldsymbol{\alpha}}.\boldsymbol{Q} = \boldsymbol{Q}^T.\delta\boldsymbol{Q}; \delta\overline{\boldsymbol{\alpha}} = \boldsymbol{Q}^T.\delta\boldsymbol{\alpha}. \tag{32}$$

It follows from the discussion above that $\partial_{\xi_1}\boldsymbol{Q}, \delta\boldsymbol{Q} \in T_{\boldsymbol{Q}}SO(3)$, $\delta\boldsymbol{\Phi} \in T_{\boldsymbol{\Phi}}\mathbb{C}, \delta\hat{\overline{\boldsymbol{\alpha}}} \in so(3)$ and $(\boldsymbol{\Phi}, \delta\boldsymbol{\Phi}) \in T\mathbb{C}$. Like the relationship between $\boldsymbol{\kappa}$ and $\partial_{\xi_1}\boldsymbol{\theta}$ defined in Eq. (7) of Chadha and Todd (2019a), we can arrive at the relation between $\delta\boldsymbol{\alpha}$ and $\delta\boldsymbol{\theta}$. We redefine $\delta\boldsymbol{\Phi}$ as,

$$\delta\boldsymbol{\Phi} = [\delta\boldsymbol{\varphi}; \delta\boldsymbol{\alpha}; \delta p]. \tag{33}$$

Having understood the varied configuration space, the expressions derived in this section can be directly used to obtain the variation of other quantities using straightforward application of the chain rule.

3.2. Variation of the strain quantities and their derivatives

In this section, we obtain the variation of finite strain quantities in terms of $(\delta\boldsymbol{\varphi}, \delta\boldsymbol{\alpha}, \delta p)$ and their derivatives. The virtual material strain vectors $\delta\overline{\boldsymbol{\lambda}}_i$ are strain conjugate to material form of first PK stress vectors (discussed later in Section 4.2). Deriving the expression of $\delta\overline{\boldsymbol{\lambda}}_i$ requires us to first find variation of $\boldsymbol{L}$-terms and $\delta\overline{\boldsymbol{\epsilon}}$ as a function of $(\delta\boldsymbol{\varphi}, \delta\boldsymbol{\alpha}, \delta p)$ and their derivatives.

3.2.1. Variation of the finite strain terms

From the definition of axial strain vector $\boldsymbol{\varepsilon}$, we obtain

$$\delta\boldsymbol{\varepsilon} = \delta\partial_{\xi_1}\boldsymbol{\varphi} - \delta\hat{\boldsymbol{\alpha}}.\boldsymbol{d}_1; \tag{34a}$$

$$\delta\overline{\boldsymbol{\varepsilon}} = \delta\left(\boldsymbol{Q}^T.\boldsymbol{\varepsilon}\right) = \boldsymbol{Q}^T\left(\delta\partial_{\xi_1}\boldsymbol{\varphi} + \partial_{\xi_1}\hat{\boldsymbol{\varphi}}.\delta\boldsymbol{\alpha}\right) = \boldsymbol{Q}^T.\tilde{\delta}\boldsymbol{\varepsilon}. \tag{34b}$$

Similarly, the variation of spatial and material curvature tensor is given by

$$\delta\hat{\boldsymbol{\kappa}} = \delta\left(\partial_{\xi_1}\boldsymbol{Q}.\boldsymbol{Q}^T\right) = \delta\partial_{\xi_1}\boldsymbol{Q}.\boldsymbol{Q}^T + \partial_{\xi_1}\boldsymbol{Q}.\delta\boldsymbol{Q}^T = \delta\partial_{\xi_1}\hat{\boldsymbol{\alpha}} + [\delta\hat{\boldsymbol{\alpha}}, \hat{\boldsymbol{\kappa}}]; \tag{35a}$$

$$\delta\hat{\overline{\boldsymbol{\kappa}}} = \delta\left(\boldsymbol{Q}^T.\partial_{\xi_1}\boldsymbol{Q}\right) = \delta\boldsymbol{Q}^T.\partial_{\xi_1}\boldsymbol{Q} + \boldsymbol{Q}^T.\delta\partial_{\xi_1}\boldsymbol{Q} = \boldsymbol{Q}^T.\delta\partial_{\xi_1}\hat{\boldsymbol{\alpha}}.\boldsymbol{Q} = \boldsymbol{Q}^T.\tilde{\delta}\hat{\boldsymbol{\kappa}}.\boldsymbol{Q}. \tag{35b}$$

The variation of the spatial and material curvature vectors are obtained as

$$\delta\boldsymbol{\kappa} = \delta\partial_{\xi_1}\boldsymbol{\alpha} + \delta\hat{\boldsymbol{\alpha}}.\boldsymbol{\kappa}; \tag{36a}$$

$$\delta\overline{\boldsymbol{\kappa}} = \boldsymbol{Q}^T.\delta\partial_{\xi_1}\boldsymbol{\alpha} = \boldsymbol{Q}^T.\tilde{\delta}\boldsymbol{\kappa}. \tag{36b}$$

Like the co-rotated derivatives, $\tilde{\delta}\boldsymbol{\varepsilon} = \left(\delta\partial_{\xi_1}\boldsymbol{\varphi} + \partial_{\xi_1}\hat{\boldsymbol{\varphi}}.\delta\boldsymbol{\alpha}\right), \tilde{\delta}\boldsymbol{\kappa} = \delta\partial_{\xi_1}\boldsymbol{\alpha}$ and $\tilde{\delta}\hat{\boldsymbol{\kappa}} = \delta\partial_{\xi_1}\hat{\boldsymbol{\alpha}}$ defines the co-rotated variation of the curvature vector, axial strain vector and curvature tensor, respectively.

3.2.2. Variation of the vector $\overline{\boldsymbol{\epsilon}}$

Since the derivative and variation can be used interchangeably, we obtain $\delta\partial_{\xi_1}\overline{\boldsymbol{\varepsilon}}, \delta\partial^n_{\xi_1}\overline{\boldsymbol{\kappa}}$ using Eqs. (34b), and (36b). These results can be used to express $\delta\overline{\boldsymbol{\epsilon}}$ in the following form

$$\delta\overline{\boldsymbol{\epsilon}} = \boldsymbol{\Lambda}^T.\boldsymbol{B}_1.\delta\boldsymbol{\Theta} = \boldsymbol{\Lambda}^T.\tilde{\delta}\boldsymbol{\epsilon}, \tag{37}$$

where,

$$\begin{aligned}
\delta\boldsymbol{\Theta} &= \left[\delta\boldsymbol{\varphi};\ \delta\partial_{\xi_1}\boldsymbol{\varphi};\ \delta\partial^2_{\xi_1}\boldsymbol{\varphi};\ \delta\boldsymbol{\alpha};\ \delta\partial_{\xi_1}\boldsymbol{\alpha};\ \delta\partial^2_{\xi_1}\boldsymbol{\alpha};\ \delta\partial^3_{\xi_1}\boldsymbol{\alpha};\ \delta\partial^4_{\xi_1}\boldsymbol{\alpha};\ \delta p;\ \delta\partial_{\xi_1}p;\ \delta\partial^2_{\xi_1}p\right];\\
\delta\overline{\boldsymbol{\epsilon}} &= \left[\delta\overline{\boldsymbol{\varepsilon}};\ \delta\partial_{\xi_1}\overline{\boldsymbol{\varepsilon}};\ \delta\overline{\boldsymbol{\kappa}};\ \delta\partial_{\xi_1}\overline{\boldsymbol{\kappa}};\ \delta\partial^2_{\xi_1}\overline{\boldsymbol{\kappa}};\ \delta\partial^3_{\xi_1}\overline{\boldsymbol{\kappa}};\ \ \delta p;\ \delta\partial_{\xi_1}p;\ \delta\partial^2_{\xi_1}p\right];\\
\tilde{\delta}\boldsymbol{\epsilon} &= \left[\tilde{\delta}\boldsymbol{\varepsilon};\ \tilde{\delta}\tilde{\partial}_{\xi_1}\boldsymbol{\varepsilon};\ \tilde{\delta}\boldsymbol{\kappa};\ \tilde{\delta}\tilde{\partial}_{\xi_1}\boldsymbol{\kappa};\ \tilde{\delta}\tilde{\partial}^2_{\xi_1}\boldsymbol{\kappa};\ \tilde{\delta}\tilde{\partial}^3_{\xi_1}\boldsymbol{\kappa};\ \delta p;\ \delta\partial_{\xi_1}p;\ \ \delta\partial^2_{\xi_1}p\right].
\end{aligned} \tag{38}$$

The virtual vector $\delta\boldsymbol{\Theta}$ can be related to $\delta\boldsymbol{\Phi}$ by means of a differential operator $\boldsymbol{B}_2$ (of size 27×7), such that

$$\delta\boldsymbol{\Theta} = \boldsymbol{B}_2.\delta\boldsymbol{\Phi}. \tag{39}$$

The Eq. (37) can then be re-written as

$$\begin{aligned}
\delta\overline{\boldsymbol{\epsilon}} &= \boldsymbol{\Lambda}^T.\boldsymbol{B}_1.\boldsymbol{B}_2.\delta\boldsymbol{\Phi};\\
\tilde{\delta}\boldsymbol{\epsilon} &= \boldsymbol{B}_1.\boldsymbol{B}_2.\delta\boldsymbol{\Phi}.
\end{aligned} \tag{40}$$

The expanded description of the matrices $\boldsymbol{B}_1$ and $\boldsymbol{B}_2$ are given in Appendices A.2.1 and A.2.2, respectively.

3.2.3. Variation of the strain vector $\overline{\boldsymbol{\lambda}}_i$ and the concatenated strain vector $\overline{\boldsymbol{\mathcal{L}}}$

From Eq. (18), we have

$$\delta\overline{\boldsymbol{\mathcal{L}}} = \delta\overline{\boldsymbol{\mathcal{L}}}.\overline{\boldsymbol{\epsilon}} + \overline{\boldsymbol{\mathcal{L}}}.\delta\overline{\boldsymbol{\epsilon}}. \tag{41}$$

We realize that, except for $\delta\boldsymbol{L}^{\lambda_1}_{\boldsymbol{\kappa}} = \delta\hat{\overline{\boldsymbol{r}}}^T$, the variation in all other $\boldsymbol{L}$-terms are $\boldsymbol{0}_3$. Thus, we have

$$\delta\overline{\boldsymbol{\mathcal{L}}}.\overline{\boldsymbol{\epsilon}} = \left[\delta\boldsymbol{L}^{\lambda_1}_{\boldsymbol{\kappa}}.\overline{\boldsymbol{\kappa}}; \boldsymbol{0}_1; \boldsymbol{0}_1\right] = \left[\delta\hat{\overline{\boldsymbol{r}}}^T.\overline{\boldsymbol{\kappa}}; \boldsymbol{0}_1; \boldsymbol{0}_1\right] \tag{42}$$

From the expression of $\overline{\boldsymbol{r}} = \boldsymbol{Q}^T.\boldsymbol{r} = \hat{\xi}_2\boldsymbol{E}_2 + \hat{\xi}_3\boldsymbol{E}_3 + W\boldsymbol{E}_1$, we can find $\delta\hat{\overline{\boldsymbol{r}}}^T$ that can be substitutes in (42) to obtain:

$$\delta\overline{\boldsymbol{\mathcal{L}}}.\overline{\boldsymbol{\epsilon}} = \overline{\boldsymbol{M}}.\delta\overline{\boldsymbol{\epsilon}}, \tag{43}$$

where,

$$\overline{\boldsymbol{M}} = \begin{bmatrix}
\overline{\boldsymbol{M}}^{\lambda_1}_{\boldsymbol{\varepsilon}} & \boldsymbol{0}_3 & \overline{\boldsymbol{M}}^{\lambda_1}_{\boldsymbol{\kappa}} & \overline{\boldsymbol{M}}^{\lambda_1}_{\partial_{\xi_1}\boldsymbol{\kappa}} & \overline{\boldsymbol{M}}^{\lambda_1}_{\partial^2_{\xi_1}\boldsymbol{\kappa}} & \boldsymbol{0}_3 & \overline{\boldsymbol{M}}^{\lambda_1}_{p} & \overline{\boldsymbol{M}}^{\lambda_1}_{\partial_{\xi_1}p} & \boldsymbol{0}_1 \\
\boldsymbol{0}_3 & \boldsymbol{0}_3 & \boldsymbol{0}_3 & \boldsymbol{0}_3 & \boldsymbol{0}_3 & \boldsymbol{0}_3 & \boldsymbol{0}_1 & \boldsymbol{0}_1 & \boldsymbol{0}_1 \\
\boldsymbol{0}_3 & \boldsymbol{0}_3 & \boldsymbol{0}_3 & \boldsymbol{0}_3 & \boldsymbol{0}_3 & \boldsymbol{0}_3 & \boldsymbol{0}_1 & \boldsymbol{0}_1 & \boldsymbol{0}_1
\end{bmatrix}. \tag{44}$$

Like $\boldsymbol{L}$-terms, we call $\overline{\boldsymbol{M}}^{\lambda_i}_{(.)}$ as $\boldsymbol{M}$-terms. Appendix A.1 gives the expression of $\boldsymbol{M}$-terms. Similar to Eq. (23), we define the spatial form of $\boldsymbol{M}$ matrix consisting of $\boldsymbol{M}^{\lambda_i}_{(.)}$, such that

$$\boldsymbol{M} = \boldsymbol{Q}_3.\overline{\boldsymbol{M}}.\boldsymbol{\Lambda}^T, \tag{45}$$

The elaborate expression of material and spatial $\boldsymbol{M}$ matrices is contained in the supplementary material. Substituting Eq. (43) into Eq. (41), we get

$$\delta\overline{\mathcal{L}} = \left[\delta\overline{\lambda}_1; \delta\overline{\lambda}_2; \delta\overline{\lambda}_3\right] = (\overline{\boldsymbol{L}} + \overline{\boldsymbol{M}}).\delta\overline{\boldsymbol{\epsilon}}. \tag{46}$$

We define the co-rotational variation of the concatenated strain vector $\mathcal{L}$ as

$$\tilde{\delta}\mathcal{L} = \left[\tilde{\delta}\lambda_1; \tilde{\delta}\lambda_2; \tilde{\delta}\lambda_3\right] = \boldsymbol{Q}_3.\delta\overline{\mathcal{L}} = \boldsymbol{Q}_3.(\overline{\boldsymbol{L}} + \overline{\boldsymbol{M}}).\delta\overline{\boldsymbol{\epsilon}} = (\boldsymbol{L} + \boldsymbol{M}).\tilde{\delta}\boldsymbol{\epsilon}. \tag{47}$$

The variation of deformation gradient tensor is obtained as

$$\begin{aligned} &\delta\boldsymbol{F} = \tilde{\delta}\boldsymbol{F} + \delta\boldsymbol{Q}.\overline{\boldsymbol{F}} = \tilde{\delta}\boldsymbol{F} + \delta\hat{\boldsymbol{\alpha}}.\boldsymbol{F};\\ &\tilde{\delta}\boldsymbol{F} = \boldsymbol{Q}.\delta\overline{\boldsymbol{F}} = \tilde{\delta}\lambda_i \otimes \boldsymbol{E}_i;\\ &\delta\overline{\boldsymbol{F}} = \delta\overline{\lambda}_i \otimes \boldsymbol{E}_i. \end{aligned} \tag{48}$$

3.3. Variation of displacement field

We need the variation of displacement field to evaluate the virtual work done by external load. We define the displacement field $\boldsymbol{u}(\xi_1, \xi_2, \xi_3)$ as $\boldsymbol{u} = \boldsymbol{R} - \boldsymbol{R}_0$. Since, $\delta\boldsymbol{R}_0 = \boldsymbol{0}_1$, we have $\delta\boldsymbol{u} = \delta\boldsymbol{R}$. Thus, Eq. (3) yields

$$\delta\boldsymbol{R} = \delta\boldsymbol{\varphi} + \delta\boldsymbol{r}; \tag{49a}$$

$$\delta\boldsymbol{r} = \tilde{\delta}\boldsymbol{r} + \delta\hat{\boldsymbol{\alpha}}.\boldsymbol{r}; \tag{49b}$$

$$\tilde{\delta}\boldsymbol{r} = \delta\tilde{\xi}_2\boldsymbol{d}_2 + \delta\tilde{\xi}_3\boldsymbol{d}_3 + \delta W\boldsymbol{d}_1. \tag{49c}$$

We can manipulate the expression of $\tilde{\delta}\boldsymbol{r}$ in Eq. (49c) to a following desirable form

$$\begin{aligned} \tilde{\delta}\boldsymbol{r} &= \boldsymbol{L}^{\lambda_1}_{\partial_{\xi_1}\boldsymbol{\varepsilon}}.\tilde{\delta}\boldsymbol{\varepsilon} + \boldsymbol{L}^{\lambda_1}_{\partial_{\xi_1}\boldsymbol{\kappa}}.\tilde{\delta}\boldsymbol{\kappa} + \boldsymbol{L}^{\lambda_1}_{\partial^2_{\xi_1}\boldsymbol{\kappa}}.\left(\boldsymbol{Q}.\delta\partial_{\xi_1}\overline{\boldsymbol{\kappa}}\right) + \boldsymbol{L}^{\lambda_1}_{\partial^3_{\xi_1}\boldsymbol{\kappa}}.\left(\boldsymbol{Q}.\delta\partial^2_{\xi_1}\overline{\boldsymbol{\kappa}}\right)\\ &+ \delta p.\boldsymbol{L}^{\lambda_1}_{\partial_{\xi_1}p} + \delta\partial_{\xi_1}p.\boldsymbol{L}^{\lambda_1}_{\partial^2_{\xi_1}p}; = \boldsymbol{L}^{\lambda_1}_{\partial_{\xi_1}\boldsymbol{\varepsilon}}.\tilde{\delta}\boldsymbol{\varepsilon} + \boldsymbol{L}^{\lambda_1}_{\partial_{\xi_1}\boldsymbol{\kappa}}.\tilde{\delta}\boldsymbol{\kappa} + \boldsymbol{L}^{\lambda_1}_{\partial^2_{\xi_1}\boldsymbol{\kappa}}.\left(\tilde{\delta}\tilde{\partial}_{\xi_1}\boldsymbol{\kappa}\right)\\ &+ \boldsymbol{L}^{\lambda_1}_{\partial^3_{\xi_1}\boldsymbol{\kappa}}.\left(\tilde{\delta}\tilde{\partial}^2_{\xi_1}\boldsymbol{\kappa}\right) + \delta p.\boldsymbol{L}^{\lambda_1}_{\partial_{\xi_1}p} + \delta\partial_{\xi_1}p.\boldsymbol{L}^{\lambda_1}_{\partial^2_{\xi_1}p}. \end{aligned} \tag{50}$$

4. Weak form of governing differential equation

4.1. General virtual work principle

We define the unsymmetric two-point first Piola Kirchoff stress tensor $\boldsymbol{P} = \boldsymbol{P}_i \otimes \boldsymbol{E}_i$ referenced to the undeformed configuration Ω_0 such that the vector $\boldsymbol{P}_i$ represents the associated stress-vectors. We can write the integral or residual form of equilibrium equation as

$$\int_{\Omega_0} \delta\boldsymbol{u} \cdot (\mathrm{Div}\boldsymbol{P} + \rho_0\boldsymbol{b} - \rho_0\partial_t^2\boldsymbol{R})\mathrm{d}\Omega_0 = 0. \tag{51}$$

Here, Div is divergence operator referenced to the configuration Ω_0. The quantities $\rho_0(\xi_1, \xi_2, \xi_3) = \rho_0$ and $\boldsymbol{b}(\xi_1, \xi_2, \xi_3) = \boldsymbol{b}$ give the mass density field in the undeformed state and the body force per unit mass respectively. Since $\boldsymbol{F} = \boldsymbol{I}_3 + \mathrm{Grad}(\boldsymbol{u})$, we have $\delta\boldsymbol{F} = \mathrm{Grad}(\delta\boldsymbol{u})$. Here, Grad is the gradient operator with respect to the configuration Ω_0. Using this result and divergence theorem on Eq. (51), we get the general virtual work principle

$$G(\boldsymbol{\Phi}, \delta\boldsymbol{\Phi}) = \delta\mathrm{U}_{\mathrm{strain}} + \delta\mathrm{W}_{\mathrm{inertial}} - \delta\mathrm{W}_{\mathrm{ext}} = 0, \tag{52}$$

where,

$$\delta\mathrm{U}_{\mathrm{strain}} = \int_{\Omega_0} \boldsymbol{P} : \delta\boldsymbol{F}\mathrm{d}\Omega_0 = \int_{\Omega_0} \mathrm{trace}\left(\boldsymbol{P}^T.\delta\boldsymbol{F}\right)\mathrm{d}\Omega_0; \tag{53a}$$

$$\delta\mathrm{W}_{\mathrm{inertial}} = \int_{\Omega_0} \rho_0\delta\boldsymbol{u} \cdot \partial_t^2\boldsymbol{R}\mathrm{d}\Omega_0; \tag{53b}$$

$$\delta\mathrm{W}_{\mathrm{ext}} = \int_{\mathfrak{S}_0} \delta\boldsymbol{u} \cdot (\boldsymbol{P}.\boldsymbol{N})\mathrm{d}\mathfrak{S}_0 + \int_{\Omega_0} \delta\boldsymbol{u} \cdot \boldsymbol{b}\mathrm{d}\Omega_0 = \delta\mathrm{W}^{\mathrm{st}}_{\mathrm{ext}} + \delta\mathrm{W}^{\mathrm{b}}_{\mathrm{ext}}. \tag{53c}$$

The virtual work due to external forces is contributed by surface tractions ($\delta\mathrm{W}^{\mathrm{st}}_{\mathrm{ext}}$) and body forces ($\delta\mathrm{W}^{\mathrm{b}}_{\mathrm{ext}}$). In the equation above, $\boldsymbol{N}$ represents the normal vector to the surface $\mathfrak{S}_0$ of the beam.

4.2. Virtual strain energy

The expression of strain energy in Eq. (53a) can be further simplified by using Eq. (48), such that

$$\delta\mathrm{U}_{\mathrm{strain}} = \int_{\Omega_0} \boldsymbol{P} : \delta\boldsymbol{F}\mathrm{d}\Omega_0 = \int_{\Omega_0} \boldsymbol{P} : \tilde{\delta}\boldsymbol{F}\mathrm{d}\Omega_0 + \int_{\Omega_0} \boldsymbol{P} : (\delta\hat{\boldsymbol{\alpha}}.\boldsymbol{F})\mathrm{d}\Omega_0. \tag{54}$$

We observe that $\boldsymbol{P} : (\delta\hat{\boldsymbol{\alpha}}.\boldsymbol{F}) = \boldsymbol{P}\boldsymbol{F}^T : \delta\hat{\boldsymbol{\alpha}} = 0$. This is because, $\boldsymbol{P}\boldsymbol{F}^T$ is symmetric and $\delta\hat{\boldsymbol{\alpha}}$ is an anti-symmetric matrix. We define the concatenated stress vector $\mathcal{P} = [\boldsymbol{P}_1; \boldsymbol{P}_2; \boldsymbol{P}_3]$ and its material counterpart $\overline{\mathcal{P}} = [\overline{\boldsymbol{P}}_1; \overline{\boldsymbol{P}}_2; \overline{\boldsymbol{P}}_3]$, such that $\mathcal{P} = \boldsymbol{Q}_3.\overline{\mathcal{P}}$. This further simplifies Eq. (54) to the following

$$\begin{aligned} &\delta\mathrm{U}_{\mathrm{strain}} = \textstyle\int_{\Omega_0} \boldsymbol{P} : \tilde{\delta}\boldsymbol{F}\mathrm{d}\Omega_0 = \int_{\Omega_0} \boldsymbol{P}_i.\tilde{\delta}\lambda_i\mathrm{d}\Omega_0 = \int_{\Omega_0} \overline{\boldsymbol{P}}_i.\delta\overline{\lambda}_i\mathrm{d}\Omega_0;\\ &\delta\mathrm{U}_{\mathrm{strain}} = \textstyle\int_{\Omega_0} \mathcal{P} \cdot \tilde{\delta}\mathcal{L}\mathrm{d}\Omega_0 = \int_{\Omega_0} \overline{\mathcal{P}} \cdot \delta\overline{\mathcal{L}}\mathrm{d}\Omega_0. \end{aligned} \tag{55}$$

Using the results in Eqs. (46) and (47) we have,

$$\delta\mathrm{U}_{\mathrm{strain}} = \int_{\Omega_0} \tilde{\delta}\boldsymbol{\epsilon} \cdot \left((\boldsymbol{L} + \boldsymbol{M})^T.\mathcal{P}\right)\mathrm{d}\Omega_0 = \int_0^L \tilde{\delta}\boldsymbol{\epsilon} \cdot \mathcal{N}_{\mathrm{int}}\mathrm{d}\xi_1; \tag{56a}$$

$$\delta\mathrm{U}_{\mathrm{strain}} = \int_{\Omega_0} \delta\overline{\boldsymbol{\epsilon}} \cdot \left((\overline{\boldsymbol{L}} + \overline{\boldsymbol{M}})^T.\overline{\mathcal{P}}\right)\mathrm{d}\Omega_0 = \int_0^L \delta\overline{\boldsymbol{\epsilon}} \cdot \overline{\mathcal{N}}_{\mathrm{int}}\mathrm{d}\xi_1. \tag{56b}$$

We define the spatial and material reduced section force vectors $\mathcal{N}_{\mathrm{int}}(\xi_1)$ and $\overline{\mathcal{N}}_{\mathrm{int}}(\xi_1)$ (refer to Appendix A.3.1) as

$$\begin{aligned} \mathcal{N}_{\mathrm{int}} &= \left[\mathcal{N}_{\boldsymbol{\varepsilon}}; \mathcal{N}_{\partial_{\xi_1}\boldsymbol{\varepsilon}}; \mathcal{N}_{\boldsymbol{\kappa}}; \mathcal{N}_{\partial_{\xi_1}\boldsymbol{\kappa}}; \mathcal{N}_{\partial^2_{\xi_1}\boldsymbol{\kappa}}; \mathcal{N}_{\partial^3_{\xi_1}\boldsymbol{\kappa}}; N_p; N_{\partial_{\xi_1}p}; N_{\partial^2_{\xi_1}p}\right]\\ &= \int_{B_0} (\boldsymbol{L} + \boldsymbol{M})^T.\mathcal{P}\mathrm{d}B_0;\\ \overline{\mathcal{N}}_{\mathrm{int}} &= \left[\overline{\mathcal{N}}_{\boldsymbol{\varepsilon}}; \overline{\mathcal{N}}_{\partial_{\xi_1}\boldsymbol{\varepsilon}}; \overline{\mathcal{N}}_{\boldsymbol{\kappa}}; \overline{\mathcal{N}}_{\partial_{\xi_1}\boldsymbol{\kappa}}; \overline{\mathcal{N}}_{\partial^2_{\xi_1}\boldsymbol{\kappa}}; \overline{\mathcal{N}}_{\partial^3_{\xi_1}\boldsymbol{\kappa}}; \overline{N}_p; \overline{N}_{\partial_{\xi_1}p}; \overline{N}_{\partial^2_{\xi_1}p}\right]\\ &= \int_{B_0} (\overline{\boldsymbol{L}} + \overline{\boldsymbol{M}})^T.\overline{\mathcal{P}}\mathrm{d}B_0, \end{aligned} \tag{57}$$

Using Eq. (40), we arrive at the desired matrix form of virtual strain energy expression

$$\delta\mathrm{U}_{\mathrm{strain}} = \int_0^L \delta\boldsymbol{\Phi}^T\boldsymbol{B}_2^T\boldsymbol{B}_1^T\mathcal{N}_{\mathrm{int}}\mathrm{d}\xi_1. \tag{58}$$

4.3. Virtual work done due to external and inertial forces

4.3.1. Virtual work done due to external forces

The virtual work due to external forces is contributed by surface traction and body force. We first consider the surface traction term

$$\begin{aligned} \delta\mathrm{W}^{\mathrm{st}}_{\mathrm{ext}} = \int_{\mathfrak{S}_0} \delta\boldsymbol{u} \cdot (\boldsymbol{P}.\boldsymbol{N})\mathrm{d}\mathfrak{S}_0 = \int_0^L \Bigg(&\int_{B_0(\xi_1+\mathrm{d}\xi_1)} \delta\boldsymbol{u} \cdot \boldsymbol{P}_1\mathrm{d}B_0\\ &- \int_{B_0(\xi_1)} \delta\boldsymbol{u} \cdot \boldsymbol{P}_1\mathrm{d}B_0 + \int_{\Gamma_0(\xi_1)} \delta\boldsymbol{u} \cdot (\boldsymbol{P}.\boldsymbol{N})\mathrm{d}\Gamma_0\Bigg)\mathrm{d}\xi_1 \end{aligned} \tag{59}$$

Recall the expression of $\delta\boldsymbol{u} = \delta\boldsymbol{\varphi} + \delta\hat{\boldsymbol{\alpha}}.\boldsymbol{r} + \tilde{\delta}\boldsymbol{r}$ as discussed in Section 3.3. We simplify the first two integrals to obtain boundary terms. We note the following results

$$\begin{aligned} &\int_{B_0(\xi_1+\mathrm{d}\xi_1)} \delta\boldsymbol{\varphi} \cdot \boldsymbol{P}_1\mathrm{d}B_0 - \int_{B_0(\xi_1)} \delta\boldsymbol{\varphi} \cdot \boldsymbol{P}_1\mathrm{d}B_0 = \partial_{\xi_1}(\delta\boldsymbol{\varphi} \cdot \boldsymbol{B}_{\boldsymbol{\varphi}})\mathrm{d}\xi_1\\ &\int_{B_0(\xi_1+\mathrm{d}\xi_1)} (\delta\hat{\boldsymbol{\alpha}}.\boldsymbol{r}) \cdot \boldsymbol{P}_1\mathrm{d}B_0 - \int_{B_0(\xi_1)} (\delta\hat{\boldsymbol{\alpha}}.\boldsymbol{r}) \cdot \boldsymbol{P}_1\mathrm{d}B_0 = \partial_{\xi_1}(\delta\boldsymbol{\alpha} \cdot .\boldsymbol{B}_{\boldsymbol{\alpha}})\mathrm{d}\xi_1\\ &\int_{B_0(\xi_1+\mathrm{d}\xi_1)} \tilde{\delta}\boldsymbol{r} \cdot \boldsymbol{P}_1\mathrm{d}B_0 - \int_{B_0(\xi_1)} \tilde{\delta}\boldsymbol{r} \cdot \boldsymbol{P}_1\mathrm{d}B_0 = \partial_{\xi_1}\\ &\quad\times\left(\tilde{\delta}\boldsymbol{\varepsilon} \cdot \boldsymbol{B}_{\boldsymbol{\varepsilon}} + \tilde{\delta}\boldsymbol{\kappa} \cdot \boldsymbol{B}_{\boldsymbol{\kappa}} + \left(\boldsymbol{Q}.\delta\partial_{\xi_1}\overline{\boldsymbol{\kappa}}\right) \cdot \boldsymbol{B}_{\partial_{\xi_1}\boldsymbol{\kappa}} + \left(\boldsymbol{Q}.\delta\partial^2_{\xi_1}\overline{\boldsymbol{\kappa}}\right) \cdot \boldsymbol{B}_{\partial^2_{\xi_1}\boldsymbol{\kappa}}\right.\\ &\quad\left. + \delta p.B_p + \delta\partial_{\xi_1}p.B_{\partial_{\xi_1}p}\right)\mathrm{d}\xi_1. \end{aligned} \tag{60}$$

Here, the quantities $\boldsymbol{B}_{(.)}$ and $B_{(.)}$ represents the reduced end boundary force terms, and are defined in appendix A.3.2. Therefore, the virtual work due to end boundary terms associated with the traction $\delta \mathrm{W}^{\mathrm{st}}_{\mathrm{ext}}|_{B(0)\cup B(L)}$ is given by:

$$\begin{aligned}\delta \mathrm{W}^{\mathrm{st}}_{\mathrm{ext}}|_{B(0)\cup B(L)} &= \int_0^L \left(\int_{B_0(\xi_1+\mathrm{d}\xi_1)} \delta\boldsymbol{u}\cdot\boldsymbol{P}_1 \mathrm{d}B_0 - \int_{B_0(\xi_1)} \delta\boldsymbol{u}\cdot\boldsymbol{P}_1 \mathrm{d}B_0 \right)\mathrm{d}\xi_1 \\ &= \Big[\delta\boldsymbol{\varphi}\cdot\boldsymbol{B}_{\boldsymbol{\varphi}} + \delta\boldsymbol{\alpha}\cdot\boldsymbol{B}_{\boldsymbol{\alpha}} + \tilde{\delta}\boldsymbol{\varepsilon}\cdot\boldsymbol{B}_{\boldsymbol{\varepsilon}} + \tilde{\delta}\boldsymbol{\kappa}\cdot\boldsymbol{B}_{\boldsymbol{\kappa}} + \left(\boldsymbol{Q}\cdot\delta\partial_{\xi_1}\overline{\boldsymbol{\kappa}}\right)\cdot\boldsymbol{B}_{\partial_{\xi_1}\boldsymbol{\kappa}} \\ &\quad + \left(\boldsymbol{Q}.\delta\partial^2_{\xi_1}\overline{\boldsymbol{\kappa}}\right)\cdot\boldsymbol{B}_{\partial^2_{\xi_1}\boldsymbol{\kappa}} + \delta p.B_p + \delta\partial_{\xi_1}p.B_{\partial_{\xi_1}p} \Big]_0^L . \end{aligned} \tag{61}$$

Note that $\boldsymbol{B}_{\boldsymbol{\varphi}}$, $\boldsymbol{B}_{\boldsymbol{\alpha}}$ and B_p represents the reduced section force, moment and bi-shear as in Simo and Vu-Quoc (1991). We now consider the virtual work due to surface traction on the peripheral boundary $\cup_{\forall\xi_1}\Gamma_0(\xi_1)$, denoted by $\delta \mathrm{W}^{\mathrm{st}}_{\mathrm{ext}}|_{\cup_{\forall\xi_1}\Gamma_0(\xi_1)}$, where

$$\begin{aligned}\delta \mathrm{W}^{\mathrm{st}}_{\mathrm{ext}}|_{\cup_{\forall\xi_1}\Gamma_0(\xi_1)} &= \int_0^L \left(\int_{\Gamma_0(\xi_1)} \delta\boldsymbol{u}\cdot(\boldsymbol{P}.\boldsymbol{N})\mathrm{d}\Gamma_0 \right)\mathrm{d}\xi_1 \\ &= \int_0^L \Big(\delta\boldsymbol{\varphi}\cdot\boldsymbol{N}^{\mathrm{st}}_{\boldsymbol{\varphi}} + \delta\boldsymbol{\alpha}\cdot\boldsymbol{N}^{\mathrm{st}}_{\boldsymbol{\alpha}} + \tilde{\delta}\boldsymbol{\varepsilon}\cdot\boldsymbol{N}^{\mathrm{st}}_{\boldsymbol{\varepsilon}} + \tilde{\delta}\boldsymbol{\kappa}\cdot\boldsymbol{N}^{\mathrm{st}}_{\boldsymbol{\kappa}} \\ &\quad + \left(\boldsymbol{Q}.\delta\partial_{\xi_1}\overline{\boldsymbol{\kappa}}\right)\cdot\boldsymbol{N}^{\mathrm{st}}_{\partial_{\xi_1}\boldsymbol{\kappa}} + \left(\boldsymbol{Q}.\delta\partial^2_{\xi_1}\overline{\boldsymbol{\kappa}}\right)\cdot\boldsymbol{N}^{\mathrm{st}}_{\partial^2_{\xi_1}\boldsymbol{\kappa}} + \delta p.N^{\mathrm{st}}_p \\ &\quad + \delta\partial_{\xi_1}p.N^{\mathrm{st}}_{\partial_{\xi_1}p} \Big)\mathrm{d}\xi_1 . \end{aligned} \tag{62}$$

In the equation above, the quantities $\boldsymbol{N}^{\mathrm{st}}_{(.)}$ and $N^{\mathrm{st}}_{(.)}$ represents the reduced external force due to surface traction (represented by the super script st), and are defined in appendix A.3.3. Similarly, the virtual work due to body force field $\boldsymbol{b}$ is obtained as

$$\begin{aligned}\delta \mathrm{W}^{\mathrm{b}}_{\mathrm{ext}} = \int_0^L \Big(&\delta\boldsymbol{\varphi}\cdot\boldsymbol{N}^{\mathrm{b}}_{\boldsymbol{\varphi}} + \delta\boldsymbol{\alpha}\cdot\boldsymbol{N}^{\mathrm{b}}_{\boldsymbol{\alpha}} + \tilde{\delta}\boldsymbol{\varepsilon}\cdot\boldsymbol{N}^{\mathrm{b}}_{\boldsymbol{\varepsilon}} + \tilde{\delta}\boldsymbol{\kappa}\cdot\boldsymbol{N}^{\mathrm{b}}_{\boldsymbol{\kappa}} + \left(\boldsymbol{Q}.\delta\partial_{\xi_1}\overline{\boldsymbol{\kappa}}\right)\cdot\boldsymbol{N}^{\mathrm{b}}_{\partial_{\xi_1}\boldsymbol{\kappa}} \\ &+ \left(\boldsymbol{Q}.\delta\partial^2_{\xi_1}\overline{\boldsymbol{\kappa}}\right)\cdot\boldsymbol{N}^{\mathrm{b}}_{\partial^2_{\xi_1}\boldsymbol{\kappa}} + \delta p.N^{\mathrm{b}}_p + \delta\partial_{\xi_1}p.N^{\mathrm{b}}_{\partial_{\xi_1}p} \Big)\mathrm{d}\xi_1 . \end{aligned} \tag{63}$$

The quantities $\boldsymbol{N}^{\mathrm{b}}_{(.)}$ and $N^{\mathrm{b}}_{(.)}$ represents the reduced external force due to body force (represented by the super script b). Hence,

$$\delta \mathrm{W}_{\mathrm{ext}} = \left(\delta \mathrm{W}^{\mathrm{st}}_{\mathrm{ext}}|_{\cup_{\forall\xi_1}\Gamma_0(\xi_1)} + \delta \mathrm{W}^{\mathrm{b}}_{\mathrm{ext}}\right) + \delta \mathrm{W}^{\mathrm{st}}_{\mathrm{ext}}|_{B(0)\cup B(L)} . \tag{64}$$

Defining the (total) reduced external forces as $\boldsymbol{N}_{(.)} = \boldsymbol{N}^{\mathrm{st}}_{(.)} + \boldsymbol{N}^{\mathrm{b}}_{(.)}$ and $N_{(.)} = N^{\mathrm{st}}_{(.)} + N^{\mathrm{b}}_{(.)}$, we have,

$$\begin{aligned}\left(\delta \mathrm{W}^{\mathrm{st}}_{\mathrm{ext}}|_{\cup_{\forall\xi_1}\Gamma_0(\xi_1)} + \delta \mathrm{W}^{\mathrm{b}}_{\mathrm{ext}}\right) = \int_0^L \Big(&\delta\boldsymbol{\varphi}\cdot\boldsymbol{N}_{\boldsymbol{\varphi}} + \delta\boldsymbol{\alpha}\cdot\boldsymbol{N}_{\boldsymbol{\alpha}} + \tilde{\delta}\boldsymbol{\varepsilon}\cdot\boldsymbol{N}_{\boldsymbol{\varepsilon}} \\ &+ \tilde{\delta}\boldsymbol{\kappa}\cdot\boldsymbol{N}_{\boldsymbol{\kappa}} + \left(\boldsymbol{Q}.\delta\partial_{\xi_1}\overline{\boldsymbol{\kappa}}\right)\cdot\boldsymbol{N}_{\partial_{\xi_1}\boldsymbol{\kappa}} \\ &+ \left(\boldsymbol{Q}.\delta\partial^2_{\xi_1}\overline{\boldsymbol{\kappa}}\right)\cdot\boldsymbol{N}_{\partial^2_{\xi_1}\boldsymbol{\kappa}} + \delta p.N_p + \delta\partial_{\xi_1}p.N_{\partial_{\xi_1}p} \Big)\mathrm{d}\xi_1 \end{aligned} \tag{65}$$

To proceed further, we intend to obtain virtual work in terms of the virtual quantities $\delta\boldsymbol{\varphi}, \delta\boldsymbol{\alpha}$ and δp and their derivatives. Eqs. (61) and (65) can be further condensed in matrix form as

$$\begin{aligned}\delta \mathrm{W}^{\mathrm{st}}_{\mathrm{ext}}|_{B(0)\cup B(L)} &= \left[\delta\boldsymbol{\Theta}\cdot\left(\boldsymbol{B}_3\boldsymbol{\mathcal{N}}_{\mathrm{boundary}}\right)\right]_0^L = \left[\delta\boldsymbol{\Theta}^T\boldsymbol{B}_3\boldsymbol{\mathcal{N}}_{\mathrm{boundary}}\right]_0^L \\ &= \left[\delta\boldsymbol{\Phi}^T\boldsymbol{B}_2^T\boldsymbol{B}_3\boldsymbol{\mathcal{N}}_{\mathrm{boundary}}\right]_0^L ; \left(\delta \mathrm{W}^{\mathrm{st}}_{\mathrm{ext}}|_{\cup_{\forall\xi_1}\Gamma_0(\xi_1)} + \delta \mathrm{W}^{\mathrm{b}}_{\mathrm{ext}}\right) \\ &= \int_0^L \delta\boldsymbol{\Theta}\cdot\left(\boldsymbol{B}_3\boldsymbol{\mathcal{N}}_{\mathrm{ext}}\right)\mathrm{d}\xi_1 = \int_0^L \delta\boldsymbol{\Theta}^T\boldsymbol{B}_3\boldsymbol{\mathcal{N}}_{\mathrm{ext}}\mathrm{d}\xi_1 \\ &= \int_0^L \delta\boldsymbol{\Phi}^T\boldsymbol{B}_2^T\boldsymbol{B}_3\boldsymbol{\mathcal{N}}_{\mathrm{ext}}\mathrm{d}\xi_1 ; \end{aligned} \tag{66}$$

where,

$$\begin{aligned}\boldsymbol{\mathcal{N}}_{\mathrm{boundary}} &= \left[\boldsymbol{B}_{\boldsymbol{\varphi}}; \boldsymbol{B}_{\boldsymbol{\varepsilon}}; \boldsymbol{B}_{\boldsymbol{\alpha}}; \boldsymbol{B}_{\boldsymbol{\kappa}}; \boldsymbol{B}_{\partial_{\xi_1}\boldsymbol{\kappa}}; \boldsymbol{B}_{\partial^2_{\xi_1}\boldsymbol{\kappa}}; B_p; B_{\partial_{\xi_1}p}\right]; \\ \boldsymbol{\mathcal{N}}_{\mathrm{ext}} &= \left[\boldsymbol{N}_{\boldsymbol{\varphi}}; \boldsymbol{N}_{\boldsymbol{\varepsilon}}; \boldsymbol{N}_{\boldsymbol{\alpha}}; \boldsymbol{N}_{\boldsymbol{\kappa}}; \boldsymbol{N}_{\partial_{\xi_1}\boldsymbol{\kappa}}; \boldsymbol{N}_{\partial^2_{\xi_1}\boldsymbol{\kappa}}; N_p; N_{\partial_{\xi_1}p}\right]. \end{aligned} \tag{67}$$

The vectors $\boldsymbol{\mathcal{N}}_{\mathrm{boundary}}$ and $\boldsymbol{\mathcal{N}}_{\mathrm{ext}}$ represent concatenated end *boundary forces* and *reduced external forces* respectively. Refer to Appendix A.2.3 for the expression of matrix $\boldsymbol{B}_3$.

4.3.2. Virtual work done due to inertial forces

Realize that the body force $\boldsymbol{b}$ and the acceleration $\partial_t^2\boldsymbol{R}$ is defined over the volume Ω_0. Therefore, like the expression of virtual work contribution due to body force in Eq. (63), we can arrive at the following

$$\begin{aligned}\delta \mathrm{W}_{\mathrm{inertial}} = \int_0^L \Big(&\delta\boldsymbol{\varphi}\cdot\boldsymbol{F}_{\boldsymbol{\varphi}} + \delta\boldsymbol{\alpha}\cdot\boldsymbol{F}_{\boldsymbol{\alpha}} + \tilde{\delta}\boldsymbol{\varepsilon}\cdot\boldsymbol{F}_{\boldsymbol{\varepsilon}} + \tilde{\delta}\boldsymbol{\kappa}\cdot\boldsymbol{F}_{\boldsymbol{\kappa}} + \left(\boldsymbol{Q}.\delta\partial_{\xi_1}\overline{\boldsymbol{\kappa}}\right)\cdot\boldsymbol{F}_{\partial_{\xi_1}\boldsymbol{\kappa}} \\ &+ \left(\boldsymbol{Q}.\delta\partial^2_{\xi_1}\overline{\boldsymbol{\kappa}}\right)\cdot\boldsymbol{F}_{\partial^2_{\xi_1}\boldsymbol{\kappa}} + \delta p.F_p + \delta\partial_{\xi_1}p.F_{\partial_{\xi_1}p} \Big)\mathrm{d}\xi_1 . \end{aligned} \tag{68}$$

The equation above can be written in a matrix form as:

$$\delta \mathrm{W}_{\mathrm{inertial}} = \int_0^L \delta\boldsymbol{\Phi}^T\boldsymbol{B}_2^T\boldsymbol{B}_3\boldsymbol{\mathcal{N}}_{\mathrm{inertial}}\mathrm{d}\xi_1 . \tag{69}$$

The concatenated inertial force vector $\boldsymbol{\mathcal{N}}_{\mathrm{inertial}}$ with its components defined in Appendix A.3.2 is

$$\boldsymbol{\mathcal{N}}_{\mathrm{inertial}} = \left[\boldsymbol{F}_{\boldsymbol{\varphi}}; \boldsymbol{F}_{\boldsymbol{\alpha}}; \boldsymbol{F}_{\boldsymbol{\varepsilon}}; \boldsymbol{F}_{\boldsymbol{\kappa}}; \boldsymbol{F}_{\partial_{\xi_1}\boldsymbol{\kappa}}; \boldsymbol{F}_{\partial^2_{\xi_1}\boldsymbol{\kappa}}; F_p; F_{\partial_{\xi_1}p}\right]. \tag{70}$$

4.4. Virtual work principle revisited

We restate the weak form of governing differential Eq. (52) for the beam kinematics at hand by using the expression of virtual strain energy in Eq. (58), virtual work due to external forces in Eq. (64) and (66) and the virtual work contribution due to inertial work obtained in Eq. (69) as

$$\begin{aligned}G(\boldsymbol{\Phi}, \delta\boldsymbol{\Phi}) = &\int_0^L \delta\boldsymbol{\Phi}^T\boldsymbol{B}_2^T\left(\boldsymbol{B}_1^T\boldsymbol{\mathcal{N}}_{\mathrm{int}} + \boldsymbol{B}_3\boldsymbol{\mathcal{N}}_{\mathrm{inertial}} - \boldsymbol{B}_3\boldsymbol{\mathcal{N}}_{\mathrm{ext}}\right)\mathrm{d}\xi_1 \\ &- \delta \mathrm{W}^{\mathrm{st}}_{\mathrm{ext}}|_{B(0)\cup B(L)} = 0. \end{aligned} \tag{71}$$

5. Strong form of governing differential equation

We can obtain the strong form (governing differential equations) from the weak form using the equivalence principle. The strong form essentially represents the local balance laws governing the deformation of the beam. The analysis carried to obtain the strong form can be summarized in two steps. Firstly, we transform the weak form in Eq. (71) using integration by parts to obtain an equation of the form

$$G(\boldsymbol{\Phi}, \delta\boldsymbol{\Phi}) = \int_0^L \left(\delta\boldsymbol{\varphi}\cdot\boldsymbol{\mathcal{E}}_{\boldsymbol{\varphi}} + \delta\boldsymbol{\alpha}\cdot\boldsymbol{\mathcal{E}}_{\boldsymbol{\alpha}} + \delta p.E_p\right)\mathrm{d}\xi_1 + G^* = 0, \tag{72}$$

where

$$G^* = \delta \mathrm{U}^*_{\mathrm{strain}} + \delta \mathrm{W}^*_{\mathrm{inertial}} - \delta \mathrm{W}^*_{\mathrm{ext}} - \delta \mathrm{W}^{\mathrm{st}}_{\mathrm{ext}}|_{B(0)\cup B(L)} . \tag{73}$$

The terms $\delta \mathrm{U}^*_{\mathrm{strain}} + \delta \mathrm{W}^*_{\mathrm{inertial}} - \delta \mathrm{W}^*_{\mathrm{ext}}$ are the boundary terms arising as a result of carrying integration by part on the integral in Eq. (71). Since the strong form equations are local in nature, the boundary terms arising due to integration by part must be $-\delta \mathrm{W}^{\mathrm{st}}_{\mathrm{ext}}|_{B(0)\cup B(L)}$ such that no boundary term appears in the transformed equation of the form

$$G(\boldsymbol{\Phi}, \delta\boldsymbol{\Phi}) = \int_0^L \left(\delta\boldsymbol{\varphi}\cdot\boldsymbol{\mathcal{E}}_{\boldsymbol{\varphi}} + \delta\boldsymbol{\alpha}\cdot\boldsymbol{\mathcal{E}}_{\boldsymbol{\alpha}} + \delta p.E_p\right)\mathrm{d}\xi_1 = 0. \tag{74}$$

It can be proved that $G^* = 0$. The proof is detailed in the supplementary material. This result should not come as a surprise because the strong form describes local equilibrium of forces. The proof of

$G^* = 0$ also provides a check for correctness of the work discussed so far. In Eq. 74, we have

$$\boldsymbol{\mathcal{E}}_{\boldsymbol{\varphi}} = \partial_{\xi_1}\boldsymbol{n} + \boldsymbol{N}_{\boldsymbol{\varphi}} - \boldsymbol{F}_{\boldsymbol{\varphi}}; \tag{75a}$$

$$\boldsymbol{\mathcal{E}}_{\boldsymbol{\alpha}} = \partial_{\xi_1}\boldsymbol{m} + \partial_{\xi_1}\hat{\boldsymbol{\varphi}}.\boldsymbol{n} + \boldsymbol{N}_{\boldsymbol{\alpha}} - \boldsymbol{F}_{\boldsymbol{\alpha}}; \tag{75b}$$

$$E_p = \partial_{\xi_1} M_\Psi - N_p + \boldsymbol{N}_p - F_p. \tag{75c}$$

In Eq. ((75c), N_p represents the bi-shear. Here we define the reduced cross-section force, moment vector, and the bi-moment as

$$\boldsymbol{n} = \left(\left(\boldsymbol{\mathcal{N}}_{\boldsymbol{\varepsilon}} - \tilde{\partial}_{\xi_1}\boldsymbol{\mathcal{N}}_{\partial_{\xi_1}\boldsymbol{\varepsilon}}\right) + \left(\boldsymbol{F}_{\boldsymbol{\varepsilon}} - \boldsymbol{N}_{\boldsymbol{\varepsilon}}\right)\right); \tag{76a}$$

$$\begin{aligned}\boldsymbol{m} = &\left(\boldsymbol{\mathcal{N}}_{\boldsymbol{\kappa}} - \tilde{\partial}_{\xi_1}\boldsymbol{\mathcal{N}}_{\partial_{\xi_1}\boldsymbol{\kappa}} + \tilde{\partial}^2_{\xi_1}\boldsymbol{\mathcal{N}}_{\partial^2_{\xi_1}\boldsymbol{\kappa}} - \tilde{\partial}^3_{\xi_1}\boldsymbol{\mathcal{N}}_{\partial^3_{\xi_1}\boldsymbol{\kappa}}\right)\\ &+ \left(\boldsymbol{F}_{\boldsymbol{\kappa}} - \tilde{\partial}_{\xi_1}\boldsymbol{F}_{\partial_{\xi_1}\boldsymbol{\kappa}} + \tilde{\partial}^2_{\xi_1}\boldsymbol{F}_{\partial^2_{\xi_1}\boldsymbol{\kappa}}\right)\\ &- \left(\boldsymbol{N}_{\boldsymbol{\kappa}} - \tilde{\partial}_{\xi_1}\boldsymbol{N}_{\partial_{\xi_1}\boldsymbol{\kappa}} + \tilde{\partial}^2_{\xi_1}\boldsymbol{N}_{\partial^2_{\xi_1}\boldsymbol{\kappa}}\right);\end{aligned} \tag{76b}$$

$$M_\Psi = \left(\left(N_{\partial_{\xi_1}p} - \partial_{\xi_1}N_{\partial^2_{\xi_1}p}\right) + \left(F_{\partial_{\xi_1}p} - N_{\partial_{\xi_1}p}\right)\right). \tag{76c}$$

Since $G^* = 0$, the arbitrary nature of the virtual displacement field $\delta\boldsymbol{\Phi}$ leads us to conservation of linear and angular momentum and the balance laws for bi-shear and bi-moment: $\boldsymbol{\mathcal{E}}_{\boldsymbol{\varphi}} = \boldsymbol{0}_1, \boldsymbol{\mathcal{E}}_{\boldsymbol{\alpha}} = \boldsymbol{0}_1$ and $E_p = 0$, respectively. The strong form of equation described in Eq. set (75) appears similar to the governing equations discussed in Simo and Vu-Quoc (1991), except for the definition of reduced section forces and bi-moment $\boldsymbol{n}, \boldsymbol{m}$ and M_Ψ. The fact that reduced forces in Eq. (76), contains inertial and external force terms is distracting. However, the results obtained in the process of proving $G^* = 0$, helps us to simplify $\boldsymbol{n}, \boldsymbol{m}$ and M_Ψ defined above to a desirable form independent of inertial and external force terms (see the supplementary material for derivation).

$$\begin{aligned}&\boldsymbol{n} = \int_{B_0}\left(\boldsymbol{L}^{\lambda_1}_{\boldsymbol{\varepsilon}}\right)^T.\boldsymbol{P}_1 dB_0 = \int_{B_0}\boldsymbol{P}_1 dB_0;\\ &\boldsymbol{m} = \int_{B_0}\left(\boldsymbol{L}^{\lambda_1}_{\boldsymbol{\kappa}}\right)^T.\boldsymbol{P}_1 dB_0 = \int_{B_0}\boldsymbol{r}\times\boldsymbol{P}_1 dB_0;\\ &M_\Psi = \int_{B_0}\boldsymbol{L}^{\lambda_1}_{\partial_{\xi_1}p}.\boldsymbol{P}_1 dB_0.\end{aligned} \tag{77}$$

As expected, the expression of reduced section force, couple and bi-moment is independent of any external and inertial force terms. The reduced forces obtained above are identical to the respective quantities discussed in Simo and Vu-Quoc (1991).

6. Constitutive law

6.1. Saint–Venant/Kirchhoff constitutive law for small strains

In this Section, we define the multi-axial linearly elastic constitutive law considering large deformation but small strain. Recall, the expression of material form of deformation gradient tensor in Eq. (14b): $\overline{\boldsymbol{F}} = \boldsymbol{I}_3 + \overline{\boldsymbol{H}}$. The small strain assumption is imposed by assuming $\|\overline{\boldsymbol{H}}\| = O(\epsilon)$ for a small parameter $\epsilon > 0$ such that $\lim_{\epsilon\to 0}\frac{O(\epsilon)}{\epsilon} =$ constant. Keeping this in mind, we can linearize the material deformation gradient tensor about $\boldsymbol{I}_3$ such that

$$\overline{\boldsymbol{F}}_\epsilon = \boldsymbol{I}_3 + \frac{\partial\overline{\boldsymbol{F}}}{\partial\epsilon}|_{\epsilon=0}.\epsilon + O(\epsilon^2) = \boldsymbol{I}_3 + \epsilon\overline{\boldsymbol{H}} + O(\epsilon^2). \tag{78}$$

The spatial form can be obtained by linearizing $\boldsymbol{F}$ about $\boldsymbol{Q}$, or simply by left translation of $\overline{\boldsymbol{F}}_\epsilon$ as

$$\boldsymbol{F}_\epsilon = \boldsymbol{Q} + \epsilon\boldsymbol{H} + O(\epsilon^2). \tag{79}$$

It is advantageous to postulate linear isotropic constitutive law (Saint–Venant/Kirchhoff material) by relating the linear part of second PK stress tensor $\boldsymbol{S} = S_{ij}\boldsymbol{E}_i\otimes\boldsymbol{E}_j$ with the linear part of the corresponding strain conjugate: Lagrangian strain tensor (symmetric) $\boldsymbol{E} = E_{ij}\boldsymbol{E}_i\otimes\boldsymbol{E}_j$. This is because of the material nature of these quantities. We have (refer to Marsden and Hughes, 1994)

$$\boldsymbol{S} = 2G\boldsymbol{E} + \lambda\text{trace}(\boldsymbol{E}). \tag{80}$$

Here, G and $\lambda = \frac{Ev}{(1+v)(1-2v)}$ are the Lamé's constant. The quantities G and E represents shear and Young's modulus respectively. For small strain, up to order $O(\epsilon)$, it can be proved that: $\overline{\boldsymbol{P}} = \boldsymbol{S}$ and $\boldsymbol{E} = \frac{1}{2}(\overline{\boldsymbol{H}} + \overline{\boldsymbol{H}}^T) = \overline{\boldsymbol{H}}^S$ (see supplementary material for proof). This brings us to the definition of constitutive relation in terms of $\overline{\boldsymbol{P}}$ and $\overline{\boldsymbol{H}}^S$. Using Eq. (80), we have

$$\overline{\boldsymbol{P}} = 2G\overline{\boldsymbol{H}}^S + \lambda\text{trace}\left(\overline{\boldsymbol{H}}^S\right). \tag{81}$$

Using the constitutive law given by (81), we can express the material form of stress vector $\overline{\boldsymbol{P}}_i$ in terms of material form of strain vectors $\overline{\boldsymbol{\lambda}}_i$ as

$$\overline{\boldsymbol{\mathcal{P}}} = \begin{bmatrix}\overline{\boldsymbol{P}}_1\\ \overline{\boldsymbol{P}}_2\\ \overline{\boldsymbol{P}}_3\end{bmatrix} = \begin{bmatrix}\overline{\boldsymbol{C}}_{11} & \overline{\boldsymbol{C}}_{12} & \overline{\boldsymbol{C}}_{13}\\ \overline{\boldsymbol{C}}_{21} & \overline{\boldsymbol{C}}_{22} & \overline{\boldsymbol{C}}_{23}\\ \overline{\boldsymbol{C}}_{31} & \overline{\boldsymbol{C}}_{32} & \overline{\boldsymbol{C}}_{33}\end{bmatrix}\begin{bmatrix}\overline{\boldsymbol{\lambda}}_1\\ \overline{\boldsymbol{\lambda}}_2\\ \overline{\boldsymbol{\lambda}}_3\end{bmatrix} = \overline{\boldsymbol{C}}.\overline{\boldsymbol{\mathcal{L}}}. \tag{82}$$

The matrices $\overline{\boldsymbol{C}}_{ij}$ are constant material matrix that is defined in Appendix (137). In spatial form, the stress vectors can be related to the spatial strain vectors as

$$\boldsymbol{\mathcal{P}} = \boldsymbol{C}.\boldsymbol{\mathcal{L}}, \text{where } \boldsymbol{C} = \boldsymbol{Q}_3.\overline{\boldsymbol{C}}.\boldsymbol{Q}_3^T. \tag{83}$$

6.2. Reduced constitutive law

The goal is to obtain a linear relationship between the internal force vector $\overline{\boldsymbol{\mathcal{N}}}_{\text{int}}$ with the vector $\overline{\boldsymbol{\epsilon}}$. We ignore terms of the order $O(\epsilon^2)$ in the expression of $\overline{\boldsymbol{\lambda}}_i$. To start with, we make use of the two following observations to redefine the internal force vector for first order strain:

First, we realize that except for $\overline{\boldsymbol{L}}^{\lambda_i}_{\boldsymbol{\kappa}}$, all the other $\overline{\boldsymbol{L}}^{\lambda_i}_{(.)}$ are independent of any strain measurements. Realizing $\overline{\boldsymbol{P}}_1 \longrightarrow O(\epsilon)$, we have

$$\left(\int_{B_0}\overline{\boldsymbol{L}}^{\lambda_i}_{\boldsymbol{\kappa}}.\overline{\boldsymbol{P}}_1 dB_0\right)_\epsilon = \epsilon.\int_{B_0}\hat{\overline{\boldsymbol{r}}}^T_1.\overline{\boldsymbol{P}}_1 dB_0 + O(\epsilon^2). \tag{84}$$

Therefore, from here on $\overline{\boldsymbol{L}}^{\lambda_i}_{\boldsymbol{\kappa}} = \hat{\overline{\boldsymbol{r}}}^T_1$. Secondly, we note that the $\boldsymbol{M}$-matrix are of order $O(\epsilon)$. Therefore,

$$\int_{B_0}\overline{\boldsymbol{M}}^{\lambda_1}_{(.)}.\boldsymbol{P}_1 dB_0 \longrightarrow O(\epsilon^2). \tag{85}$$

Using Eqs. (84) and (85), we redefine the material form of reduced forces by ignoring higher-order terms as: $\overline{\boldsymbol{\mathcal{N}}}_{\text{int}} = \int_{B_0}\overline{\boldsymbol{L}}^T.\overline{\boldsymbol{\mathcal{P}}} dB_0$, where $\overline{\boldsymbol{L}}$ is defined in Eq. (22) with $\overline{\boldsymbol{L}}^{\lambda_i}_{\boldsymbol{\kappa}} = \hat{\overline{\boldsymbol{r}}}^T_1$. Using Eq. (82) and the relation given in Eq. (18) we get:

$$\overline{\boldsymbol{\mathcal{N}}}_{\text{int}} = \int_{B_0}\overline{\boldsymbol{L}}^T.\overline{\boldsymbol{C}}.\overline{\boldsymbol{\mathcal{L}}} dB_0 = \int_{B_0}\overline{\boldsymbol{L}}^T.\overline{\boldsymbol{C}}.\overline{\boldsymbol{L}}.\overline{\boldsymbol{\epsilon}} dB_0 = \left(\int_{B_0}\overline{\boldsymbol{L}}^T.\overline{\boldsymbol{C}}.\overline{\boldsymbol{L}} dB_0\right).\overline{\boldsymbol{\epsilon}} = \overline{\mathfrak{C}}.\overline{\boldsymbol{\epsilon}}. \tag{86}$$

The elements of the matrix $\overline{\mathfrak{C}}$ can be obtained from Eq. (86) by substituting the expressions of $\boldsymbol{L}$-Matrix and $\overline{\boldsymbol{C}}$ defined in Appendices A.1 and A.4. The symmetric matrix $\overline{\mathfrak{C}}$ relates the reduced force vectors with the finite strains and their derivatives, the expanded form of which is given in Appendix A.4. The spatial form can be written as $\mathfrak{C} = \boldsymbol{\Lambda}.\overline{\mathfrak{C}}.\boldsymbol{\Lambda}^T$. The elaborate expression of the matrices associated with the constitutive law is detailed in the supplementary material.

7. Linearization and numerical formulation for static case

In this Section, we consider the numerical formulation of the beam discussed in this paper for static case assuming a linear elastic small strain constitutive law discussed in Section 6. We assume displacement prescribed boundary condition. For these assumed conditions, the weak form obtained in Eq. (71) becomes

$$G(\boldsymbol{\Phi},\delta\boldsymbol{\Phi}) = \delta \mathrm{U}_{\mathrm{strain}} - \delta \mathrm{W}_{\mathrm{ext}} = \int_0^L \delta\boldsymbol{\Phi}^T \boldsymbol{B}_2^T \boldsymbol{B}_1^T \boldsymbol{\mathcal{N}}_{\mathrm{int}} \mathrm{d}\xi_1 - \int_0^L \delta\boldsymbol{\Phi}^T \boldsymbol{B}_2^T \boldsymbol{B}_3 \boldsymbol{\mathcal{N}}_{\mathrm{ext}} \mathrm{d}\xi_1 = 0. \tag{87}$$

7.1. Consistent linearization

7.1.1. Linearization of weak form

The linearized part of the functional $G(\boldsymbol{\Phi},\delta\boldsymbol{\Phi})$ at the configuration $\boldsymbol{\Phi}^{\#}$ in the direction of $\Delta\boldsymbol{\Phi}$, such that $\boldsymbol{\Phi}_\epsilon = \boldsymbol{\Phi}^{\#} + \epsilon\Delta\boldsymbol{\Phi}$, is given as

$$L[G(\boldsymbol{\Phi},\delta\boldsymbol{\Phi})]_{(\boldsymbol{\Phi}^{\#},\Delta\boldsymbol{\Phi})} = G(\boldsymbol{\Phi}^{\#},\delta\boldsymbol{\Phi}) + \mathrm{D}G(\boldsymbol{\Phi}^{\#},\delta\boldsymbol{\Phi}).\Delta\boldsymbol{\Phi}. \tag{88}$$

In the equation above, $\mathrm{D}G(\boldsymbol{\Phi}^{\#},\delta\boldsymbol{\Phi}).\Delta\boldsymbol{\Phi}$ is the Frećhet differential defined by directional derivative formula as

$$\mathrm{D}G(\boldsymbol{\Phi}^{\#},\delta\boldsymbol{\Phi}).\Delta\boldsymbol{\Phi} = \frac{\mathrm{d}G(\boldsymbol{\Phi}_\epsilon,\delta\boldsymbol{\Phi})}{\mathrm{d}\epsilon}|_{\epsilon=0}. \tag{89}$$

In Eq. (88), the term $G(\boldsymbol{\Phi}^{\#},\delta\boldsymbol{\Phi})$ is responsible for the unbalanced forces, whereas the term $\mathrm{D}G(\boldsymbol{\Phi}^{\#},\delta\boldsymbol{\Phi}).\Delta\boldsymbol{\Phi}$ (linear in $\Delta\boldsymbol{\Phi}$) yields the tangent stiffness matrix. For simplicity, we assume that $\boldsymbol{\Phi}^{\#} = \boldsymbol{\Phi}$ and define the linear increment in the weak form ΔG as

$$\mathrm{D}G(\boldsymbol{\Phi}^{\#},\delta\boldsymbol{\Phi}).\Delta\boldsymbol{\Phi} = \Delta G(\boldsymbol{\Phi}^{\#},\delta\boldsymbol{\Phi}) = \Delta G(\boldsymbol{\Phi},\delta\boldsymbol{\Phi})|_{\boldsymbol{\Phi}=\boldsymbol{\Phi}^{\#}} = \Delta G(\boldsymbol{\Phi},\delta\boldsymbol{\Phi}) = \Delta\delta \mathrm{U}_{\mathrm{strain}} - \Delta\delta \mathrm{W}_{\mathrm{ext}}. \tag{90}$$

7.1.2. Linearization of virtual strain energy

The expression of virtual strain energy can be written using Eq. (58) as

$$\delta \mathrm{U}_{\mathrm{strain}} = \int_0^L \delta\boldsymbol{\Phi}^T \boldsymbol{B}_2^T \boldsymbol{B}_1^T \boldsymbol{\mathcal{N}}_{\mathrm{int}} \mathrm{d}\xi_1 = \int_0^L \delta\boldsymbol{\Phi}^T \boldsymbol{B}_2^T \boldsymbol{B}_1^T \boldsymbol{\Lambda} \overline{\boldsymbol{\mathcal{N}}}_{\mathrm{int}} \mathrm{d}\xi_1. \tag{91}$$

Thus, the linearized virtual strain energy is obtained as

$$\Delta\delta \mathrm{U}_{\mathrm{strain}} = \overbrace{\int_0^L \delta\boldsymbol{\Phi}^T \boldsymbol{B}_2^T \boldsymbol{B}_1^T \boldsymbol{\Lambda} \Delta\overline{\boldsymbol{\mathcal{N}}}_{\mathrm{int}} \mathrm{d}\xi_1}^{\Delta\delta \mathrm{U}_{\mathrm{strain1}}} + \overbrace{\int_0^L \delta\boldsymbol{\Phi}^T \boldsymbol{B}_2^T \boldsymbol{B}_1^T \Delta\boldsymbol{\Lambda} \overline{\boldsymbol{\mathcal{N}}}_{\mathrm{int}} \mathrm{d}\xi_1}^{\Delta\delta \mathrm{U}_{\mathrm{strain2}}} + \overbrace{\int_0^L \delta\boldsymbol{\Phi}^T \boldsymbol{B}_2^T \Delta\boldsymbol{B}_1^T \boldsymbol{\Lambda} \overline{\boldsymbol{\mathcal{N}}}_{\mathrm{int}} \mathrm{d}\xi_1}^{\Delta\delta \mathrm{U}_{\mathrm{strain3}}}. \tag{92}$$

Since the process of linearization is similar to the variation, using Eq. (40), we get $\Delta\overline{\boldsymbol{\epsilon}} = \boldsymbol{\Lambda}^T \boldsymbol{B}_1 \boldsymbol{B}_2 \Delta\boldsymbol{\Phi}$. Using the constitutive law given in Eq. (86), we can obtain the linear increment in the material internal force vector

$$\Delta\overline{\boldsymbol{\mathcal{N}}}_{\mathrm{int}} = \overline{\mathfrak{C}} \Delta\overline{\boldsymbol{\epsilon}} = \overline{\mathfrak{C}} \boldsymbol{\Lambda}^T \boldsymbol{B}_1 \boldsymbol{B}_2 \Delta\boldsymbol{\Phi}. \tag{93}$$

Thus,

$$\Delta\delta \mathrm{U}_{\mathrm{strain1}} = \mathrm{D}\delta \mathrm{U}_{\mathrm{strain1}}(\boldsymbol{\Phi},\delta\boldsymbol{\Phi}).\Delta\boldsymbol{\Phi} = \int_0^L \delta\boldsymbol{\Phi}^T \boldsymbol{B}_2^T \boldsymbol{B}_1^T \mathfrak{C} \boldsymbol{B}_1 \boldsymbol{B}_2 \Delta\boldsymbol{\Phi} \mathrm{d}\xi_1. \tag{94}$$

Similarly, we have $\Delta\boldsymbol{Q} = \Delta\hat{\boldsymbol{\alpha}}.\boldsymbol{Q}$, using which, we get

$$\Delta\boldsymbol{\Lambda}.\overline{\boldsymbol{\mathcal{N}}}_{\mathrm{int}} = \left[\Delta\hat{\boldsymbol{\alpha}}.\boldsymbol{\mathcal{N}}_{\boldsymbol{\varepsilon}}; \Delta\hat{\boldsymbol{\alpha}}.\boldsymbol{\mathcal{N}}_{\partial_{\xi_1}\boldsymbol{\varepsilon}}; \Delta\hat{\boldsymbol{\alpha}}.\boldsymbol{\mathcal{N}}_{\boldsymbol{\kappa}}; \Delta\hat{\boldsymbol{\alpha}}.\boldsymbol{\mathcal{N}}_{\partial_{\xi_1}\boldsymbol{\kappa}}; \Delta\hat{\boldsymbol{\alpha}}.\boldsymbol{\mathcal{N}}_{\partial^2_{\xi_1}\boldsymbol{\kappa}}; \Delta\hat{\boldsymbol{\alpha}}.\boldsymbol{\mathcal{N}}_{\partial^3_{\xi_1}\boldsymbol{\kappa}}; 0; 0; 0\right] = \boldsymbol{B}_4 \Delta\boldsymbol{\Theta} = \boldsymbol{B}_4 \boldsymbol{B}_2 \Delta\boldsymbol{\Phi}. \tag{95}$$

Appendix A.2.4 gives expression of the matrix $\boldsymbol{B}_4$. Thus,

$$\Delta\delta \mathrm{U}_{\mathrm{strain2}} = \mathrm{D}\delta \mathrm{U}_{\mathrm{strain2}}(\boldsymbol{\Phi},\delta\boldsymbol{\Phi}).\Delta\boldsymbol{\Phi} = \int_0^L \delta\boldsymbol{\Phi}^T \boldsymbol{B}_2^T \boldsymbol{B}_1^T \boldsymbol{B}_4 \boldsymbol{B}_2 \Delta\boldsymbol{\Phi} \mathrm{d}\xi_1. \tag{96}$$

To derive the expression of $\Delta\delta \mathrm{U}_{\mathrm{strain3}}$, we use the expression of $\boldsymbol{B}_1^T$ in Eq. (123) and obtain

$$\Delta\boldsymbol{B}_1^T \boldsymbol{\mathcal{N}}_{\mathrm{int}} = \boldsymbol{B}_5 \Delta\boldsymbol{\Theta} = \boldsymbol{B}_5 \boldsymbol{B}_2 \Delta\boldsymbol{\Phi}. \tag{97}$$

Appendix A.2.5 defines the matrix $\boldsymbol{B}_5$. Therefore, we have

$$\Delta\delta \mathrm{U}_{\mathrm{strain3}} = \mathrm{D}\delta \mathrm{U}_{\mathrm{strain3}}(\boldsymbol{\Phi},\delta\boldsymbol{\Phi}).\Delta\boldsymbol{\Phi} = \int_0^L \delta\boldsymbol{\Phi}^T \boldsymbol{B}_2^T \boldsymbol{B}_5 \boldsymbol{B}_2 \Delta\boldsymbol{\Phi} \mathrm{d}\xi_1. \tag{98}$$

Finally, if $\boldsymbol{B}_6 = \boldsymbol{B}_5 + \boldsymbol{B}_1^T.\boldsymbol{B}_4$, we define

$$\Delta\delta \mathrm{U}_{\mathrm{strain23}} = \Delta\delta \mathrm{U}_{\mathrm{strain2}} + \Delta\delta \mathrm{U}_{\mathrm{strain3}} = \mathrm{D}\delta \mathrm{U}_{\mathrm{strain23}}(\boldsymbol{\Phi},\delta\boldsymbol{\Phi}).\Delta\boldsymbol{\Phi} = \int_0^L \delta\boldsymbol{\Phi}^T \boldsymbol{B}_2^T \boldsymbol{B}_6 \boldsymbol{B}_2 \Delta\boldsymbol{\Phi} \mathrm{d}\xi_1. \tag{99}$$

The term $\Delta\delta \mathrm{U}_{\mathrm{strain1}}$ leads to the symmetric material stiffness matrix whereas, the term $\Delta\delta \mathrm{U}_{\mathrm{strain23}}$ yields geometric stiffness matrix (not necessarily symmetric).

7.1.3. Linearization of virtual external work done

From the expression of virtual external work, we have

$$\Delta\delta \mathrm{W}_{\mathrm{ext}} = \overbrace{\int_0^L \delta\boldsymbol{\Phi}^T \boldsymbol{B}_2^T \Delta\boldsymbol{B}_3 \boldsymbol{\mathcal{N}}_{\mathrm{ext}} \mathrm{d}\xi_1}^{\Delta\delta \mathrm{W}_{\mathrm{ext1}}} + \overbrace{\int_0^L \delta\boldsymbol{\Phi}^T \boldsymbol{B}_2^T \boldsymbol{B}_3 \Delta\boldsymbol{\mathcal{N}}_{\mathrm{ext}} \mathrm{d}\xi_1}^{\Delta\delta \mathrm{W}_{\mathrm{ext2}}}. \tag{100}$$

The term $\Delta\delta \mathrm{W}_{\mathrm{ext1}}$ arises due to geometric dependence of $\Delta\delta \mathrm{W}_{\mathrm{ext}}$; whereas the term $\Delta\delta \mathrm{W}_{\mathrm{ext2}}$ is due to non-conservative nature of the external forces. We can represent $\Delta\boldsymbol{B}_3\boldsymbol{\mathcal{N}}_{\mathrm{ext}}$ and $\boldsymbol{B}_3\Delta\boldsymbol{\mathcal{N}}_{\mathrm{ext}}$ in a more desirable form,

$$\begin{aligned} \Delta\boldsymbol{B}_3 \boldsymbol{\mathcal{N}}_{\mathrm{ext}} &= \boldsymbol{B}_7 \Delta\boldsymbol{\Theta} = \boldsymbol{B}_7 \boldsymbol{B}_2 \Delta\boldsymbol{\Phi}; \\ \boldsymbol{B}_3 \Delta\boldsymbol{\mathcal{N}}_{\mathrm{ext}} &= \boldsymbol{B}_8 \Delta\boldsymbol{\Theta} = \boldsymbol{B}_8 \boldsymbol{B}_2 \Delta\boldsymbol{\Phi}. \end{aligned} \tag{101}$$

Appendix A.2.6 gives the matrix $\boldsymbol{B}_7$. The matrix $\boldsymbol{B}_8$ depends on the characteristic of external loading (for example: follower load, pressure load, etc) and is determined on a case by case basis. The supplementary material contains a discussion on handling the point load and it details the $\boldsymbol{B}_8$ matrix for such loading.

7.2. Discretization and Galerkin form of equilibrium equation

We discretize the domain using N_e elements. Any element e consist of N_{en} number of nodes and has length $L_e = \xi^e_{1b} - \xi^e_{1a}$, where, ξ^e_{1b} and ξ^e_{1a} are the arc-length of the first and last node of the element e, such that $\xi^e_{1b} > \xi^e_{1a}$ and $\xi^e_1 \in [\xi^e_{1a}, \xi^e_{1b}]$. We approximate the admissible incremental displacement field $\Delta\boldsymbol{\Phi}$ by a finite dimensional subspace that is subset of the variationally admissible tangent space. The incremental displacement field $(\Delta\boldsymbol{\varphi}^e, \Delta\boldsymbol{\alpha}^e, \Delta p^e)$ restricted to element e can then be interpolated by means of shape functions as

$$\Delta\boldsymbol{\varphi}^e = \sum_{I=1}^{N_{en}} N_I \Delta\boldsymbol{\varphi}^e_I; \quad \Delta\boldsymbol{\alpha}^e = \sum_{I=1}^{N_{en}} N_I \Delta\boldsymbol{\alpha}^e_I; \quad \Delta p^e = \sum_{I=1}^{N_{en}} N_I \Delta p^e_I. \tag{102}$$

Here, $\Delta\boldsymbol{\varphi}^e_I, \Delta\boldsymbol{\alpha}^e_I$ and Δp^e_I represents the nodal incremental displacement, vorticity and warping amplitude at node I of element e respectively; N_I is the shape-function associated with I^{th} node.

7.2.1. Unbalanced force vector

We first obtain the *nodal internal load vector* $\boldsymbol{f}^e_{\text{int}I}$. The approximated virtual strain energy can be written as

$$\delta \mathrm{U}^h_{\text{strain}} = \sum_{e=1}^{N_e}\sum_{I=1}^{N_{en}} \delta\boldsymbol{\Phi}_I^{eT} \overbrace{\left(\int_{\xi^e_{1a}}^{\xi^e_{1b}} \mathbb{B}_I^T \boldsymbol{B}_1^{eT} \mathcal{N}^e_{\text{int}} \mathrm{d}\xi_1\right)}^{\boldsymbol{f}^e_{\text{int}I}} = \sum_{e=1}^{N_e}\sum_{I=1}^{N_{en}} \delta\boldsymbol{\Phi}_I^{eT} \boldsymbol{f}^e_{\text{int}I}. \tag{103}$$

The matrix $\mathbb{B}_I$, defined in Appendix A.2.7, consists of the shape-functions and its derivatives. The superscript e on any quantity represents the restriction of that quantity on element e.

In order to define incremental load steps necessary for numerical formulation, we first define the load coefficient $x \in [0,1]$ with $\mathcal{N}_{\text{ext}}(x) = x\mathcal{N}_{\text{ext0}}$, such that

$$\delta \mathrm{W}_{\text{ext}}(x) = x\delta \mathrm{W}_{\text{ext0}} = x\int_0^L \delta\boldsymbol{\Phi}^T \boldsymbol{B}_2^T \boldsymbol{B}_3 \mathcal{N}_{\text{ext0}} \mathrm{d}\xi_1. \tag{104}$$

The approximated virtual external work is obtained as

$$\delta \mathrm{W}^h_{\text{ext0}} = \sum_{e=1}^{N_e}\sum_{I=1}^{N_{en}} \delta\boldsymbol{\Phi}_I^{eT} \overbrace{\left(\int_{\xi^e_{1a}}^{\xi^e_{1b}} \mathbb{B}_I^T \boldsymbol{B}_3 \mathcal{N}^e_{\text{ext0}} \mathrm{d}\xi_1\right)}^{\boldsymbol{f}^e_{\text{ext0}I}} = \sum_{e=1}^{N_e}\sum_{I=1}^{N_{en}} \delta\boldsymbol{\Phi}_I^{eT} \boldsymbol{f}^e_{\text{ext0}I}.$$
$$\delta \mathrm{W}^h_{\text{ext}}(x) = \sum_{e=1}^{N_e}\sum_{I=1}^{N_{en}} \delta\boldsymbol{\Phi}_I^{eT} \boldsymbol{f}^e_{\text{ext}I}(x); \text{ where } \boldsymbol{f}^e_{\text{ext}I}(x) = x\boldsymbol{f}^e_{\text{ext0}I}. \tag{105}$$

Refer to Appendices A.3.4 and A.3.5 for the expression of internal and external force vectors: $\boldsymbol{f}^e_{\text{int}I}$ and $\boldsymbol{f}^e_{\text{ext}I}(x)$. The unbalanced force vector associated with element e at node I is defined as

$$\boldsymbol{F}^e_I(\boldsymbol{\Phi}^e, x) = \boldsymbol{f}^e_{\text{ext}I}(\boldsymbol{\Phi}^e, x) - \boldsymbol{f}^e_{\text{int}I}(\boldsymbol{\Phi}^e). \tag{106}$$

7.2.2. Element tangent stiffness

The approximated form of linearized virtual strain energy obtained in Section 7.1.2 is given by:

$$\Delta\delta \mathrm{U}^h_{\text{strain}} = \sum_{e=1}^{N_e}\sum_{I=1}^{N_{en}}\sum_{J=1}^{N_{en}} \delta\boldsymbol{\Phi}_I^{eT} \left(\underbrace{\overbrace{\int_{\xi^e_{1a}}^{\xi^e_{1b}} \mathbb{B}_I^T \boldsymbol{B}_1^{eT} \mathfrak{C} \boldsymbol{B}_1^e \mathbb{B}_J \,\mathrm{d}\xi_1}^{\boldsymbol{K}^e_{\text{mat}IJ}} + \overbrace{\int_{\xi^e_{1a}}^{\xi^e_{1b}} \mathbb{B}_I^T \boldsymbol{B}_6^e \mathbb{B}_J \,\mathrm{d}\xi_1}^{\boldsymbol{K}^e_{gIJ}}}_{\boldsymbol{K}^e_{\text{int}IJ}}\right) \Delta\boldsymbol{\Phi}^e_J. \tag{107}$$

Here, the element tangential stiffness matrix corresponding to internal loads $\boldsymbol{K}^e_{\text{int}IJ} = \boldsymbol{K}^e_{\text{m}IJ} + \boldsymbol{K}^e_{gIJ}$ consist of a symmetric material part $\boldsymbol{K}^e_{mIJ}$ and a geometric part $\boldsymbol{K}^e_{gIJ}$ (not necessarily symmetric). Similarly, the contribution to stiffness matrix due to external loads can be obtained by using results in Section 7.1.3, such that the approximated linearized virtual work is obtained as

$$\Delta\delta \mathrm{W}^h_{\text{ext}}(x) = x\Delta\delta \mathrm{W}^h_{\text{ext0}} = \sum_{e=1}^{N_e}\sum_{I=1}^{N_{en}}\sum_{J=1}^{N_{en}} \delta\boldsymbol{\Phi}_I^{eT} \left(\underbrace{\overbrace{\int_{\xi^e_{1a}}^{\xi^e_{1b}} \mathbb{B}_I^T \boldsymbol{B}_7^e \mathbb{B}_J \,\mathrm{d}\xi_1}^{\boldsymbol{K}^e_{\text{ext1}IJ}} + \overbrace{\int_{\xi^e_{1a}}^{\xi^e_{1b}} \mathbb{B}_I^T \boldsymbol{B}_8^e \mathbb{B}_J \,\mathrm{d}\xi_1}^{\boldsymbol{K}^e_{\text{ext2}IJ}}}_{\boldsymbol{K}^e_{\text{ext}IJ}}\right) \Delta\boldsymbol{\Phi}^e_J. \tag{108}$$

Here, the element tangential stiffness matrix corresponding to internal loads $\boldsymbol{K}^e_{\text{ext}IJ} = \boldsymbol{K}^e_{\text{ext1}IJ} + \boldsymbol{K}^e_{\text{ext2}IJ}$ consist of two parts: the matrix $\boldsymbol{K}^e_{\text{ext1}IJ}$ gives contribution due to dependence of external work on the configuration of the system, assuming the force vectors are conservative; whereas, the matrix $\boldsymbol{K}^e_{\text{ext2}IJ}$ is due to non-conservative nature of the external forces. The element stiffness matrix is given as

$$\begin{aligned}\boldsymbol{K}^e_{IJ}(\boldsymbol{\Phi}^e, x) &= \boldsymbol{K}^e_{\text{int}IJ}(\boldsymbol{\Phi}^e) - \boldsymbol{K}^e_{\text{ext}IJ}(\boldsymbol{\Phi}^e, x) \\ &= \boldsymbol{K}^e_{\text{m}IJ}(\boldsymbol{\Phi}^e) + \boldsymbol{K}^e_{gIJ}(\boldsymbol{\Phi}^e) - \boldsymbol{K}^e_{\text{ext1}IJ}(\boldsymbol{\Phi}^e, x) - \boldsymbol{K}^e_{\text{ext2}IJ}(\boldsymbol{\Phi}^e, x).\end{aligned} \tag{109}$$

7.2.3. Matrix form of linearized equation of motion and iterative solution

The unbalanced force vector and the element tangent stiffness can be assembled using assembly operator $\mathbb{A}$ such that the global stiffness and global unbalanced force is obtained as

$$\begin{aligned}&\boldsymbol{K} = \mathbb{A}\left(\boldsymbol{K}^e_{IJ}\right); \\ &\boldsymbol{F}(\boldsymbol{\Phi}, x) = \mathbb{A}\left(\boldsymbol{F}^e_I\right) = x\mathbb{A}\left(\boldsymbol{f}^e_{\text{ext0}I}(\boldsymbol{\Phi}^e)\right) - \mathbb{A}\left(\boldsymbol{f}^e_{\text{int}I}(\boldsymbol{\Phi}^e)\right) = x\boldsymbol{f}_{\text{ext0}}(\boldsymbol{\Phi}) - \boldsymbol{f}_{\text{int}}(\boldsymbol{\Phi}).\end{aligned} \tag{110}$$

We use standard Newton Raphson's iterative procedure. We divide the external loading into n load steps. Let $\boldsymbol{\Phi}_n$ represents the discretized form of degrees of freedom vector at load step n, such that $\Delta\boldsymbol{\Phi}_n = \boldsymbol{\Phi}_{n+1} - \boldsymbol{\Phi}_n$. At equilibrium state corresponding to load step n (converged state), the unbalanced force vanishes, i.e., $\boldsymbol{F}(\boldsymbol{\Phi}_n, x_n) = \boldsymbol{0}$. Provided the n^{th} load step has converged, we aim to find $\Delta\boldsymbol{\Phi}_n$, such that $\boldsymbol{F}(\boldsymbol{\Phi}_{n+1}, x_{n+1}) = \boldsymbol{0}$. At i^{th} iteration, we can linearize the equation $\boldsymbol{F}(\boldsymbol{\Phi}_{n+1}, x_{n+1}) = \boldsymbol{0}$ about $\boldsymbol{F}(\boldsymbol{\Phi}^i_{n+1}, x^i_{n+1})$, such that $\boldsymbol{\Phi}^{i+1}_{n+1} = \boldsymbol{\Phi}^i_{n+1} + \Delta\boldsymbol{\Phi}^{i+1}_n$ and $x^i_{n+1} = x_n$ as

$$\begin{aligned}\boldsymbol{F}(\boldsymbol{\Phi}^{i+1}_{n+1}, x_{n+1}) = \boldsymbol{F}(\boldsymbol{\Phi}^i_{n+1}, x_n) &+ \frac{\partial \boldsymbol{F}}{\partial \boldsymbol{\Phi}}|_{(\boldsymbol{\Phi}^i_{n+1}, x_n)}.\Delta\boldsymbol{\Phi}^{i+1}_n \\ &+ \frac{\partial \boldsymbol{F}}{\partial x}|_{(\boldsymbol{\Phi}^i_{n+1}, x_n)}.(x_{n+1} - x_n) = \boldsymbol{0}.\end{aligned} \tag{111}$$

We define the global tangent stiffness matrix (obtained in (110)) and obtain the following results from Eq. (110),

$$\begin{aligned}&\boldsymbol{F}(\boldsymbol{\Phi}^i_{n+1}, x_n) = x_n\boldsymbol{f}_{\text{ext0}}(\boldsymbol{\Phi}^i_{n+1}) - \boldsymbol{f}_{\text{int}}(\boldsymbol{\Phi}^i_{n+1}); \\ &\boldsymbol{K}(\boldsymbol{\Phi}^i_{n+1}, x_n) = -\frac{\partial \boldsymbol{F}(\boldsymbol{\Phi}_{n+1}, x_{n+1})}{\partial \boldsymbol{\Phi}_{n+1}}|_{(\boldsymbol{\Phi}^i_{n+1}, x_n)}; \\ &\boldsymbol{f}_{\text{ext0}}(\boldsymbol{\Phi}^i_{n+1}) = \frac{\partial \boldsymbol{F}(\boldsymbol{\Phi}_{n+1}, x_{n+1})}{\partial x_{n+1}}|_{(\boldsymbol{\Phi}^i_{n+1}, x_n)}.\end{aligned} \tag{112}$$

Substituting the results obtained above into the Eq. (111), we get

$$\boldsymbol{K}(\boldsymbol{\Phi}^i_{n+1}, x_n).\Delta\boldsymbol{\Phi}^{i+1}_n = x_{n+1}\boldsymbol{f}_{\text{ext0}}(\boldsymbol{\Phi}^i_{n+1}) - \boldsymbol{f}_{\text{int}}(\boldsymbol{\Phi}^i_{n+1}) = \boldsymbol{F}(\boldsymbol{\Phi}^i_{n+1}, x_{n+1}). \tag{113}$$

7.3. Updating the axial strain vector, curvature vector and their derivatives

7.3.1. Updating configuration

Solving Eq. (113), yields an incremental change in configuration space due to deformation, say $\Delta\boldsymbol{\Phi} = \{\Delta\boldsymbol{\varphi}, \Delta\boldsymbol{\alpha}, \Delta p\}$. The derivatives of these increments can be obtained by using the approximation in Eq. (102) such that $\partial^n_{\xi_1}\Delta\boldsymbol{\Phi}^e(\xi^e_1) = \partial^n_{\xi_1}N_I(\xi^e_1).\Delta\boldsymbol{\Phi}^e$, $\partial^n_{\xi_1}\Delta\boldsymbol{\alpha}^e(\xi^e_1) = \partial^n_{\xi_1}N_I(\xi^e_1).\Delta\boldsymbol{\alpha}^e_I$ and $\partial^n_{\xi_1}\Delta p^e(\xi^e_1) = \partial^n_{\xi_1}N_I(\xi^e_1).\Delta p^e_I$. Let the *initial* and *final* configuration be given as $\boldsymbol{\Phi}_{\text{i}} = \{\boldsymbol{\varphi}_{\text{i}}, \boldsymbol{Q}_{\text{i}}, p_{\text{i}}\}$ and $\boldsymbol{\Phi}_{\text{f}} = \{\boldsymbol{\varphi}_{\text{f}}, \boldsymbol{Q}_{\text{f}}, p_{\text{f}}\}$, such that

$$\boldsymbol{\varphi}_{\text{f}} = \boldsymbol{\varphi}_{\text{i}} + \Delta\boldsymbol{\varphi}; \quad \partial^n_{\xi_1}\boldsymbol{\varphi}_{\text{f}} = \partial^n_{\xi_1}\boldsymbol{\varphi}_{\text{i}} + \partial^n_{\xi_1}\Delta\boldsymbol{\varphi}; \tag{114a}$$

$$p_{\text{f}} = p_{\text{i}} + \Delta p; \quad \partial^n_{\xi_1}p_{\text{f}} = \partial^n_{\xi_1}p_{\text{i}} + \partial^n_{\xi_1}\Delta p; \tag{114b}$$

$$\boldsymbol{Q}_{\text{f}} = \exp(\Delta\hat{\boldsymbol{\alpha}}).\boldsymbol{Q}_{\text{i}} = \boldsymbol{Q}_{+}.\boldsymbol{Q}_{\text{i}} \text{ where, } \boldsymbol{Q}_{+} = \exp(\Delta\hat{\boldsymbol{\alpha}}). \tag{114c}$$

From the expressions of $\boldsymbol{B}_i$ with $i \in \{1,3,4,5,6\}$ in appendix A.2, the following quantities other than the configuration space itself need to be updated: $\partial_{\xi_1}\boldsymbol{\varphi}$, $\partial^2_{\xi_1}\boldsymbol{\varphi}$, $\hat{\boldsymbol{\kappa}}$, $\partial_{\xi_1}\hat{\boldsymbol{\kappa}}$, and $\partial^2_{\xi_1}\hat{\boldsymbol{\kappa}}$ and the finite strain quantities constituting $\overline{\boldsymbol{\epsilon}}$. Once we update $\overline{\boldsymbol{\epsilon}}$, we can obtain the material (and then spatial) form of internal force vector, eventually getting the updates $\boldsymbol{B}_i$ with $i \in \{4,5,6\}$.

Remark 2. We note that in Eq. (114c), we use multiplicative updating rule for the rotation tensor. The incremental rotation $\boldsymbol{Q}_{+} = \exp(\Delta\hat{\boldsymbol{\alpha}})$ becomes singular when $\|\Delta\boldsymbol{\alpha}\| = 2n\pi$ for $n = 1, 2, 3, \ldots$. Refer to Ibrahimbegović et al. (1995) for a rescaling

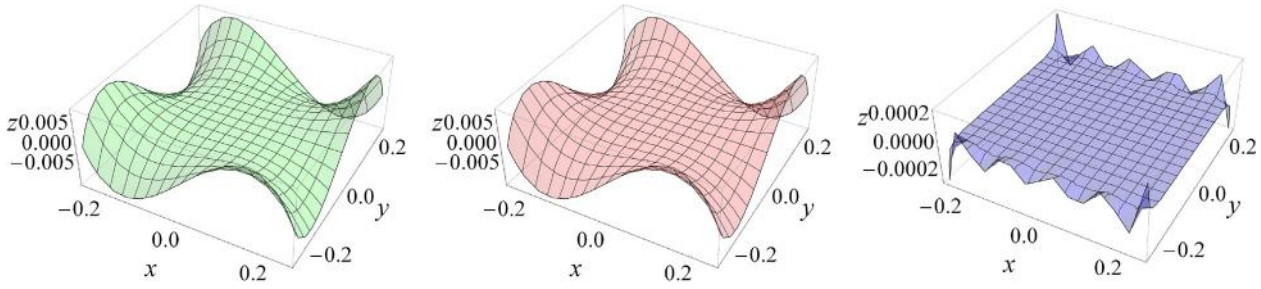

Fig. 4. Saint Venant's warping function for a square cross-section.

remedy to avoid this singularity. In this paper, we make sure that our load step size is small enough such that the singularity does not arise.

7.3.2. Updating axial strain, curvature and its derivatives

Readers are recommended to refer to Chadha and Todd (2019a, b) (particularly the appendix) that details method for obtaining and updating the higher order derivatives of curvature. So far, we have obtained all the elements constituting $\overline{\epsilon}$ except for $\overline{\boldsymbol{\varepsilon}}$ and $\partial_{\xi_1}\overline{\boldsymbol{\varepsilon}}$. These can be obtained using the definition of axial strain vector in Eq. (6), such that:

$$\overline{\boldsymbol{\varepsilon}} = \boldsymbol{Q}^T.\partial_{\xi_1}\boldsymbol{\varphi} - \boldsymbol{E}_1; \tag{115a}$$

$$\partial_{\xi_1}\overline{\boldsymbol{\varepsilon}} = \boldsymbol{Q}^T.\left(\partial^2_{\xi_1}\boldsymbol{\varphi} - \hat{\boldsymbol{\kappa}}.\partial_{\xi_1}\boldsymbol{\varphi}\right) = \boldsymbol{Q}^T.\left(\tilde{\partial}_{\xi_1}\partial_{\xi_1}\boldsymbol{\varphi}\right). \tag{115b}$$

Using the results in *Proposition 3*, presented in Chadha and Todd (2019a), we get $\partial_{\xi_1}\overline{\boldsymbol{\varepsilon}} = \boldsymbol{Q}^T.\tilde{\partial}_{\xi_1}\boldsymbol{\varepsilon}$. From Eq. (115b), $\tilde{\partial}_{\xi_1}\boldsymbol{\varepsilon} = \tilde{\partial}_{\xi_1}(\partial_{\xi_1}\boldsymbol{\varphi})$. Using *Proposition 1* (that also defines the operator $\hat{\partial}_{\xi_1}$ used below) presented in Chadha and Todd (2019a), we have the following

$$\tilde{\partial}^n_{\xi_1}\boldsymbol{\varepsilon} = \tilde{\partial}^n_{\xi_1}(\partial_{\xi_1}\boldsymbol{\varphi}) = \left(\partial_{\xi_1} - \hat{\partial}_{\xi_1}\right)^n(\partial_{\xi_1}\boldsymbol{\varphi}); \tag{116a}$$

$$\partial^n_{\xi_1}\overline{\boldsymbol{\varepsilon}} = \boldsymbol{Q}^T.\tilde{\partial}^n_{\xi_1}(\partial_{\xi_1}\boldsymbol{\varphi}) = \boldsymbol{Q}^T.\left(\sum_{i=0}^{n}(-1)^{(n-i)}\left(\frac{n!}{i!(n-i)!}\right)\partial^n_{\xi_1}\hat{\partial}^{(n-i)}_{\xi_1}\right)\partial_{\xi_1}\boldsymbol{\varphi}. \tag{116b}$$

The following section presents few numerical example concerning the formulation described so far.

8. Numerical examples

We consider three numerical examples based on the formulation described in this chapter using the constitutive model defined in Section 6. The set of problems chosen emphasizes on a large 3D deformation of beam/framed structure.

We consider the tolerance of 10^{-5} in the Euclidean norm of force residue $\|\boldsymbol{P}(\boldsymbol{\Phi})\| = \|\boldsymbol{xf}_{\text{ext0}}(\boldsymbol{\Phi}) - \boldsymbol{f}_{\text{int}}(\boldsymbol{\Phi})\|$ as a measure of convergence. The numerical results, including the deformation map and finite strains, obtained by the current formulation (referred to as Chadha-Todd (CT) beam) are compared with the Simo-Reissener beam model (SR) described in Simo (1985), Simo Vu-Quoc beam model (SV) discussed in Simo and Vu-Quoc (1991), and Crisfield co-rotational formulation detailed in Crisfield (1990). As per the description of deformed configuration in Fig. 1, the SR beam is defined by the configuration Ω_1; the SV beam is defined by a special case of configuration Ω_2 that considers non-uniform St. Venant warping but ignores bending induced shear contribution to warping; the CT beam is described by the state Ω, and the CF beam is a special case of SR (defined by Ω_1) that ignores the shear deformation. We also note that SV and CT beam becomes identical if we ignore Poisson's deformation and warping due to bending induced shear; SR and CF beam formulation becomes identical if shear deformation is ignored; all the four beams are the same if the structure is infinitely slender.

In the following simulations, we consider rectangular cross-section with the edge dimensions $b \times d$, such that $d \geqslant b$. The warping function Ψ_1 pertaining to the torsion can be obtained using the St. Venant's Neumann boundary value problem. There exists a closed-form solution of this differential equation for rectangular cross-section (refer to Sokolnikoff (1956)) given by

$$\Psi_1(\xi_2,\xi_3) = \xi_2\xi_3 - \frac{8d^2}{\pi^3}\sum_{n=0}^{\infty}\frac{(-1)^n\sin(k_n\xi_2)\sinh(k_n\xi_3)}{(2n+1)^3\cosh(k_n b)}; \tag{117}$$

$$k_n = \tfrac{(2n+1)\pi}{d} \quad \text{for } n = 0,1,2,\ldots.$$

Fig. 4a illustrates the warping function Ψ_{1a} for a square cross-section with the edge dimension 0.5 units obtained by solving the concerned Neumann boundary value problem. Similarly, Fig. 4b represents the warping function Ψ_{1b} obtained using Eq. (117) considering $0 \leqslant n \leqslant 3$. We observe from Fig. 4c that Eq. (117) with $0 \leqslant n \leqslant 3$ gives an excellent estimate of the warping function Ψ_1.

The bending induced shear warping functions are obtained in the Appendices A1.5 and A1.6 of Chadha and Todd (2019). We consider the warping functions defined in Eq. (85) of Chadha and Todd (2019) as Ψ_2 and Ψ_3. This warping function includes the non-linear shear induced warping and it ignores the uniform shear deformation of the cross-section as it is taken care of by the director triad. Therefore, we have

$$\Psi_3 = -\frac{E}{2G}\left(\frac{\xi_2^3}{3}\right); \quad \Psi_2 = -\frac{E}{2G}\left(\frac{\xi_3^3}{3}\right). \tag{118}$$

8.1. A discussion on convergence

The weak form requires obtaining updated curvature field $\partial^r_{\xi_1}\boldsymbol{\kappa}$ (see components of $\boldsymbol{B}_1$ matrix in Eq. (123)) and $\Delta\partial^s_{\xi_1}\boldsymbol{\kappa}$ (see Eqs. (38) and (40)) at each iteration, such that $r = 0,1,2$ and $s = 0,1,2,3$. This demands C^3 continuity in $\Delta\boldsymbol{\alpha}$ as obtaining $\Delta\partial^r_{\xi_1}\boldsymbol{\kappa}$ requires up to $(r+1)$ derivatives of $\Delta\boldsymbol{\alpha}$. Secondly, the weak form has up to the second-order derivative of the position vector, and the warping amplitude requiring a C^1 continuity in $\Delta\boldsymbol{\varphi}$ and Δp. Maintaining a global C^3 continuity in the incremental rotation angle will impose 8 continuity conditions at element boundary that can be fulfilled by a seventh-order polynomial (e.g.: eight, seventh-order Hermite polynomials obtained by imposing Kronecker-delta properties at the element junction; or considering seventh-order Lagrangian-polynomials on an eight-noded element). We denote k as the order of the approximating polynomial used, and m is the highest order of derivative in the weak form, which for our case is $m = 4$. A

fourth-order Lagrangian polynomial $k = 4$ satisfies the minimum requirement for the weak form to be square-integrable, and a seventh-order polynomial $k = 7$ is required for the continuity at the element boundary. Although $k = 4$ violates continuity requirements, it yields a converging solution (since $k + 1 > m$) satisfying the compatibility requirement and yields a continuous curvature and mid-curve axial-strain vector at the element junctions (despite committing a variational crime). In this case, care must be taken to avoid using quadrature rules that require element end nodes (like, Gauss–Lobatto). We use a full Newton–Raphson iterative solution procedure with uniformly reduced Gauss–Legendre quadrature to avoid shear locking.

The rate of convergence β in s^{th} Sobolev norm H^s, with $0 \geqslant s \geqslant m$ and $H^0 \equiv L_2$, using Aubin-Nitsche's (refer to Chapter 4 of Hughes (2012)) criterion is given by $\beta = \min(k + 1 - s, 2(k + 1 - m))$. With these criteria, all seven degrees of freedom exhibit a positive rate of convergence for both fourth and seventh order polynomial. For instance, the convergence rate in L_2-norm of rotational degree of freedom is $\beta = 2$ for $k = 4$, and $\beta = 8$ for $k = 7$. Therefore, the seventh-order shape function not only enforces continuity requirements at the element boundary, but it also increases the rate of convergence. On the other hand, the numerical solution with a seventh-order shape function is computationally expensive as compared to a fourth-order polynomial (see Fig. 6), and might lead to oscillatoric strain response at the Gauss-points depending on the shape functions used (see Fig. 10).

From Eq. (114), we note that the rotation quantified by a nonlinear quantity $\mathbf{Q} \in SO(3)$ is updated by the multiplicative rule that utilizes the *current incremental rotation vector* $\Delta\boldsymbol{\alpha}$. Unlike $\Delta\boldsymbol{\alpha}$, it is meaningless to define the quantity $\boldsymbol{\alpha}$, because the rotation is parameterized by the vector $\boldsymbol{\theta}$, not $\boldsymbol{\alpha}$. Therefore, the traditional definition of the L_2 norm does not exist for the *current incremental rotation vector* $\Delta\boldsymbol{\alpha}$. It is a stand-alone quantity and is not defined as a vector difference between two vectors, or $\Delta\boldsymbol{\alpha} \neq \boldsymbol{\alpha}_{\text{f}} - \boldsymbol{\alpha}_{\text{i}}$ as the vector $\boldsymbol{\alpha}$ is undefined. However, we could have adapted a total Lagrangian updating scheme (as in Ibrahimbegović, 1995) and used $\Delta\boldsymbol{\theta}$ instead of $\Delta\boldsymbol{\alpha}$ that would allow updating the rotation vector using additive rule, or $\boldsymbol{\theta}_{\text{f}} = \boldsymbol{\theta}_{\text{i}} + \Delta\boldsymbol{\theta}$, and $\mathbf{Q}_{\text{f}} = \exp(\boldsymbol{\theta}_{\text{f}})$. The traditional definition of L_2-norm would then be valid for the rotation vector $\boldsymbol{\theta}$.

8.2. Numerical Example 1: Cantilever beam subjected to conservative concentrated end load

For simulation 1, we consider a cantilever beam with a uniform square cross-section with edge length 0.5 units subjected to the conservative concentrated load $\boldsymbol{N}_{\boldsymbol{\varphi}} = [18; 5; 5]$ units and $\boldsymbol{N}_{\boldsymbol{\alpha}} = [120; 500; 200]$ units at end node. The beam has the material and geometric properties as: $E = 150 \times 10^3$ units, $L = 10$ units, $G = 62.5 \times 10^3$ units and $\nu = 0.2$. The Vlasov warping constant for this case is significantly small: $\overline{\mathfrak{C}}_{88} = 0.796$. We report the displacement at the end node obtained using CT-beam for 100 elements as: $\boldsymbol{\varphi}(L) = (1.3030, 1.6435, 0.4488)$ units, $p(L) = 0.2591$ units, and $\theta(L) = \|\log(\boldsymbol{Q}(L))\| = 1.2093$ units.

The results discussed in the remaining part of this section is obtained by considering 15 elements, seventh-order Lagrangian polynomial and 30 load steps (implying $x_{n+1} - x_n = \frac{1}{30}$). Tables 1 and 2, gives the norm of force residue for the selective load step. The convergence rates of the Newton method are observed.

Fig. 5 represents the mid-curve and director triad field of the considered beam for selective load steps respectively. The plot compares the undeformed state Ω_0 and the deformed state obtained using SR, SV, CT, and CF beam models. Fig. 6a demonstrates the convergence of the degrees of freedom for fourth (blue color) and seventh (red color) order Lagrangian shape function. Fig. 6b illustrates the run time of FEM code considering fourth (blue color) and seventh (red color) order Lagrangian shape function. The finite element code can further be optimized, therefore, the relevant quantity to look for in Fig. 6b is the ratio of the run time. The formulation with $k = 7$ is around 4.6 times computationally more expensive than $k = 4$. The quantities $e_{\boldsymbol{\varphi}}$ and $e_{\mathbf{Q}}$ (defined in Eq. (9)) represent the error in the mid-curve position vector and the rotation tensor of SR and SV beam relative to the CT beam for four different load steps are plotted in the Figs. 7 and 8.

Table 1
Numerical Example 1: Force residue for the load steps (5, 10, 20, 30) obtained using the CT beam.

Iter.	Force residual norm			
	Load step 5	Load step 10	Load step 20	Load step 30
0	1.840×10^1	1.840×10^1	1.840×10^1	1.840×10^1
1	6.336×10^2	6.0931×10^2	1.781×10^3	6.750×10^2
2	1.996×10^0	2.210×10^0	1.079×10^1	1.547×10^0
3	2.599×10^{-2}	1.081×10^{-1}	3.987×10^0	2.222×10^{-1}
4	1.309×10^{-5}	6.785×10^{-5}	1.022×10^{-3}	2.489×10^{-5}
5	3.068×10^{-7}	3.128×10^{-7}	1.099×10^{-5}	3.066×10^{-7}
6	–	–	3.088×10^{-7}	–

There is significant difference in the position vector of the mid-curve obtained using CT beam model relative to SR, CF, and SV beams. This is primarily because the bending stiffness for CT beam is greater than the bending section modulus for SR, SV, and CF beam by a factor of $f = \left(\frac{3\nu^2+2\nu-2}{4\nu^2+2\nu-2} + \frac{\nu^2}{2(1+\nu)}\left(\frac{I_{11}}{I_{xx}}\right)\right) \geqslant 1$, such that $\overline{\mathfrak{C}}_{33_{xx}} = fEI_{xx}$, where the subscript xx is either 22 or 33 (refer to Fig. 9c). Secondly, CT beam is flexible in torsion relative to the other beam models. We also observe that the error $e_{\boldsymbol{\varphi}}$, increases with the arc-length ξ_1, or equivalently $\partial_{\xi_1} e_{\boldsymbol{\varphi}} > 0$. This phenomenon is very similar to the problem of dead-reckoning (also called a coning effect) in path-estimation.

In Fig. 10a, we observe that CT and SV predicts almost the same warping amplitude p. This is because the parameters $\overline{\mathfrak{C}}_{78}, \overline{\mathfrak{C}}_{79}, \overline{\mathfrak{C}}_{89}, \overline{\mathfrak{C}}_{99}, \overline{\mathfrak{C}}_{98}, \overline{\mathfrak{C}}_{97}$ are small for the considered cross-section. We observe oscillations in the warping amplitude p (a possible reason is discussed in next section). The beam is subjected to conservative torsional moment, leading to constant warping amplitude away from the boundary. Since the aforementioned material constants $\overline{\mathfrak{C}}_{ij}$ are negligible and the cross-section is symmetric (shear center and the centroid of the cross-section coincides), the warping amplitude $p(\xi_1)$ converges with the torsional curvature field $\overline{\kappa}_1(\xi_1)$ as depicted in Fig. 10b. Fig. 11 shows the curvatures (left column) and axial strain components (right column) for load steps (5, 10, 20, 30) obtained using Simo-Reissener (SR), Simo Vu-Quoc (SV) and Chadha-Todd (CT) beam models.

8.3. Numerical Example 2: Cantilever beam subjected to pure torsion and elongation

We consider a beam with the same geometry and material property as Example 1 discussed in Section 8.2, except for the changes in cross-sectional dimensions. For current example, we consider a rectangular cross-section with the dimensions $b = 0.5$ units and $d = 4b = 2 = \frac{L}{5}$ units. The Vlasov constant for the considered cross-section is $\overline{\mathfrak{C}}_{88} = 1261.65$. The beam is subjected to a torsion of 10,000 units and an axial pull of 10000 units at the free end. This structure can not be considered as a slender beam because the depth of the cross-section is 20% of its length. The goal of this example is to demonstrate the performance of the CT beam relative

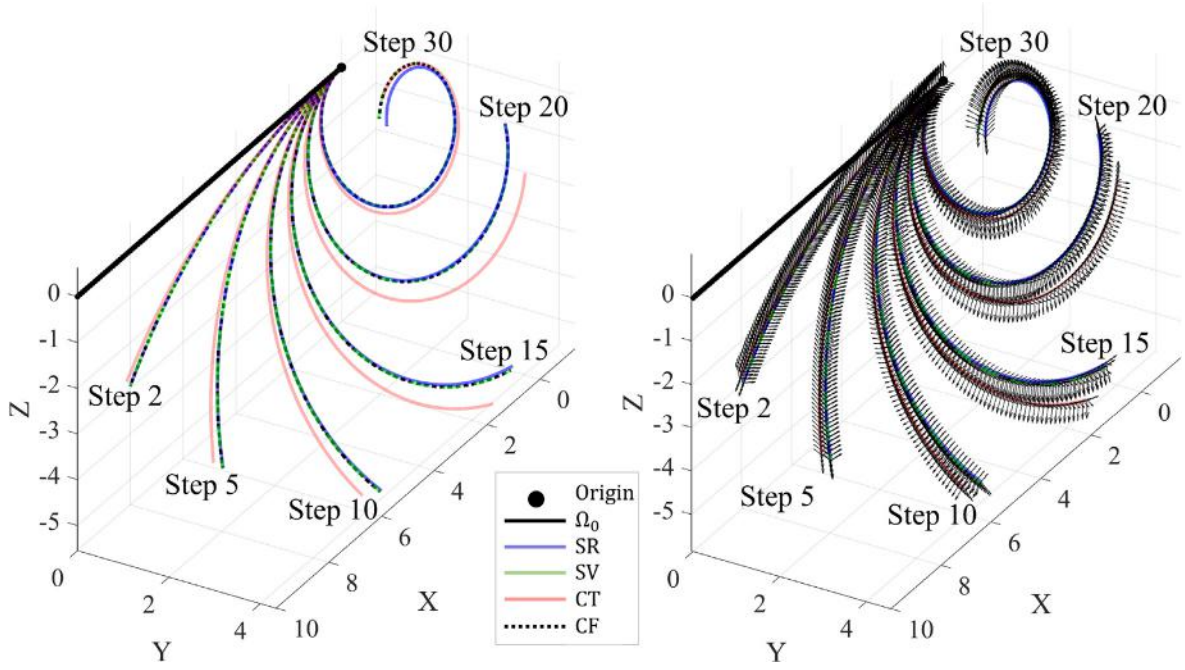

Fig. 5. Numerical Example 1: Deformed configuration.

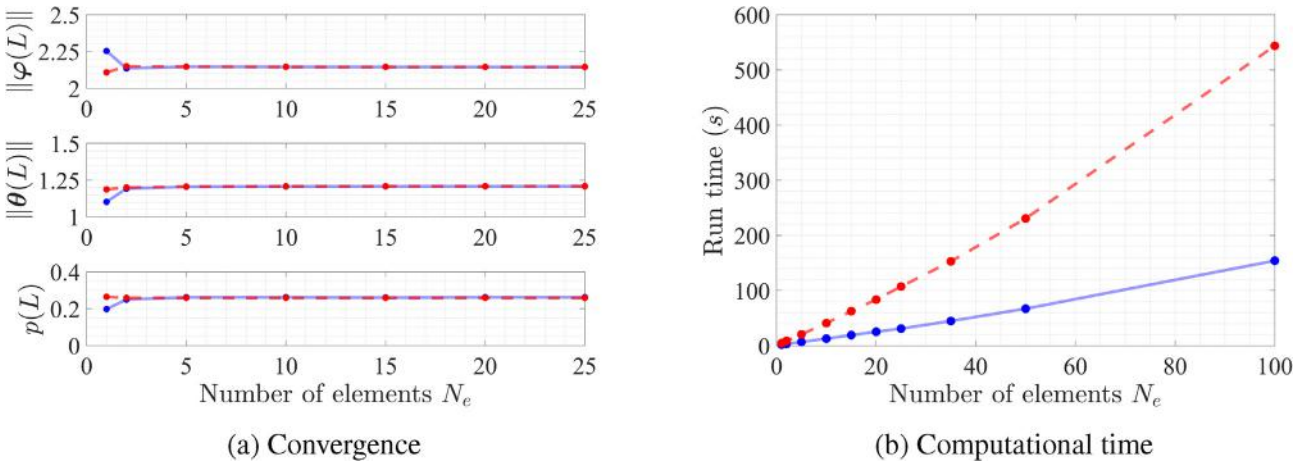

Fig. 6. Numerical Example 1: Convergence and computational time plot. The red and blue represents the results for the 7th and the 4th order shape-function.

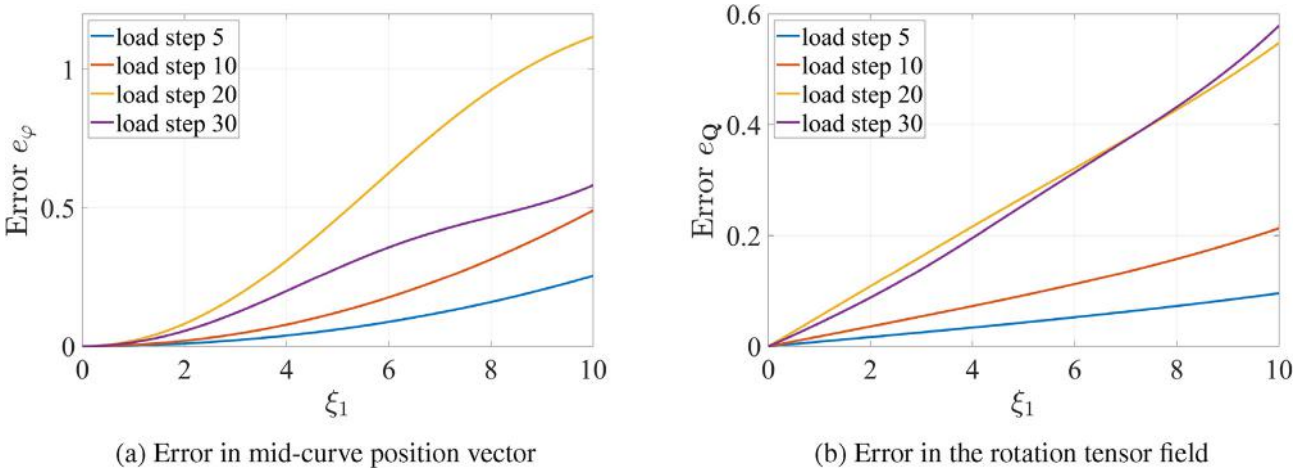

Fig. 7. Numerical Example 1: Error in the Simo-Reissener beam relative to the Chadha-Todd beam.

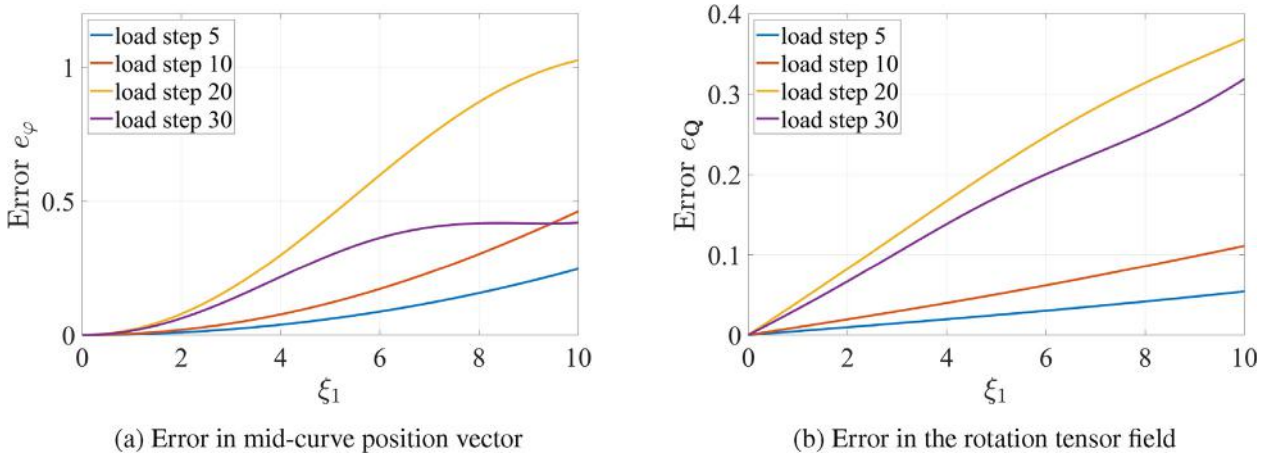

(a) Error in mid-curve position vector (b) Error in the rotation tensor field

Fig. 8. Numerical Example 1: Error in the Simo Vu-Quoc beam relative to the Chadha-Todd beam.

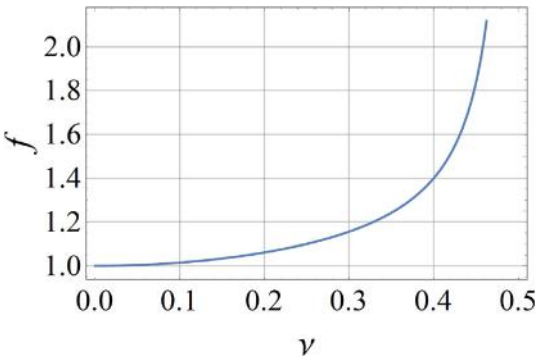

Fig. 9. Factor f as a function of Poisson's ratio for a square cross-section.

to SV, SR, and CF beam when Poisson's and warping effects are dominant. We expect a significant deviation of CT and SV beam relative to the SR and CF beam. We consider 30 load steps, 15 elements, and fourth-order Lagrangian polynomial.

Fig. 12 represents the deformed state for SR (and CF), SV and CT beam models. We observe a few expected results. The error in e_φ is negligible for SR (Fig. 13a) and SV (Fig. 14a) beams. This is because the mid-cure of the beam is effected by pure elongation. However, as observed in Figs. 12 and 13b, there is a significant error in rotation triad obtained for SR and CF beam relative to CT beam (or even SV beam). We can infer from Fig. 12a that the deviation of the director triad in the SR beam relative to the CT beam (obtained at the Gauss points) increases linearly along the length of the beam. However, at first glimpse, the triangular shape of the error plot $e_{\mathbf{Q}}$ (Fig. 13b) depicts a linear increase followed by a decrease in the error. This observation is misleading and contradicting to our previous inference. The wave nature of error plot $e_{\mathbf{Q}}$ is due to the local homeomorphism of exponential map discussed in Section 3.2.2 of Chadha and Todd (2019). In fact, the error plot 13b does show continuous increase of error since $e_{\mathbf{Q}} \in [0, \pi)$.

We attribute large error in the deformation map predicted by SR beam to the fact that the considered structure can no longer be considered slender and the deformation is significantly effected by fully coupled Poisson's and warping effect. The inclusion of all deformation effects in the CT beam makes it more flexible (or less stiff).

Fig. 15 shows the first component of the axial strain vector $\overline{\varepsilon}_1$ and the mid-curve axial strain e. Since the beam is not subjected to bending and shear, $\overline{\varepsilon}_2 = \overline{\varepsilon}_3 = 0, \overline{\kappa}_2 = \overline{\kappa}_3 = 0$, and $\overline{\varepsilon}_1 = e$. As expected, we observe that all four beams have excellent agreement on the mid-curve deformation and the axial strains.

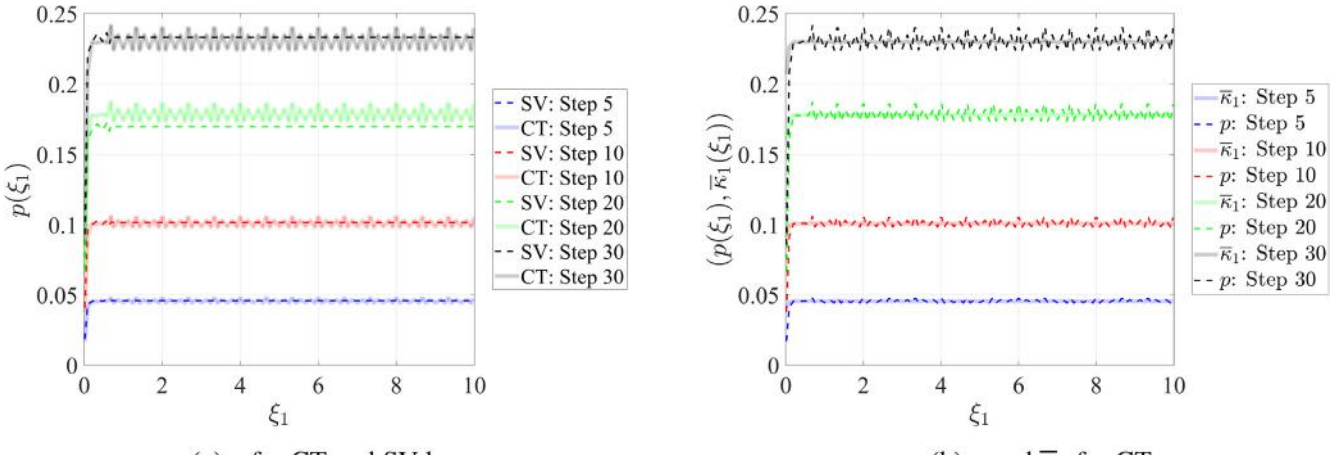

(a) p for CT and SV beam (b) p and $\overline{\kappa}_1$ for CT

Fig. 10. Numerical Example 1: Torsional curvature and warping amplitude.

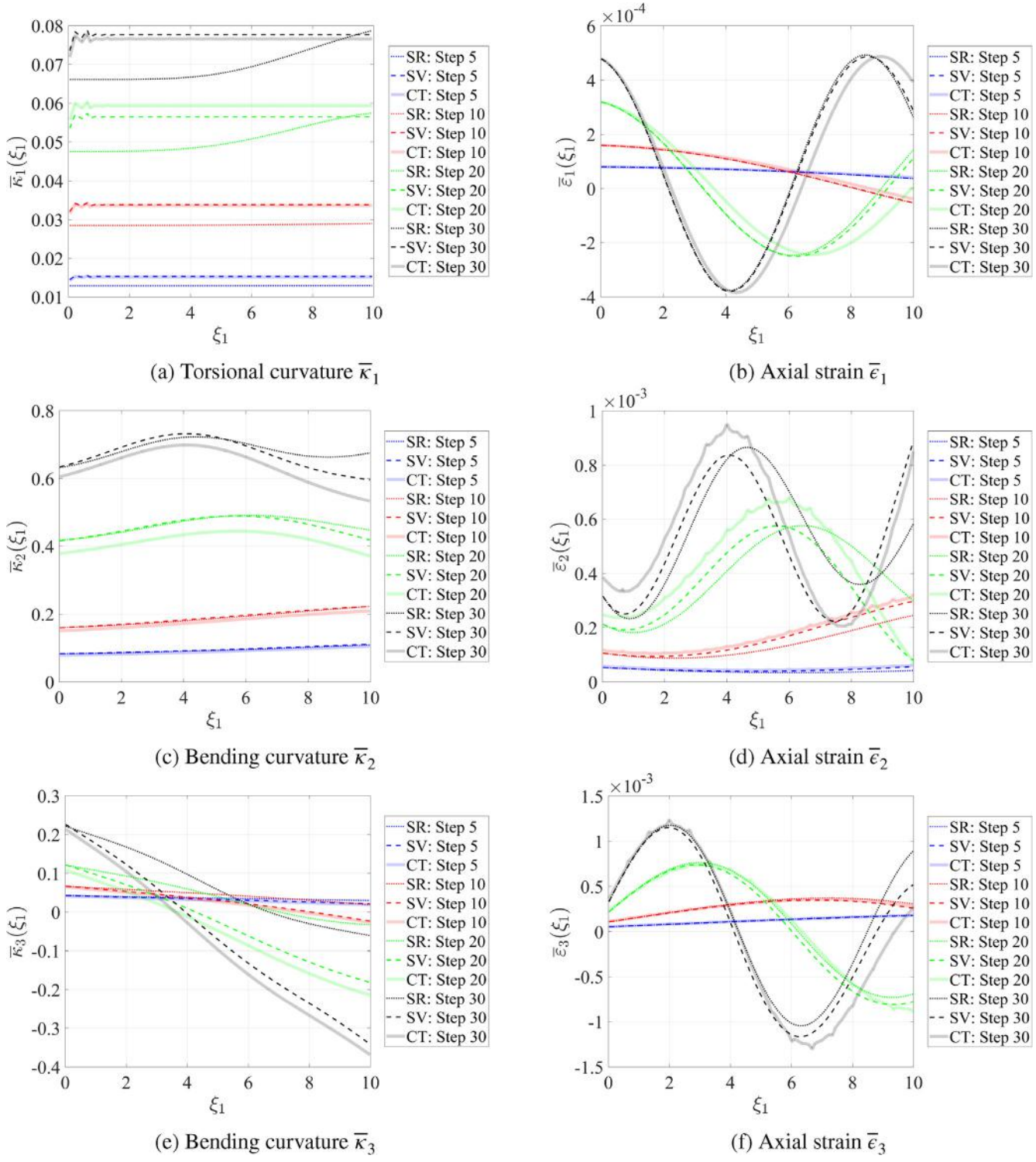

(a) Torsional curvature $\overline{\kappa}_1$ (b) Axial strain $\overline{\epsilon}_1$

(c) Bending curvature $\overline{\kappa}_2$ (d) Axial strain $\overline{\epsilon}_2$

(e) Bending curvature $\overline{\kappa}_3$ (f) Axial strain $\overline{\epsilon}_3$

Fig. 11. Numerical Example 1: Components of the material curvature vector (left column) and the axial strain vector (right column).

Fig. 16a illustrates the torsional curvature field obtained using SR, CF, SV, and CT beam models; and Fig. 16b illustrates the warping amplitude obtained using SV and CT for the load steps in the multiple of five. We make the following observations. Firstly, we observe a significant underestimation of the torsional curvature obtained by the SR or CF beam. This is because the beam is no longer slender. The CT and SV beams are more flexible in torsion relative to SR and CF beam. In case of uniform torsion, we have $p = \overline{\kappa}_1$. If T represents torsion at the end node (here, $T = 10000$ units), the torsional curvature converges to a constant value for CT and SV beam as $\overline{\kappa}_1(L) = \frac{T}{\overline{\mathfrak{C}}_{33_{11}} + \overline{\mathfrak{C}}_{37_{11}}} = 2.306$ (note that $\overline{\mathfrak{C}}_{37_{11}} < 0$), whereas, the curvature for SR and CF beam can be obtained as $\overline{\kappa}_1(L) = \frac{T}{\overline{\mathfrak{C}}_{33_{11}}} = 0.456$.

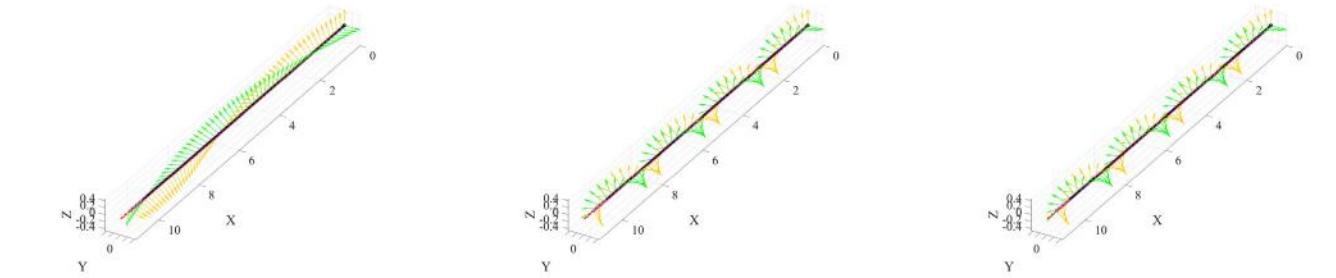

Fig. 12. Numerical Example 2: Deformed state.

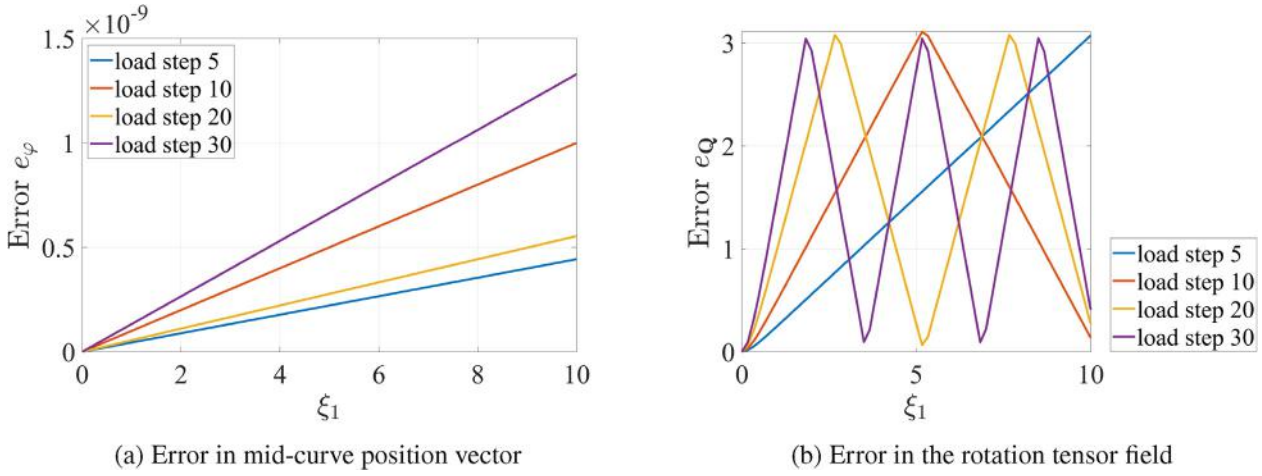

Fig. 13. Numerical Example 2: Error in the Simo-Reissener beam relative to the Chadha-Todd beam.

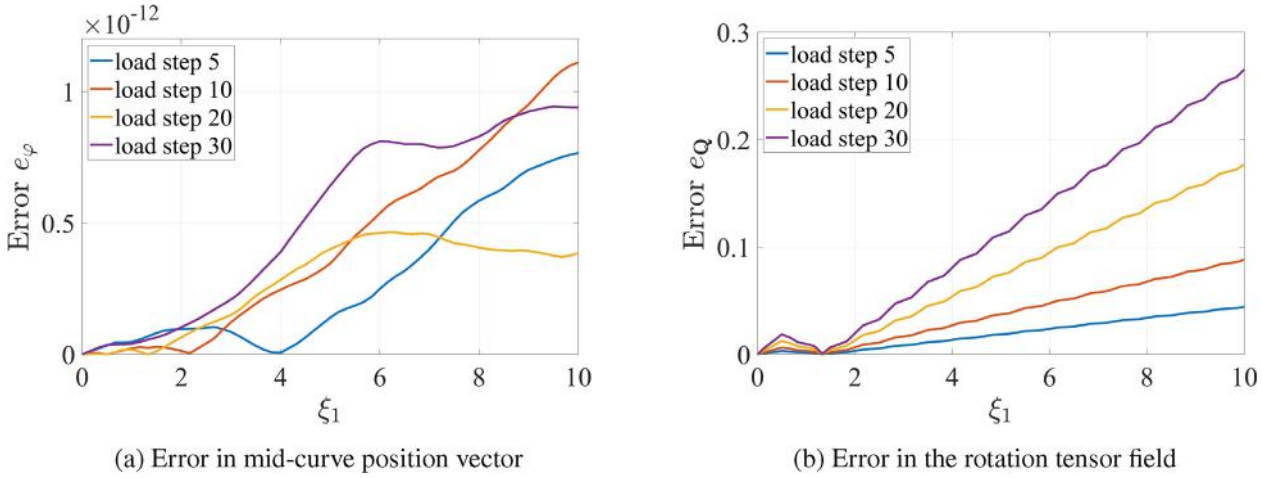

Fig. 14. Numerical Example 2: Error in the Simo Vu-Quoc beam relative to the Chadha-Todd beam.

Secondly, for the given loading, we anticipate a constant torsion field (as in SR beam), but the torsional curvature transitions from zero to constant value in SV and CT beam. Similar is the case with the warping amplitude. We also know that for uniform torsion, the warping amplitude equals the torsional curvature, as observed in Fig. 17. The fixed boundary on the left end implies $p(0) = 0$. Seemingly, the warping amplitude guides the value of torsional curvature leading to an anomaly in the value of curvature near the boundary. Thirdly, we observe oscillations in the torsional curvature and warping amplitude in plot 16. We suspect that the oscillation in the warping amplitude is because of the dependence of the bi-shear on $\partial^2_{\xi_1} p$. Since the quantity $\partial^2_{\xi_1} p$ is highly oscillatory at Gauss points it leads to oscillations in the warping amplitude. As noted before, in the case of uniform torsion, the torsional curvature is guided by the warping amplitude. Therefore, we observe the same oscillations in $\overline{\kappa}_1(\xi_1)$.

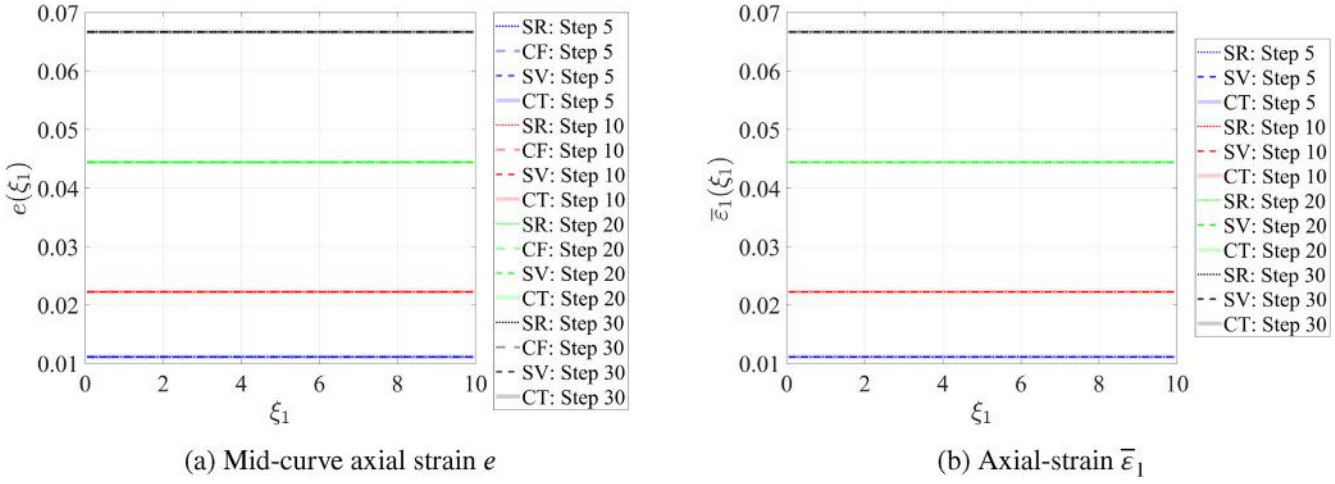

(a) Mid-curve axial strain e (b) Axial-strain $\overline{\varepsilon}_1$

Fig. 15. Numerical Example 2: Axial strains.

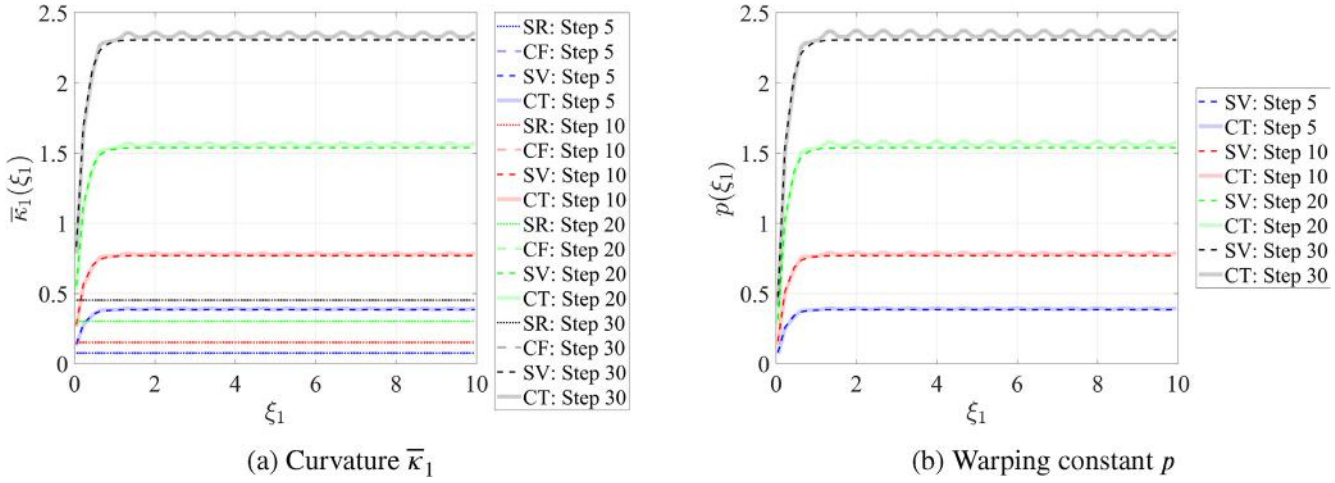

(a) Curvature $\overline{\kappa}_1$ (b) Warping constant p

Fig. 16. Numerical Example 2: Torsional curvature and warping amplitude.

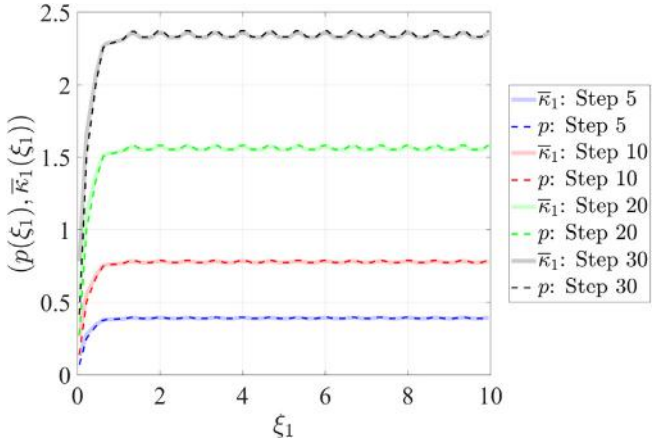

Fig. 17. Numerical Example 2: Warping amplitude and torsional curvature for CT beam.

8.4. Numerical Example 3: 3D frame subjected to concentrated conservative loads at multiple nodes

We consider a structure with the geometry depicted in Fig. 18 subjected to two different cases of loading and cross-section. The local element frames are defined by $\{\boldsymbol{e}_i\}$. The only global to local transformation that we make here is for the material matrix $\overline{\mathbb{C}}$. We consider 150 load steps and fourth-order Lagrangian shape-function for this example.

Table 2
Numerical Example 3: Position vector $\boldsymbol{\varphi} = \varphi_i \boldsymbol{E}_i$ for different beam models at node A and B.

		Node A			Node B		
		φ_1	φ_2	φ_3	φ_1	φ_2	φ_3
Case 1	CT	14.150	−5.483	10.460	7.705	11.190	8.463
	SV	14.380	−5.484	9.893	10.410	9.330	8.397
	SR	13.930	−4.768	11.660	14.210	7.144	12.750
	CF	13.960	−4.761	11.650	14.090	7.247	12.640
Case 2	CT	15.780	4.388	4.792	6.364	11.010	9.937
	SV	15.770	5.353	3.738	6.702	10.790	9.738
	SR	14.210	7.144	12.750	5.773	11.060	10.720
	CF	14.090	7.247	12.640	5.766	11.040	10.670

8.4.1. Case 1

For case 1, we consider a moderately slender structure with the cross-sectional dimension as $b = 0.5$ units and $d = 5b$ units. We subject the structure to 3 times the load showed in Fig. 18.

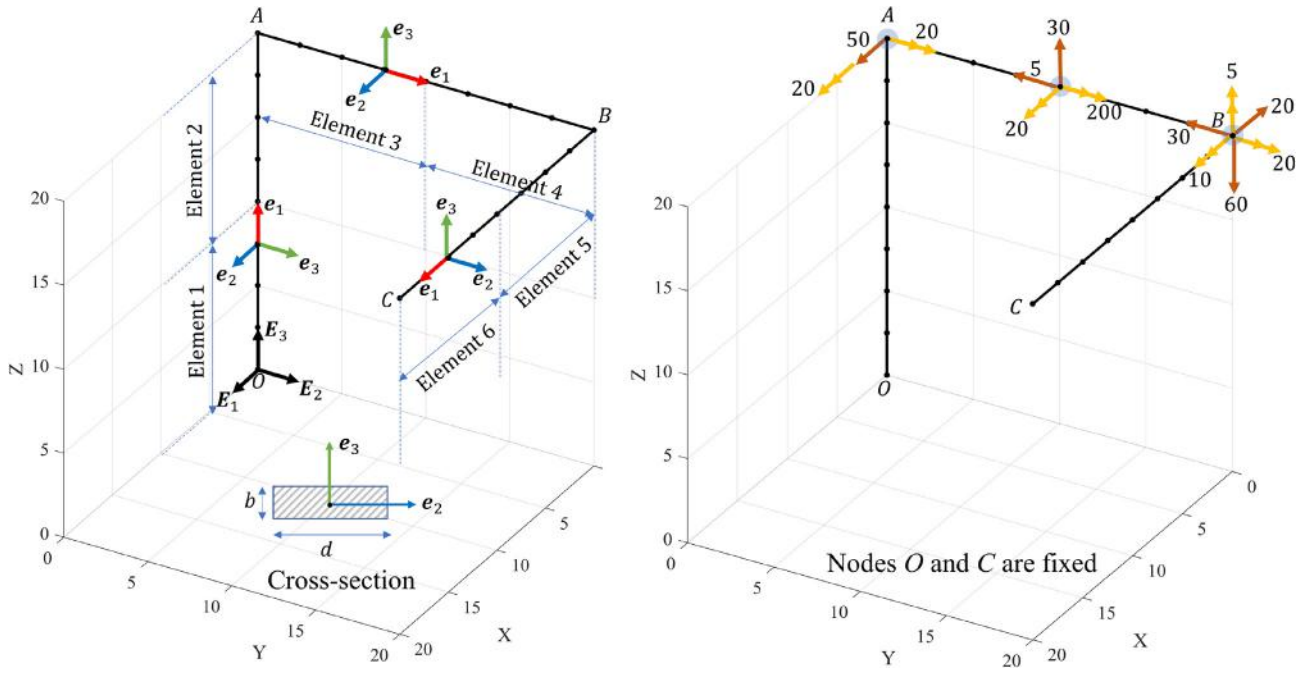

Fig. 18. Numerical Example 3: Geometry and load pattern.

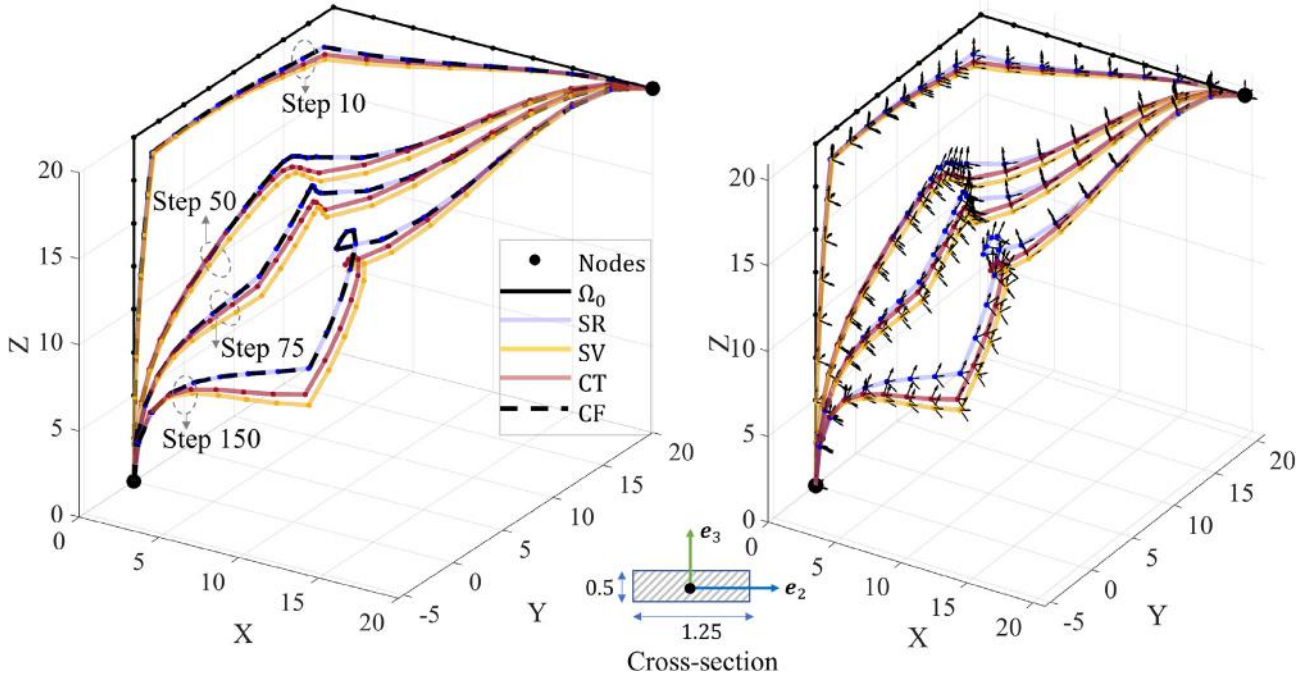

Fig. 19. Numerical Example 3, case 1: Deformed configuration.

Fig. 19 illustrates the deformed shape for various load-steps using CT, SV, SR, and CF beam models. As is expected, SR and CF formulation yields a very similar deformation field. Figs. 19 and 20 shows the error in the mid-curve position vector and rotation triads predicted by SR and SV beams relative to CT beam respectively. CT beam prediction is closer to the SV beam as compared to the SR beam. Figs. 21 and 22 compares the curvature and warping amplitude fields interpolated linearly from their values at the Gauss points obtained by CT, SV, and SR beam models for various load steps. The yellow plane represents a positive plot. We note that the strain fields are in the global coordinate system, for example, in the local element coordinate system, $\overline{\kappa}_1$ represents bending curvature about $\boldsymbol{e}_2$ for elements 1, 2, 3, and 4, whereas it represents torsional curvature for elements 5 and 6. Similarly, the torsional curvature for elements 1 and 2 is given by $\overline{\kappa}_3$, for elements 3 and 4 by $\overline{\kappa}_2$ (the local and global system aligns for elements 4 and 5).

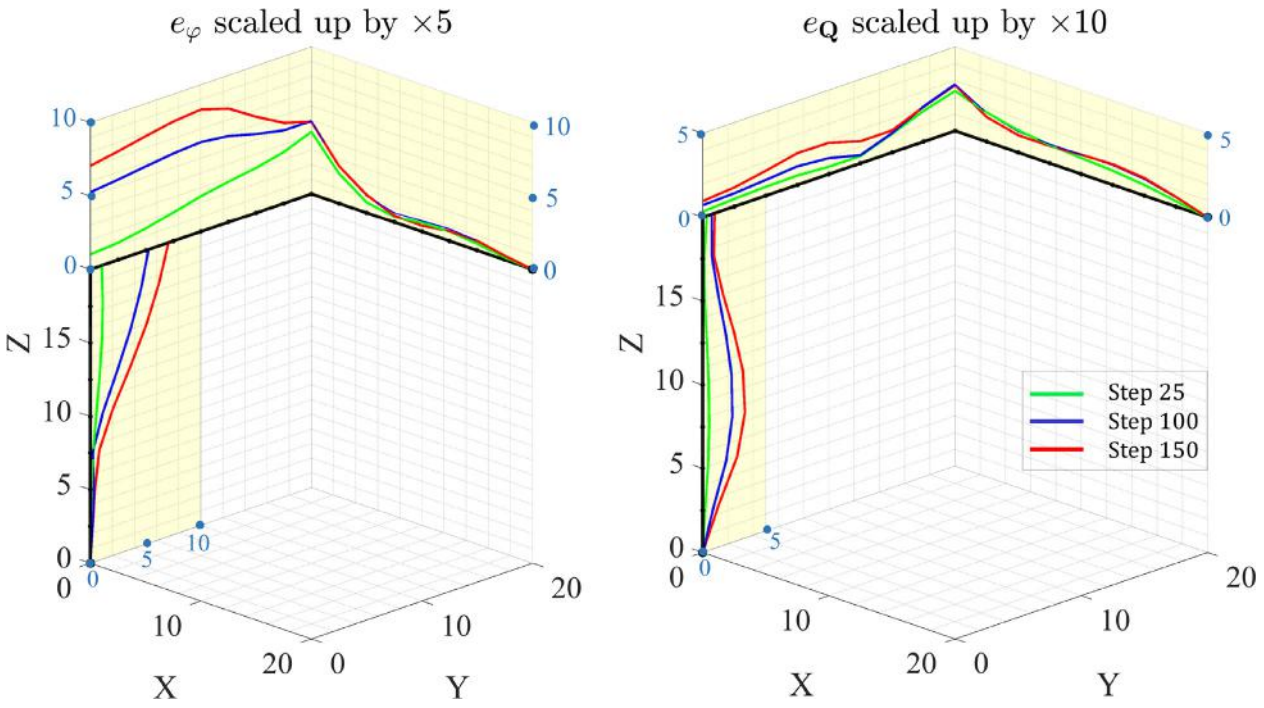

Fig. 20. Numerical Example 3, case 1: Error in the Simo-Reissener beam relative to the Chadha-Todd beam.

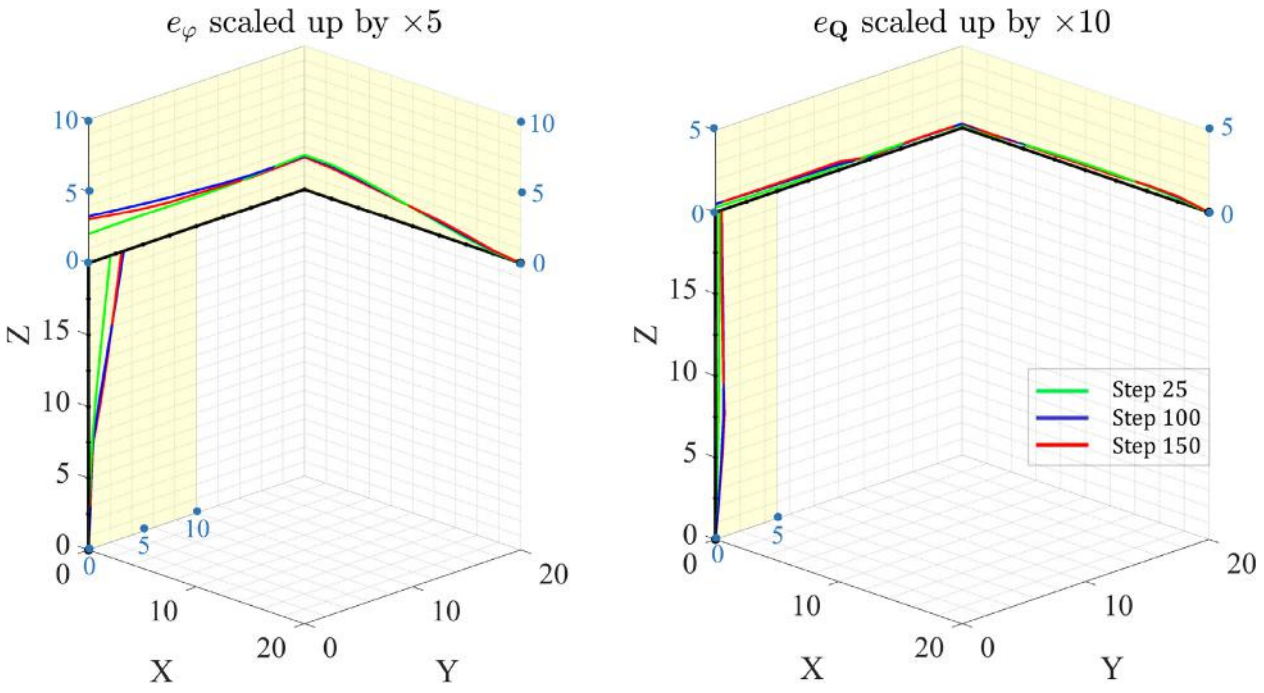

Fig. 21. Numerical Example 3, case 1: Error in the Simo Vu-Quoc beam relative to the Chadha-Todd beam.

A clear resemblance in the warping amplitude p can be observed with $\overline{\kappa}_3$ for elements 1 and 2; with $\overline{\kappa}_2$ for elements 3 and 4; and with $\overline{\kappa}_1$ for elements 5 and 6. see Fig. 23.

8.4.2. Case 2

For case 2, we consider a more slender structure with the cross-sectional dimension as $b = 0.2$ units and $d = 8b$ units (higher aspect ratio of the cross-section as compared to case 1). We subject the structure to 2 times the load showed in Fig. 18. Fig. 24 illustrates the deformed shape for various load-steps using CT, SV, SR, and CF beam models. As is expected, SR and CF formulation yields a very close displacement field. The difference in the displacement fields obtained by various beam models is very prominent in this example because the slenderness of the structure and the higher

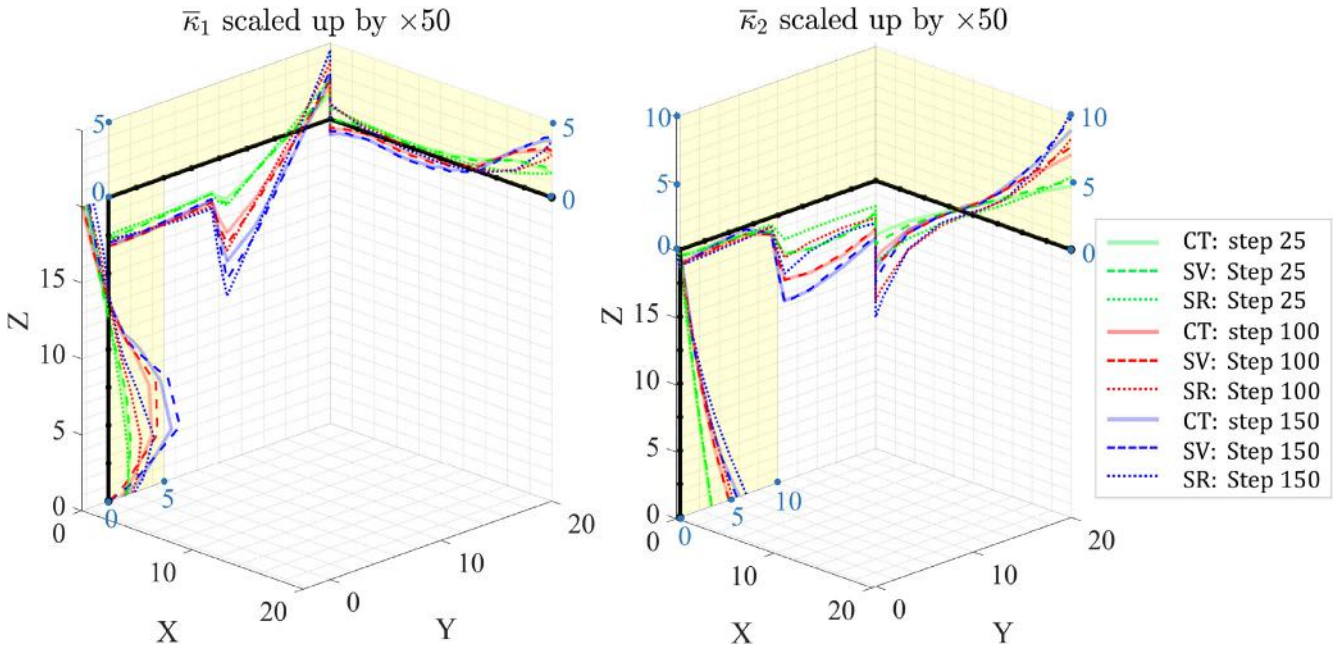

Fig. 22. Numerical Example 3, case 1: The component of material curvatures $\bar{\kappa}_1$, and $\bar{\kappa}_2$ in global coordinates.

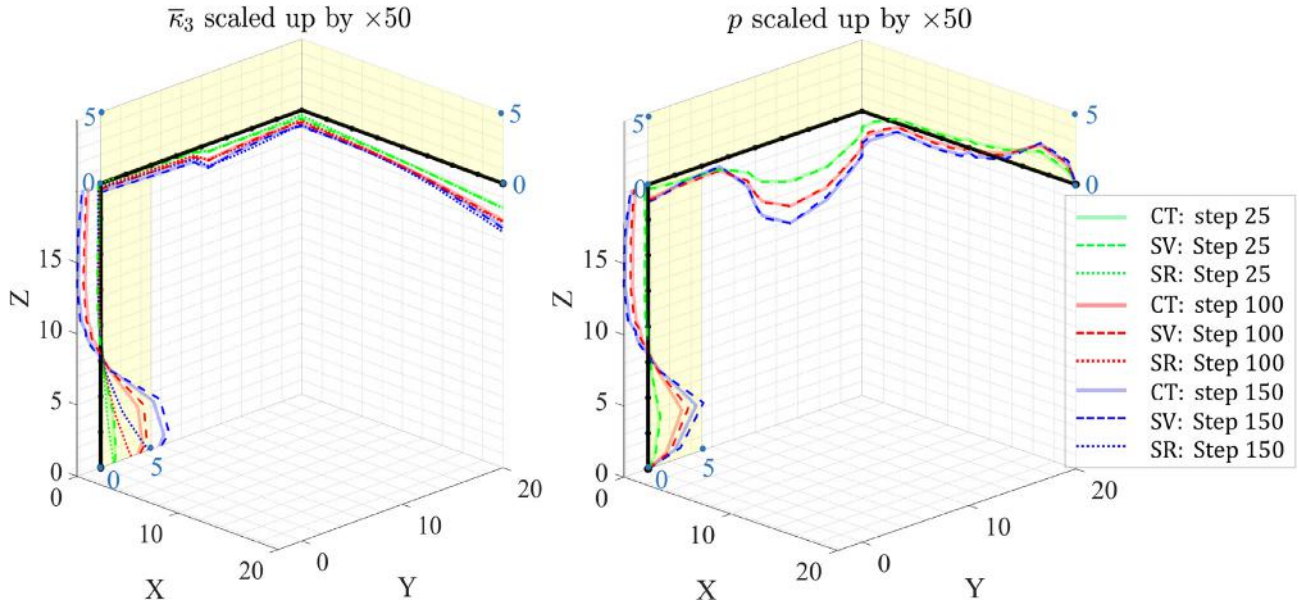

Fig. 23. Numerical Example 3, case 1: The component of material curvature $\bar{\kappa}_3$ in global coordinates, and warping amplitude p.

aspect ratio of the cross-section brings out the effect of fully coupled Poisson's and warping effect in the displacement and strain fields. We report the deformed position vector $\boldsymbol{\varphi}$ (in consistent units) at the nodes A and B marked in Fig. 18 for both Case 1 and Case 2.

9. Summary and conclusion

In this paper, we have detailed the variational formulation (including dynamic behavior) and numerical implementation (restricted to the static case) of geometrically-exact Cosserat beams with a deforming cross-section. In this regard, the current investigation is a sequel to our previous work on generalizing the kinematics of beam to encompass major deformation effects of the beam in the setting of single-manifold characterized geometrically-exact Cosserat beams.

On a broader level, this paper can be divided into five parts. In the first part, we briefly lay down the foundation of kinematics used in this study. Since the configuration of the system at hand is a product space $\mathbb{R}^3 \times SO(3) \times \mathbb{R}$, we describe the important concepts related to finite rotation, curvature, material, and spatial quantities. Finally, we define the tangent space and tangent bundle associated with the deformed configuration.

To arrive at the virtual work principle, we evaluate the variation of necessary quantities. The attempt to capture fully coupled Poisson's and warping effects (including bending induced non-uniform

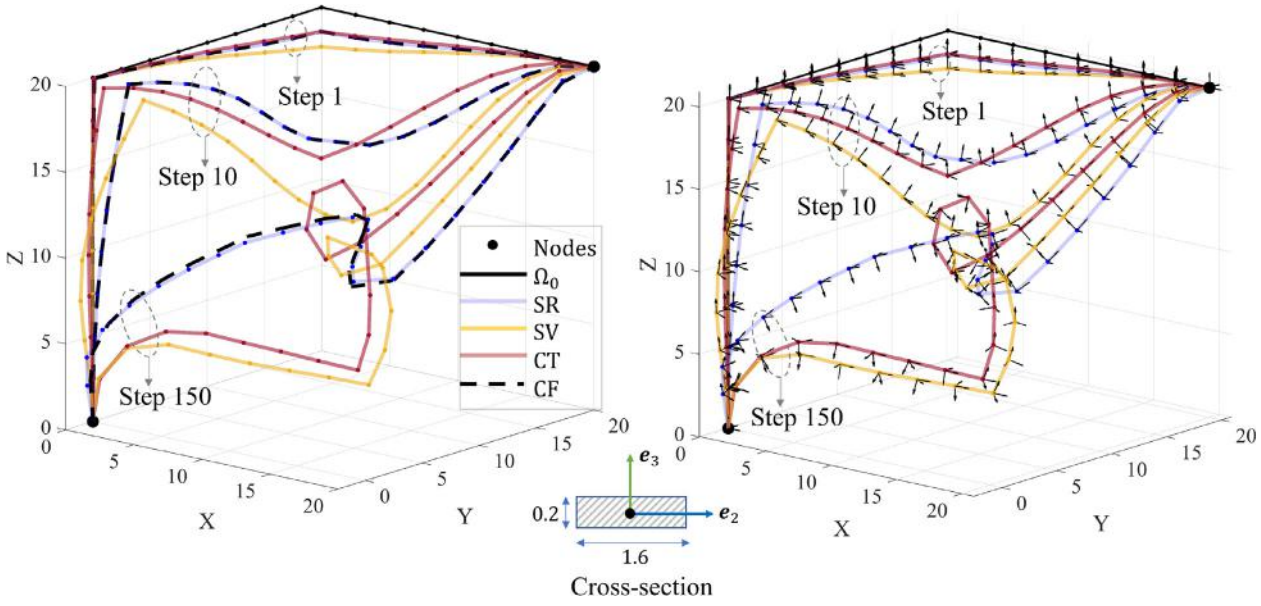

Fig. 24. Numerical Example 3, case 2: Deformed configuration.

shear) results in the dependence of deformation map on derivatives of curvature fields (up to second-order). This makes the calculation of variations rather demanding. The second part of this paper is dedicated to the calculation of variations of kinematic quantities required to obtain the weak form.

The third domain of this work deals with deriving the weak equilibrium equation in a form desirable to computationally solve the problem. This beam model has higher regularity requirements as compared to the conventional Simo-Reissner beam. We expected to obtain an exactly similar balance of linear momentum, angular momentum, and bi-moment as given in Simo and Vu-Quoc (1991). Despite using an advanced kinematic model, the strong form, when expressed using the first PK stress tensor, does not change.

The last part of this paper deals with developing a finite element model considering a small strain linear constitutive model for the static case. For the considered constitutive model, the material stiffness matrix is symmetric, whereas, in general, the geometric stiffness is not symmetric. Finally, numerical simulations comparing various beam models are presented.

Declaration of Competing Interest

The authors declare that they have no known competing financial interests or personal relationships that could have appeared to influence the work reported in this paper.

Acknowledgments

Funding for this work was provided by the USACE through the U.S. Army Engineer Research and Development Center Research Cooperative Agreement W912HZ-17–2-0024. We thank Prof. Joel P. Conte, Prof. J. S. Chen, and Mr. Mukesh K. Ramancha in the Department of Structural Engineering at UC San Diego for providing us with valuable discussions, advice, and comments.

Appendix A. Appendix

A.1. Expressions of $\boldsymbol{L}$ and $\boldsymbol{M}$-terms

A.1.1. Material form of $\boldsymbol{L}$-terms associated with λ_1

$$
\begin{aligned}
&\overline{\boldsymbol{L}}^{\lambda_1}_{\boldsymbol{\varepsilon}} = \boldsymbol{I}_3 \\
&\overline{\boldsymbol{L}}^{\lambda_1}_{\partial_{\xi_1}\boldsymbol{\varepsilon}} = -v\overline{\boldsymbol{r}}_1 \otimes \boldsymbol{E}_1 \\
&\overline{\boldsymbol{L}}^{\lambda_1}_{\boldsymbol{\kappa}} = \hat{\overline{\boldsymbol{r}}}^T \\
&\overline{\boldsymbol{L}}^{\lambda_1}_{\partial_{\xi_1}\boldsymbol{\kappa}} = v\xi_2\overline{\boldsymbol{r}}_1 \otimes \boldsymbol{E}_3 - v\xi_3\overline{\boldsymbol{r}}_1 \otimes \boldsymbol{E}_2 \\
&\overline{\boldsymbol{L}}^{\lambda_1}_{\partial^2_{\xi_1}\boldsymbol{\kappa}} = \boldsymbol{E}_1 \otimes \overline{\boldsymbol{\Psi}}_{23} \\
&\overline{\boldsymbol{L}}^{\lambda_1}_{\partial^3_{\xi_1}\boldsymbol{\kappa}} = -v\overline{\boldsymbol{r}}_1 \otimes \overline{\boldsymbol{\Psi}}_{23} \\
&\overline{\boldsymbol{L}}^{\lambda_1}_{p} = \boldsymbol{0}_1 \\
&\overline{\boldsymbol{L}}^{\lambda_1}_{\partial_{\xi_1}p} = \Psi_1\boldsymbol{E}_1 \\
&\overline{\boldsymbol{L}}^{\lambda_1}_{\partial^2_{\xi_1}p} = -v\Psi_1\overline{\boldsymbol{r}}_1
\end{aligned}
\tag{119}
$$

$$
\begin{aligned}
&\overline{\boldsymbol{L}}^{\lambda_2}_{\boldsymbol{\varepsilon}} = -v\boldsymbol{E}_2 \otimes \boldsymbol{E}_1 \\
&\overline{\boldsymbol{L}}^{\lambda_2}_{\partial_{\xi_1}\boldsymbol{\varepsilon}} = \boldsymbol{0}_3 \\
&\overline{\boldsymbol{L}}^{\lambda_2}_{\boldsymbol{\kappa}} = 2v\xi_2\boldsymbol{E}_2 \otimes \boldsymbol{E}_3 - v\xi_3\boldsymbol{E}_2 \otimes \boldsymbol{E}_2 \quad + v\xi_3\boldsymbol{E}_3 \otimes \boldsymbol{E}_3 \\
&\overline{\boldsymbol{L}}^{\lambda_2}_{\partial_{\xi_1}\boldsymbol{\kappa}} = \boldsymbol{E}_1 \otimes \partial_{\xi_2}\overline{\boldsymbol{\Psi}}_{23} \\
&\overline{\boldsymbol{L}}^{\lambda_2}_{\partial^2_{\xi_1}\boldsymbol{\kappa}} = -v\boldsymbol{E}_2 \otimes \overline{\boldsymbol{\Psi}}_{23} - v\overline{\boldsymbol{r}}_1 \otimes \partial_{\xi_2}\overline{\boldsymbol{\Psi}}_{23} \\
&\overline{\boldsymbol{L}}^{\lambda_2}_{\partial^3_{\xi_1}\boldsymbol{\kappa}} = \boldsymbol{0}_3 \\
&\overline{\boldsymbol{L}}^{\lambda_2}_{p} = \partial_{\xi_2}\Psi_1.\boldsymbol{E}_1 \\
&\overline{\boldsymbol{L}}^{\lambda_2}_{\partial_{\xi_1}p} = -v\Psi_1\boldsymbol{E}_2 - v\partial_{\xi_2}\Psi_1.\overline{\boldsymbol{r}}_1 \\
&\overline{\boldsymbol{L}}^{\lambda_2}_{\partial^2_{\xi_1}p} = \boldsymbol{0}_1
\end{aligned}
\tag{120}
$$

*A.1.2. Material form of **L**-terms associated with λ_3 and **M**-terms*

$$
\begin{aligned}
&\overline{\boldsymbol{L}}^{\lambda_3}_{\varepsilon} = -v\boldsymbol{E}_3 \otimes \boldsymbol{E}_1 \\
&\overline{\boldsymbol{L}}^{\lambda_3}_{\partial_{\xi_1}\varepsilon} = 0_3 \\
&\overline{\boldsymbol{L}}^{\lambda_3}_{\kappa} = -v\xi_2\boldsymbol{E}_2 \otimes \boldsymbol{E}_2 + v\xi_2\boldsymbol{E}_3 \otimes \boldsymbol{E}_3 \quad - 2v\xi_3\boldsymbol{E}_3 \otimes \boldsymbol{E}_2 \\
&\overline{\boldsymbol{L}}^{\lambda_3}_{\partial_{\xi_1}\kappa} = \boldsymbol{E}_1 \otimes \partial_{\xi_3}\overline{\boldsymbol{\Psi}}_{23} \\
&\overline{\boldsymbol{L}}^{\lambda_3}_{\partial^2_{\xi_1}\kappa} = -v\boldsymbol{E}_3 \otimes \overline{\boldsymbol{\Psi}}_{23} - v\overline{\boldsymbol{r}}_1 \otimes \partial_{\xi_3}\overline{\boldsymbol{\Psi}}_{23} \\
&\overline{\boldsymbol{L}}^{\lambda_3}_{\partial^3_{\xi_1}\kappa} = 0_3 \\
&\overline{\boldsymbol{L}}^{\lambda_3}_{p} = \partial_{\xi_3}\Psi_1.\boldsymbol{E}_1 \\
&\overline{\boldsymbol{L}}^{\lambda_3}_{\partial_{\xi_1}p} = -v\Psi_1\boldsymbol{E}_3 - v\partial_{\xi_3}\Psi_1.\overline{\boldsymbol{r}}_1 \\
&\overline{\boldsymbol{L}}^{\lambda_3}_{\partial^2_{\xi_1}p} = 0_1
\end{aligned}
\tag{121}
$$

$$
\begin{aligned}
&\overline{\boldsymbol{M}}^{\lambda_1}_{\varepsilon} = -v\hat{\boldsymbol{\kappa}}.\overline{\boldsymbol{r}}_1 \otimes \boldsymbol{E}_1 \\
&\overline{\boldsymbol{M}}^{\lambda_1}_{\kappa} = v\hat{\boldsymbol{\kappa}}.\overline{\boldsymbol{r}}_1 \otimes (\xi_2\boldsymbol{E}_3 - \xi_3\boldsymbol{E}_2) \\
&\overline{\boldsymbol{M}}^{\lambda_1}_{\partial_{\xi_1}\kappa} = \hat{\boldsymbol{\kappa}}.\boldsymbol{E}_1 \otimes \overline{\boldsymbol{\Psi}}_{23} \\
&\overline{\boldsymbol{M}}^{\lambda_1}_{\partial^2_{\xi_1}\kappa} = -v\hat{\boldsymbol{\kappa}}.\overline{\boldsymbol{r}}_1 \otimes \overline{\boldsymbol{\Psi}}_{23} \\
&\overline{\boldsymbol{M}}^{\lambda_1}_{p} = \Psi_1\hat{\boldsymbol{\kappa}}.\overline{\boldsymbol{E}}_1 \\
&\overline{\boldsymbol{M}}^{\lambda_1}_{\partial_{\xi_1}p} = -v\Psi_1\hat{\boldsymbol{\kappa}}.\overline{\boldsymbol{r}}_1
\end{aligned}
\tag{122}
$$

A.2. Expressions of matrices

A.2.1. Matrix $\boldsymbol{B}_1$

$$
\boldsymbol{B}_1 = \begin{bmatrix}
\boldsymbol{0}_3 & \boldsymbol{I}_3 & \boldsymbol{0}_3 & \partial_{\xi_1}\hat{\boldsymbol{\varphi}} & \boldsymbol{0}_3 & \boldsymbol{0}_3 & \boldsymbol{0}_3 & \boldsymbol{0}_3 & \boldsymbol{0}_3 \\
\boldsymbol{0}_3 & -\hat{\boldsymbol{\kappa}} & \boldsymbol{I}_3 & \left(\partial^2_{\xi_1}\hat{\boldsymbol{\varphi}} - \hat{\boldsymbol{\kappa}}.\partial_{\xi_1}\hat{\boldsymbol{\varphi}}\right) & \partial_{\xi_1}\hat{\boldsymbol{\varphi}} & \boldsymbol{0}_3 & \boldsymbol{0}_3 & \boldsymbol{0}_3 & \boldsymbol{0}_3 \\
\boldsymbol{0}_3 & \boldsymbol{0}_3 & \boldsymbol{0}_3 & \boldsymbol{0}_3 & \boldsymbol{I}_3 & \boldsymbol{0}_3 & \boldsymbol{0}_3 & \boldsymbol{0}_3 & \boldsymbol{0}_3 \\
\boldsymbol{0}_3 & \boldsymbol{0}_3 & \boldsymbol{0}_3 & \boldsymbol{0}_3 & -\hat{\boldsymbol{\kappa}} & \boldsymbol{I}_3 & \boldsymbol{0}_3 & \boldsymbol{0}_3 & \boldsymbol{0}_3 \\
\boldsymbol{0}_3 & \boldsymbol{0}_3 & \boldsymbol{0}_3 & \boldsymbol{0}_3 & (\hat{\boldsymbol{\kappa}}.\hat{\boldsymbol{\kappa}} - \partial_{\xi_1}\hat{\boldsymbol{\kappa}}) & -2\hat{\boldsymbol{\kappa}} & \boldsymbol{I}_3 & \boldsymbol{0}_3 & \boldsymbol{0}_3 \\
\boldsymbol{0}_3 & \boldsymbol{0}_3 & \boldsymbol{0}_3 & \boldsymbol{0}_3 & \begin{pmatrix}\partial_{\xi_1}\hat{\boldsymbol{\kappa}}.\hat{\boldsymbol{\kappa}} + 2\hat{\boldsymbol{\kappa}}.\partial_{\xi_1}\hat{\boldsymbol{\kappa}} \\ -\partial^2_{\xi_1}\hat{\boldsymbol{\kappa}} - \hat{\boldsymbol{\kappa}}.\hat{\boldsymbol{\kappa}}.\hat{\boldsymbol{\kappa}}\end{pmatrix} & 3(\hat{\boldsymbol{\kappa}}.\hat{\boldsymbol{\kappa}} - \partial_{\xi_1}\hat{\boldsymbol{\kappa}}) & -3\hat{\boldsymbol{\kappa}} & \boldsymbol{I}_3 & \boldsymbol{0}_3 \\
\boldsymbol{0}_3 & \boldsymbol{0}_3 & \boldsymbol{0}_3 & \boldsymbol{0}_3 & \boldsymbol{0}_3 & \boldsymbol{0}_3 & \boldsymbol{0}_3 & \boldsymbol{0}_3 & \boldsymbol{I}_3
\end{bmatrix}
\tag{123}
$$

A.2.2. Matrix $\boldsymbol{B}_2$

$$
\boldsymbol{B}_2^T = \begin{bmatrix}
\boldsymbol{I}_3 & \partial_{\xi_1}.\boldsymbol{I}_3 & \partial^2_{\xi_1}.\boldsymbol{I}_3 & \boldsymbol{0}_3 & \boldsymbol{0}_3 & \boldsymbol{0}_3 & \boldsymbol{0}_3 & \boldsymbol{0}_3 & \boldsymbol{0}_1 & \boldsymbol{0}_1 & \boldsymbol{0}_1 \\
\boldsymbol{0}_3 & \boldsymbol{0}_3 & \boldsymbol{0}_3 & \boldsymbol{I}_3 & \partial_{\xi_1}.\boldsymbol{I}_3 & \partial^2_{\xi_1}.\boldsymbol{I}_3 & \partial^3_{\xi_1}.\boldsymbol{I}_3 & \partial^4_{\xi_1}.\boldsymbol{I}_3 & \boldsymbol{0}_1 & \boldsymbol{0}_1 & \boldsymbol{0}_1 \\
\boldsymbol{0}_1^T & \boldsymbol{0}_1^T & \boldsymbol{0}_1^T & \boldsymbol{0}_1^T & \boldsymbol{0}_1^T & \boldsymbol{0}_1^T & \boldsymbol{0}_1^T & \boldsymbol{0}_1^T & 1 & \partial_{\xi_1} & \partial^2_{\xi_1}
\end{bmatrix}
\tag{124}
$$

Here, $\partial^n_{\xi_1}.\boldsymbol{I}_3 = \text{diagonal}\left[\partial^n_{\xi_1}, \partial^n_{\xi_1}, \partial^n_{\xi_1}\right]$

A.2.3. Matrix $\boldsymbol{B}_3$

$$
\boldsymbol{B}_3 = \begin{bmatrix}
\boldsymbol{I}_3 & \boldsymbol{0}_3 & \boldsymbol{0}_3 & \boldsymbol{0}_3 & \boldsymbol{0}_3 & \boldsymbol{0}_3 & \boldsymbol{0}_1 & \boldsymbol{0}_1 \\
\boldsymbol{0}_3 & \boldsymbol{I}_3 & \boldsymbol{0}_3 & \boldsymbol{0}_3 & \boldsymbol{0}_3 & \boldsymbol{0}_3 & \boldsymbol{0}_1 & \boldsymbol{0}_1 \\
\boldsymbol{0}_3 & \boldsymbol{0}_3 & \boldsymbol{0}_3 & \boldsymbol{0}_3 & \boldsymbol{0}_3 & \boldsymbol{0}_3 & \boldsymbol{0}_1 & \boldsymbol{0}_1 \\
\boldsymbol{0}_3 & -\partial_{\xi_1}\hat{\boldsymbol{\varphi}} & \boldsymbol{I}_3 & \boldsymbol{0}_3 & \boldsymbol{0}_3 & \boldsymbol{0}_3 & \boldsymbol{0}_1 & \boldsymbol{0}_1 \\
\boldsymbol{0}_3 & \boldsymbol{0}_3 & \boldsymbol{0}_3 & \boldsymbol{I}_3 & \hat{\boldsymbol{\kappa}} & (\hat{\boldsymbol{\kappa}}.\hat{\boldsymbol{\kappa}} + \partial_{\xi_1}\hat{\boldsymbol{\kappa}}) & \boldsymbol{0}_1 & \boldsymbol{0}_1 \\
\boldsymbol{0}_3 & \boldsymbol{0}_3 & \boldsymbol{0}_3 & \boldsymbol{0}_3 & \boldsymbol{I}_3 & 2\hat{\boldsymbol{\kappa}} & \boldsymbol{0}_1 & \boldsymbol{0}_1 \\
\boldsymbol{0}_3 & \boldsymbol{0}_3 & \boldsymbol{0}_3 & \boldsymbol{0}_3 & \boldsymbol{0}_3 & \boldsymbol{I}_3 & \boldsymbol{0}_1 & \boldsymbol{0}_1 \\
\boldsymbol{0}_3 & \boldsymbol{0}_3 & \boldsymbol{0}_3 & \boldsymbol{0}_3 & \boldsymbol{0}_3 & \boldsymbol{0}_3 & \boldsymbol{0}_1 & \boldsymbol{0}_1 \\
\boldsymbol{0}_1^T & \boldsymbol{0}_1^T & \boldsymbol{0}_1^T & \boldsymbol{0}_1^T & \boldsymbol{0}_1^T & \boldsymbol{0}_1^T & 1 & 0 \\
\boldsymbol{0}_1^T & \boldsymbol{0}_1^T & \boldsymbol{0}_1^T & \boldsymbol{0}_1^T & \boldsymbol{0}_1^T & \boldsymbol{0}_1^T & 0 & 1 \\
\boldsymbol{0}_1^T & \boldsymbol{0}_1^T & \boldsymbol{0}_1^T & \boldsymbol{0}_1^T & \boldsymbol{0}_1^T & \boldsymbol{0}_1^T & 0 & 0
\end{bmatrix}
\tag{125}
$$

A.2.4. Matrix $\boldsymbol{B}_4$

$$
\boldsymbol{B}_4 = \begin{bmatrix}
\boldsymbol{0}_3 & \boldsymbol{0}_3 & \boldsymbol{0}_3 & -\hat{\boldsymbol{\mathcal{N}}}_{\varepsilon} & \boldsymbol{0}_3 & \boldsymbol{0}_3 & \boldsymbol{0}_3 & \boldsymbol{0}_3 & \boldsymbol{0}_3 \\
\boldsymbol{0}_3 & \boldsymbol{0}_3 & \boldsymbol{0}_3 & -\hat{\boldsymbol{\mathcal{N}}}_{\partial_{\xi_1}\varepsilon} & \boldsymbol{0}_3 & \boldsymbol{0}_3 & \boldsymbol{0}_3 & \boldsymbol{0}_3 & \boldsymbol{0}_3 \\
\boldsymbol{0}_3 & \boldsymbol{0}_3 & \boldsymbol{0}_3 & -\hat{\boldsymbol{\mathcal{N}}}_{\kappa} & \boldsymbol{0}_3 & \boldsymbol{0}_3 & \boldsymbol{0}_3 & \boldsymbol{0}_3 & \boldsymbol{0}_3 \\
\boldsymbol{0}_3 & \boldsymbol{0}_3 & \boldsymbol{0}_3 & -\hat{\boldsymbol{\mathcal{N}}}_{\partial_{\xi_1}\kappa} & \boldsymbol{0}_3 & \boldsymbol{0}_3 & \boldsymbol{0}_3 & \boldsymbol{0}_3 & \boldsymbol{0}_3 \\
\boldsymbol{0}_3 & \boldsymbol{0}_3 & \boldsymbol{0}_3 & -\hat{\boldsymbol{\mathcal{N}}}_{\partial^2_{\xi_1}\kappa} & \boldsymbol{0}_3 & \boldsymbol{0}_3 & \boldsymbol{0}_3 & \boldsymbol{0}_3 & \boldsymbol{0}_3 \\
\boldsymbol{0}_3 & \boldsymbol{0}_3 & \boldsymbol{0}_3 & -\hat{\boldsymbol{\mathcal{N}}}_{\partial^3_{\xi_1}\kappa} & \boldsymbol{0}_3 & \boldsymbol{0}_3 & \boldsymbol{0}_3 & \boldsymbol{0}_3 & \boldsymbol{0}_3 \\
\boldsymbol{0}_3 & \boldsymbol{0}_3 & \boldsymbol{0}_3 & \boldsymbol{0}_3 & \boldsymbol{0}_3 & \boldsymbol{0}_3 & \boldsymbol{0}_3 & \boldsymbol{0}_3 & \boldsymbol{0}_3
\end{bmatrix}
\tag{126}
$$

A.2.5. Matrix $\boldsymbol{B}_5$

$$
\boldsymbol{B}_5 = \begin{bmatrix}
\boldsymbol{0}_3 & \boldsymbol{0}_3 & \boldsymbol{0}_3 & \boldsymbol{0}_3 & \boldsymbol{0}_3 & \boldsymbol{0}_3 & \boldsymbol{0}_3 & \boldsymbol{0}_3 & \boldsymbol{0}_3 \\
\boldsymbol{0}_3 & \boldsymbol{0}_3 & \boldsymbol{0}_3 & \boldsymbol{B}_{5_{24}} & \boldsymbol{B}_{5_{25}} & \boldsymbol{0}_3 & \boldsymbol{0}_3 & \boldsymbol{0}_3 & \boldsymbol{0}_3 \\
\boldsymbol{0}_3 & \boldsymbol{0}_3 & \boldsymbol{0}_3 & \boldsymbol{0}_3 & \boldsymbol{0}_3 & \boldsymbol{0}_3 & \boldsymbol{0}_3 & \boldsymbol{0}_3 & \boldsymbol{0}_3 \\
\boldsymbol{0}_3 & \boldsymbol{B}_{5_{42}} & \boldsymbol{B}_{5_{43}} & \boldsymbol{B}_{5_{44}} & \boldsymbol{B}_{5_{45}} & \boldsymbol{0}_3 & \boldsymbol{0}_3 & \boldsymbol{0}_3 & \boldsymbol{0}_3 \\
\boldsymbol{0}_3 & \boldsymbol{B}_{5_{52}} & \boldsymbol{0}_3 & \boldsymbol{B}_{5_{54}} & \boldsymbol{B}_{5_{55}} & \boldsymbol{B}_{5_{56}} & \boldsymbol{B}_{5_{57}} & \boldsymbol{0}_3 & \boldsymbol{0}_3 \\
\boldsymbol{0}_3 & \boldsymbol{0}_3 & \boldsymbol{0}_3 & \boldsymbol{B}_{5_{64}} & \boldsymbol{B}_{5_{65}} & \boldsymbol{B}_{5_{66}} & \boldsymbol{0}_3 & \boldsymbol{0}_3 & \boldsymbol{0}_3 \\
\boldsymbol{0}_3 & \boldsymbol{0}_3 & \boldsymbol{0}_3 & \boldsymbol{B}_{5_{74}} & \boldsymbol{B}_{5_{75}} & \boldsymbol{0}_3 & \boldsymbol{0}_3 & \boldsymbol{0}_3 & \boldsymbol{0}_3 \\
\boldsymbol{0}_3 & \boldsymbol{0}_3 & \boldsymbol{0}_3 & \boldsymbol{0}_3 & \boldsymbol{0}_3 & \boldsymbol{0}_3 & \boldsymbol{0}_3 & \boldsymbol{0}_3 & \boldsymbol{0}_3 \\
\boldsymbol{0}_3 & \boldsymbol{0}_3 & \boldsymbol{0}_3 & \boldsymbol{0}_3 & \boldsymbol{0}_3 & \boldsymbol{0}_3 & \boldsymbol{0}_3 & \boldsymbol{0}_3 & \boldsymbol{0}_3
\end{bmatrix}
\tag{127}
$$

where:

$$\boldsymbol{B}_{5_{24}} = \hat{\boldsymbol{\mathcal{N}}}_{\partial_{\xi_1}\varepsilon}.\hat{\boldsymbol{\kappa}}; \quad \boldsymbol{B}_{5_{25}} = -\hat{\boldsymbol{\mathcal{N}}}_{\partial_{\xi_1}\varepsilon}; \quad \boldsymbol{B}_{5_{42}} = \hat{\boldsymbol{\mathcal{N}}}_{\varepsilon} + \left[\hat{\boldsymbol{\kappa}}, \hat{\boldsymbol{\mathcal{N}}}_{\partial_{\xi_1}\varepsilon}\right];$$

$$\boldsymbol{B}_{5_{43}} = \hat{\boldsymbol{\mathcal{N}}}_{\partial_{\xi_1}\varepsilon};$$

$$\boldsymbol{B}_{5_{44}} = -\partial_{\xi_1}\hat{\boldsymbol{\varphi}}.\hat{\boldsymbol{\mathcal{N}}}_{\partial_{\xi_1}\varepsilon}.\hat{\boldsymbol{\kappa}}; \quad \boldsymbol{B}_{5_{45}} = \partial_{\xi_1}\hat{\boldsymbol{\varphi}}.\hat{\boldsymbol{\mathcal{N}}}_{\partial_{\xi_1}\varepsilon}; \quad \boldsymbol{B}_{5_{52}} = \hat{\boldsymbol{\mathcal{N}}}_{\partial_{\xi_1}\varepsilon};$$

$$
\begin{aligned}
\boldsymbol{B}_{5_{54}} = &\left(\hat{\boldsymbol{\mathcal{N}}}_{\partial_{\xi_1}\kappa} + \left[\hat{\boldsymbol{\kappa}}, \hat{\boldsymbol{\mathcal{N}}}_{\partial^2_{\xi_1}\kappa}\right] + \hat{\boldsymbol{\kappa}}.\hat{\boldsymbol{\mathcal{N}}}_{\partial^2_{\xi_1}\kappa} + \hat{\boldsymbol{\kappa}}.\left[\hat{\boldsymbol{\kappa}}, \hat{\boldsymbol{\mathcal{N}}}_{\partial^3_{\xi_1}\kappa}\right] + \left[\hat{\boldsymbol{\kappa}}, \left[\hat{\boldsymbol{\kappa}}, \hat{\boldsymbol{\mathcal{N}}}_{\partial^3_{\xi_1}\kappa}\right]\right]\right. \\
&\left. + \hat{\boldsymbol{\kappa}}.\hat{\boldsymbol{\kappa}}.\hat{\boldsymbol{\mathcal{N}}}_{\partial^3_{\xi_1}\kappa} + \left[\partial_{\xi_1}\hat{\boldsymbol{\kappa}}, \hat{\boldsymbol{\mathcal{N}}}_{\partial^3_{\xi_1}\kappa}\right] + 2\partial_{\xi_1}\hat{\boldsymbol{\kappa}}.\hat{\boldsymbol{\mathcal{N}}}_{\partial^3_{\xi_1}\kappa}\right).\hat{\boldsymbol{\kappa}} \\
&+ \left(\hat{\boldsymbol{\mathcal{N}}}_{\partial^2_{\xi_1}\kappa} + \hat{\boldsymbol{\kappa}}.\hat{\boldsymbol{\mathcal{N}}}_{\partial^3_{\xi_1}\kappa} + 2\left[\hat{\boldsymbol{\kappa}}, \hat{\boldsymbol{\mathcal{N}}}_{\partial^3_{\xi_1}\kappa}\right]\right).\partial_{\xi_1}\hat{\boldsymbol{\kappa}} + \hat{\boldsymbol{\mathcal{N}}}_{\partial^3_{\xi_1}\kappa}.\partial^2_{\xi_1}\hat{\boldsymbol{\kappa}};
\end{aligned}
$$

$$
\begin{aligned}
\boldsymbol{B}_{5_{55}} = -&\left(\hat{\boldsymbol{\mathcal{N}}}_{\partial_{\xi_1}\kappa} + \left[\hat{\boldsymbol{\kappa}}, \hat{\boldsymbol{\mathcal{N}}}_{\partial^2_{\xi_1}\kappa}\right] + \hat{\boldsymbol{\kappa}}.\hat{\boldsymbol{\mathcal{N}}}_{\partial^2_{\xi_1}\kappa} + \hat{\boldsymbol{\kappa}}.\left[\hat{\boldsymbol{\kappa}}, \hat{\boldsymbol{\mathcal{N}}}_{\partial^3_{\xi_1}\kappa}\right] + \left[\hat{\boldsymbol{\kappa}}, \left[\hat{\boldsymbol{\kappa}}, \hat{\boldsymbol{\mathcal{N}}}_{\partial^3_{\xi_1}\kappa}\right]\right]\right. \\
&\left. + \hat{\boldsymbol{\kappa}}.\hat{\boldsymbol{\kappa}}.\hat{\boldsymbol{\mathcal{N}}}_{\partial^3_{\xi_1}\kappa} + \left[\partial_{\xi_1}\hat{\boldsymbol{\kappa}}, \hat{\boldsymbol{\mathcal{N}}}_{\partial^3_{\xi_1}\kappa}\right] + 2\partial_{\xi_1}\hat{\boldsymbol{\kappa}}.\hat{\boldsymbol{\mathcal{N}}}_{\partial^3_{\xi_1}\kappa}\right) \\
&+ \left(\hat{\boldsymbol{\mathcal{N}}}_{\partial^2_{\xi_1}\kappa} + \hat{\boldsymbol{\kappa}}.\hat{\boldsymbol{\mathcal{N}}}_{\partial^3_{\xi_1}\kappa} + 2\left[\hat{\boldsymbol{\kappa}}, \hat{\boldsymbol{\mathcal{N}}}_{\partial^3_{\xi_1}\kappa}\right]\right).\hat{\boldsymbol{\kappa}} + 2\hat{\boldsymbol{\mathcal{N}}}_{\partial^3_{\xi_1}\kappa}.\partial_{\xi_1}\hat{\boldsymbol{\kappa}};
\end{aligned}
$$

$$\boldsymbol{B}_{5_{56}} = \hat{\boldsymbol{\mathcal{N}}}_{\partial^3_{\xi_1}\kappa}.\hat{\boldsymbol{\kappa}} - \left(\hat{\boldsymbol{\mathcal{N}}}_{\partial^2_{\xi_1}\kappa} + \hat{\boldsymbol{\kappa}}.\hat{\boldsymbol{\mathcal{N}}}_{\partial^3_{\xi_1}\kappa} + 2\left[\hat{\boldsymbol{\kappa}}, \hat{\boldsymbol{\mathcal{N}}}_{\partial^3_{\xi_1}\kappa}\right]\right);$$

$$\boldsymbol{B}_{5_{57}} = -\hat{\boldsymbol{\mathcal{N}}}_{\partial^3_{\xi_1}\kappa};$$

$$\boldsymbol{B}_{5_{64}} = 3\hat{\boldsymbol{\mathcal{N}}}_{\partial^3_{\xi_1}\kappa}.\partial_{\xi_1}\hat{\boldsymbol{\kappa}} + \left(2\hat{\boldsymbol{\mathcal{N}}}_{\partial^2_{\xi_1}\kappa} + 3\left[\hat{\boldsymbol{\kappa}}, \hat{\boldsymbol{\mathcal{N}}}_{\partial^3_{\xi_1}\kappa}\right] + 3\hat{\boldsymbol{\kappa}}.\hat{\boldsymbol{\mathcal{N}}}_{\partial^3_{\xi_1}\kappa}\right).\hat{\boldsymbol{\kappa}};$$

$$\boldsymbol{B}_{5_{65}} = -\left(2\hat{\boldsymbol{\mathcal{N}}}_{\partial^2_{\xi_1}\kappa} + 3\left[\hat{\boldsymbol{\kappa}}, \hat{\boldsymbol{\mathcal{N}}}_{\partial^3_{\xi_1}\kappa}\right] + 3\hat{\boldsymbol{\kappa}}.\hat{\boldsymbol{\mathcal{N}}}_{\partial^3_{\xi_1}\kappa}\right) + 3\hat{\boldsymbol{\mathcal{N}}}_{\partial^3_{\xi_1}\kappa}.\hat{\boldsymbol{\kappa}};$$

$$\boldsymbol{B}_{5_{66}} = -3\hat{\boldsymbol{\mathcal{N}}}_{\partial^3_{\xi_1}\kappa}; \quad \boldsymbol{B}_{5_{74}} = 3\hat{\boldsymbol{\mathcal{N}}}_{\partial^3_{\xi_1}\kappa}.\hat{\boldsymbol{\kappa}}; \quad \boldsymbol{B}_{5_{75}} = -3\hat{\boldsymbol{\mathcal{N}}}_{\partial^3_{\xi_1}\kappa}.$$

A.2.6. Matrix $\boldsymbol{B}_7$

$$\boldsymbol{B}_7=\begin{bmatrix}\mathbf{0}_3&\mathbf{0}_3&\mathbf{0}_3&\mathbf{0}_3&\mathbf{0}_3&\mathbf{0}_3&\mathbf{0}_3&\mathbf{0}_3&\mathbf{0}_3\\ \mathbf{0}_3&\mathbf{0}_3&\mathbf{0}_3&\mathbf{0}_3&\mathbf{0}_3&\mathbf{0}_3&\mathbf{0}_3&\mathbf{0}_3&\mathbf{0}_3\\ \mathbf{0}_3&\mathbf{0}_3&\mathbf{0}_3&\mathbf{0}_3&\mathbf{0}_3&\mathbf{0}_3&\mathbf{0}_3&\mathbf{0}_3&\mathbf{0}_3\\ \mathbf{0}_3&\boldsymbol{B}_{7_{42}}&\mathbf{0}_3&\mathbf{0}_3&\mathbf{0}_3&\mathbf{0}_3&\mathbf{0}_3&\mathbf{0}_3&\mathbf{0}_3\\ \mathbf{0}_3&\mathbf{0}_3&\mathbf{0}_3&\boldsymbol{B}_{7_{54}}&\boldsymbol{B}_{7_{55}}&\boldsymbol{B}_{7_{56}}&\mathbf{0}_3&\mathbf{0}_3&\mathbf{0}_3\\ \mathbf{0}_3&\mathbf{0}_3&\mathbf{0}_3&\boldsymbol{B}_{7_{64}}&\boldsymbol{B}_{7_{65}}&\mathbf{0}_3&\mathbf{0}_3&\mathbf{0}_3&\mathbf{0}_3\\ \mathbf{0}_3&\mathbf{0}_3&\mathbf{0}_3&\mathbf{0}_3&\mathbf{0}_3&\mathbf{0}_3&\mathbf{0}_3&\mathbf{0}_3&\mathbf{0}_3\\ \mathbf{0}_3&\mathbf{0}_3&\mathbf{0}_3&\mathbf{0}_3&\mathbf{0}_3&\mathbf{0}_3&\mathbf{0}_3&\mathbf{0}_3&\mathbf{0}_3\\ \mathbf{0}_3&\mathbf{0}_3&\mathbf{0}_3&\mathbf{0}_3&\mathbf{0}_3&\mathbf{0}_3&\mathbf{0}_3&\mathbf{0}_3&\mathbf{0}_3\end{bmatrix}. \tag{128}$$

where:

$$\begin{aligned}
\boldsymbol{B}_{7_{42}} &= \hat{\boldsymbol{N}}_{\boldsymbol{\varepsilon}};\\
\boldsymbol{B}_{7_{54}} &= \left(\hat{\boldsymbol{N}}_{\partial_{\xi_1}\boldsymbol{\kappa}}+\left[\hat{\boldsymbol{\kappa}},\hat{\boldsymbol{N}}_{\partial^2_{\xi_1}\boldsymbol{\kappa}}\right]+\hat{\boldsymbol{\kappa}}.\hat{\boldsymbol{N}}_{\partial^2_{\xi_1}\boldsymbol{\kappa}}\right).\hat{\boldsymbol{\kappa}}+\hat{\boldsymbol{N}}_{\partial^2_{\xi_1}\boldsymbol{\kappa}}.\partial_{\xi_1}\hat{\boldsymbol{\kappa}};\\
\boldsymbol{B}_{7_{55}} &= \hat{\boldsymbol{N}}_{\partial^2_{\xi_1}\boldsymbol{\kappa}}.\hat{\boldsymbol{\kappa}}-\left(\hat{\boldsymbol{N}}_{\partial_{\xi_1}\boldsymbol{\kappa}}+\left[\hat{\boldsymbol{\kappa}},\hat{\boldsymbol{N}}_{\partial^2_{\xi_1}\boldsymbol{\kappa}}\right]+\hat{\boldsymbol{\kappa}}.\hat{\boldsymbol{N}}_{\partial^2_{\xi_1}\boldsymbol{\kappa}}\right);\\
\boldsymbol{B}_{7_{56}} &= -\hat{\boldsymbol{N}}_{\partial^2_{\xi_1}\boldsymbol{\kappa}};\\
\boldsymbol{B}_{7_{64}} &= 2\hat{\boldsymbol{N}}_{\partial^2_{\xi_1}\boldsymbol{\kappa}}.\hat{\boldsymbol{\kappa}};\\
\boldsymbol{B}_{7_{65}} &= -2\hat{\boldsymbol{N}}_{\partial^2_{\xi_1}\boldsymbol{\kappa}}.
\end{aligned}$$

A.2.7. Matrix $\mathbb{B}_I$

$$\mathbb{B}_I^T=\begin{bmatrix}\boldsymbol{I}_3&\partial_{\xi_1}N_I.\boldsymbol{I}_3&\partial^2_{\xi_1}N_I.\boldsymbol{I}_3&\mathbf{0}_3&\mathbf{0}_3&\mathbf{0}_3&\mathbf{0}_3&\mathbf{0}_3&\mathbf{0}_1&\mathbf{0}_1&\mathbf{0}_1\\ \mathbf{0}_3&\mathbf{0}_3&\mathbf{0}_3&\boldsymbol{I}_3&\partial_{\xi_1}N_I.\boldsymbol{I}_3&\partial^2_{\xi_1}N_I.\boldsymbol{I}_3&\partial^3_{\xi_1}N_I.\boldsymbol{I}_3&\partial^4_{\xi_1}N_I.\boldsymbol{I}_3&\mathbf{0}_1&\mathbf{0}_1&\mathbf{0}_1\\ \mathbf{0}_1^T&\mathbf{0}_1^T&\mathbf{0}_1^T&\mathbf{0}_1^T&\mathbf{0}_1^T&\mathbf{0}_1^T&\mathbf{0}_1^T&\mathbf{0}_1^T&1&\partial_{\xi_1}N_I&\partial^2_{\xi_1}N_I\end{bmatrix} \tag{129}$$

Here, $\partial^n_{\xi_1}N_I.\boldsymbol{I}_3=\text{diagonal}\left[\partial^n_{\xi_1}N_I,\partial^n_{\xi_1}N_I,\partial^n_{\xi_1}N_I\right]$

A.3. Force vectors

A.3.1. Material form of reduced section forces

$$\begin{aligned}
\overline{\boldsymbol{\mathcal{N}}}_{\boldsymbol{\varepsilon}} &= \int_{B_0}\left(\overline{\boldsymbol{L}}^{\lambda_1}_{\boldsymbol{\varepsilon}}+\overline{\boldsymbol{M}}^{\lambda_1}_{\boldsymbol{\varepsilon}}\right)^T.\overline{\boldsymbol{P}}_1+\left(\overline{\boldsymbol{L}}^{\lambda_2}_{\boldsymbol{\varepsilon}}\right)^T.\overline{\boldsymbol{P}}_2+\left(\overline{\boldsymbol{L}}^{\lambda_3}_{\boldsymbol{\varepsilon}}\right)^T.\overline{\boldsymbol{P}}_3\mathrm{d}B_0\\
\overline{\boldsymbol{\mathcal{N}}}_{\partial_{\xi_1}\boldsymbol{\varepsilon}} &= \int_{B_0}\left(\overline{\boldsymbol{L}}^{\lambda_1}_{\partial_{\xi_1}\boldsymbol{\varepsilon}}\right)^T.\overline{\boldsymbol{P}}_1\mathrm{d}B_0\\
\overline{\boldsymbol{\mathcal{N}}}_{\boldsymbol{\kappa}} &= \int_{B_0}\left(\overline{\boldsymbol{L}}^{\lambda_1}_{\boldsymbol{\kappa}}+\overline{\boldsymbol{M}}^{\lambda_1}_{\boldsymbol{\kappa}}\right)^T.\overline{\boldsymbol{P}}_1+\left(\overline{\boldsymbol{L}}^{\lambda_2}_{\boldsymbol{\kappa}}\right)^T.\overline{\boldsymbol{P}}_2+\left(\overline{\boldsymbol{L}}^{\lambda_3}_{\boldsymbol{\kappa}}\right)^T.\overline{\boldsymbol{P}}_3\mathrm{d}B_0\\
\overline{\boldsymbol{\mathcal{N}}}_{\partial_{\xi_1}\boldsymbol{\kappa}} &= \int_{B_0}\left(\overline{\boldsymbol{L}}^{\lambda_1}_{\partial_{\xi_1}\boldsymbol{\kappa}}+\overline{\boldsymbol{M}}^{\lambda_1}_{\partial_{\xi_1}\boldsymbol{\kappa}}\right)^T.\overline{\boldsymbol{P}}_1+\left(\overline{\boldsymbol{L}}^{\lambda_2}_{\partial_{\xi_1}\boldsymbol{\kappa}}\right)^T.\overline{\boldsymbol{P}}_2+\left(\overline{\boldsymbol{L}}^{\lambda_3}_{\partial_{\xi_1}\boldsymbol{\kappa}}\right)^T.\overline{\boldsymbol{P}}_3\mathrm{d}B_0\\
\overline{\boldsymbol{\mathcal{N}}}_{\partial^2_{\xi_1}\boldsymbol{\kappa}} &= \int_{B_0}\left(\overline{\boldsymbol{L}}^{\lambda_1}_{\partial^2_{\xi_1}\boldsymbol{\kappa}}+\overline{\boldsymbol{M}}^{\lambda_1}_{\partial^2_{\xi_1}\boldsymbol{\kappa}}\right)^T.\overline{\boldsymbol{P}}_1+\left(\overline{\boldsymbol{L}}^{\lambda_2}_{\partial^2_{\xi_1}\boldsymbol{\kappa}}\right)^T.\overline{\boldsymbol{P}}_2+\left(\overline{\boldsymbol{L}}^{\lambda_3}_{\partial^2_{\xi_1}\boldsymbol{\kappa}}\right)^T.\overline{\boldsymbol{P}}_3\mathrm{d}B_0\\
\overline{\boldsymbol{\mathcal{N}}}_{\partial^3_{\xi_1}\boldsymbol{\kappa}} &= \int_{B_0}\left(\overline{\boldsymbol{L}}^{\lambda_1}_{\partial^3_{\xi_1}\boldsymbol{\kappa}}\right)^T.\overline{\boldsymbol{P}}_1\mathrm{d}B_0\\
\overline{N}_p &= \int_{B_0}\overline{\boldsymbol{M}}^{\lambda_1}_p.\overline{\boldsymbol{P}}_1+\overline{\boldsymbol{L}}^{\lambda_2}_p.\overline{\boldsymbol{P}}_2+\overline{\boldsymbol{L}}^{\lambda_3}_p.\overline{\boldsymbol{P}}_3\mathrm{d}B_0\\
\overline{N}_{\partial_{\xi_1}p} &= \int_{B_0}\left(\overline{\boldsymbol{L}}^{\lambda_1}_{\partial_{\xi_1}p}+\overline{\boldsymbol{M}}^{\lambda_1}_{\partial_{\xi_1}p}\right).\overline{\boldsymbol{P}}_1+\overline{\boldsymbol{L}}^{\lambda_2}_{\partial_{\xi_1}p}.\overline{\boldsymbol{P}}_2+\overline{\boldsymbol{L}}^{\lambda_3}_{\partial_{\xi_1}p}.\overline{\boldsymbol{P}}_3\mathrm{d}B_0\\
\overline{N}_{\partial^2_{\xi_1}p} &= \int_{B_0}\overline{\boldsymbol{L}}^{\lambda_1}_{\partial^2_{\xi_1}p}.\overline{\boldsymbol{P}}_1\mathrm{d}B_0.
\end{aligned} \tag{130}$$

A.3.2. End boundary forces, and reduced inertial forces

$$\begin{aligned}
\boldsymbol{B}_{\boldsymbol{\varphi}} &= \int_{B_0}\left(\boldsymbol{L}^{\lambda_1}_{\boldsymbol{\varepsilon}}\right)^T.\boldsymbol{P}_1\mathrm{d}B_0\\
\boldsymbol{B}_{\boldsymbol{\alpha}} &= \int_{B_0}\left(\boldsymbol{L}^{\lambda_1}_{\boldsymbol{\kappa}}\right)^T.\boldsymbol{P}_1\mathrm{d}B_0\\
\boldsymbol{B}_{\boldsymbol{\varepsilon}} &= \int_{B_0}\left(\boldsymbol{L}^{\lambda_1}_{\partial_{\xi_1}\boldsymbol{\varepsilon}}\right)^T.\boldsymbol{P}_1\mathrm{d}B_0\\
\boldsymbol{B}_{\boldsymbol{\kappa}} &= \int_{B_0}\left(\boldsymbol{L}^{\lambda_1}_{\partial_{\xi_1}\boldsymbol{\kappa}}\right)^T.\boldsymbol{P}_1\mathrm{d}B_0\\
\boldsymbol{B}_{\partial_{\xi_1}\boldsymbol{\kappa}} &= \int_{B_0}\left(\boldsymbol{L}^{\lambda_1}_{\partial^2_{\xi_1}\boldsymbol{\kappa}}\right)^T.\boldsymbol{P}_1\mathrm{d}B_0\\
\boldsymbol{B}_{\partial^2_{\xi_1}\boldsymbol{\kappa}} &= \int_{B_0}\left(\boldsymbol{L}^{\lambda_1}_{\partial^3_{\xi_1}\boldsymbol{\kappa}}\right)^T.\boldsymbol{P}_1\mathrm{d}B_0\\
B_p &= \int_{B_0}\boldsymbol{L}^{\lambda_1}_{\partial_{\xi_1}p}.\boldsymbol{P}_1\mathrm{d}B_0\\
B_{\partial_{\xi_1}p} &= \int_{B_0}\boldsymbol{L}^{\lambda_1}_{\partial^2_{\xi_1}p}.\boldsymbol{P}_1\mathrm{d}B_0
\end{aligned} \tag{131}$$

$$\begin{aligned}
\boldsymbol{F}_{\boldsymbol{\varphi}} &= \int_{\Omega_0}\rho_0\left(\boldsymbol{L}^{\lambda_1}_{\boldsymbol{\varepsilon}}\right)^T.\partial^2_t\boldsymbol{R}\mathrm{d}\Omega_0\\
\boldsymbol{F}_{\boldsymbol{\alpha}} &= \int_{\Omega_0}\rho_0\left(\boldsymbol{L}^{\lambda_1}_{\boldsymbol{\kappa}}\right)^T.\partial^2_t\boldsymbol{R}\mathrm{d}\Omega_0\\
\boldsymbol{F}_{\boldsymbol{\varepsilon}} &= \int_{\Omega_0}\rho_0\left(\boldsymbol{L}^{\lambda_1}_{\partial_{\xi_1}\boldsymbol{\varepsilon}}\right)^T.\partial^2_t\boldsymbol{R}\mathrm{d}\Omega_0\\
\boldsymbol{F}_{\boldsymbol{\kappa}} &= \int_{\Omega_0}\rho_0\left(\boldsymbol{L}^{\lambda_1}_{\partial_{\xi_1}\boldsymbol{\kappa}}\right)^T.\partial^2_t\boldsymbol{R}\mathrm{d}\Omega_0\\
\boldsymbol{F}_{\partial_{\xi_1}\boldsymbol{\kappa}} &= \int_{\Omega_0}\rho_0\left(\boldsymbol{L}^{\lambda_1}_{\partial^2_{\xi_1}\boldsymbol{\kappa}}\right)^T.\partial^2_t\boldsymbol{R}\mathrm{d}\Omega_0\\
\boldsymbol{F}_{\partial^2_{\xi_1}\boldsymbol{\kappa}} &= \int_{\Omega_0}\rho_0\left(\boldsymbol{L}^{\lambda_1}_{\partial^3_{\xi_1}\boldsymbol{\kappa}}\right)^T.\partial^2_t\boldsymbol{R}\mathrm{d}\Omega_0\\
F_p &= \int_{\Omega_0}\rho_0\boldsymbol{L}^{\lambda_1}_{\partial_{\xi_1}p}.\partial^2_t\boldsymbol{R}\mathrm{d}\Omega_0\\
F_{\partial_{\xi_1}p} &= \int_{\Omega_0}\rho_0\boldsymbol{L}^{\lambda_1}_{\partial^2_{\xi_1}p}.\partial^2_t\boldsymbol{R}\mathrm{d}\Omega_0
\end{aligned} \tag{132}$$

A.3.3. Reduced external forces due to surface traction and body force

$$\begin{aligned}
\boldsymbol{N}^{\mathrm{st}}_{\boldsymbol{\varphi}} &= \int_{\Gamma_0}\left(\boldsymbol{L}^{\lambda_1}_{\boldsymbol{\varepsilon}}\right)^T.(\boldsymbol{P}.\boldsymbol{N})\mathrm{d}\Gamma_0\\
\boldsymbol{N}^{\mathrm{st}}_{\boldsymbol{\alpha}} &= \int_{\Gamma_0}\left(\boldsymbol{L}^{\lambda_1}_{\boldsymbol{\kappa}}\right)^T.(\boldsymbol{P}.\boldsymbol{N})\mathrm{d}\Gamma_0\\
\boldsymbol{N}^{\mathrm{st}}_{\boldsymbol{\varepsilon}} &= \int_{\Gamma_0}\left(\boldsymbol{L}^{\lambda_1}_{\partial_{\xi_1}\boldsymbol{\varepsilon}}\right)^T.(\boldsymbol{P}.\boldsymbol{N})\mathrm{d}\Gamma_0\\
\boldsymbol{N}^{\mathrm{st}}_{\boldsymbol{\kappa}} &= \int_{\Gamma_0}\left(\boldsymbol{L}^{\lambda_1}_{\partial_{\xi_1}\boldsymbol{\kappa}}\right)^T.(\boldsymbol{P}.\boldsymbol{N})\mathrm{d}\Gamma_0\\
\boldsymbol{N}^{\mathrm{st}}_{\partial_{\xi_1}\boldsymbol{\kappa}} &= \int_{\Gamma_0}\left(\boldsymbol{L}^{\lambda_1}_{\partial^2_{\xi_1}\boldsymbol{\kappa}}\right)^T.(\boldsymbol{P}.\boldsymbol{N})\mathrm{d}\Gamma_0\\
\boldsymbol{N}^{\mathrm{st}}_{\partial^2_{\xi_1}\boldsymbol{\kappa}} &= \int_{\Gamma_0}\left(\boldsymbol{L}^{\lambda_1}_{\partial^3_{\xi_1}\boldsymbol{\kappa}}\right)^T.(\boldsymbol{P}.\boldsymbol{N})\mathrm{d}\Gamma_0\\
N^{\mathrm{st}}_p &= \int_{\Gamma_0}\boldsymbol{L}^{\lambda_1}_{\partial_{\xi_1}p}.(\boldsymbol{P}.\boldsymbol{N})\mathrm{d}\Gamma_0\\
N^{\mathrm{st}}_{\partial_{\xi_1}p} &= \int_{\Gamma_0}\boldsymbol{L}^{\lambda_1}_{\partial^2_{\xi_1}p}.(\boldsymbol{P}.\boldsymbol{N})\mathrm{d}\Gamma_0
\end{aligned} \tag{133}$$

$$\begin{aligned}
\boldsymbol{N}^{\mathrm{b}}_{\boldsymbol{\varphi}} &= \int_{B_0}\rho_0\left(\boldsymbol{L}^{\lambda_1}_{\boldsymbol{\varepsilon}}\right)^T.\boldsymbol{b}\mathrm{d}B_0\\
\boldsymbol{N}^{\mathrm{b}}_{\boldsymbol{\alpha}} &= \int_{B_0}\rho_0\left(\boldsymbol{L}^{\lambda_1}_{\boldsymbol{\kappa}}\right)^T.\boldsymbol{b}\mathrm{d}B_0\\
\boldsymbol{N}^{\mathrm{b}}_{\boldsymbol{\varepsilon}} &= \int_{B_0}\rho_0\left(\boldsymbol{L}^{\lambda_1}_{\partial_{\xi_1}\boldsymbol{\varepsilon}}\right)^T.\boldsymbol{b}\mathrm{d}B_0\\
\boldsymbol{N}^{\mathrm{b}}_{\boldsymbol{\kappa}} &= \int_{B_0}\rho_0\left(\boldsymbol{L}^{\lambda_1}_{\partial_{\xi_1}\boldsymbol{\kappa}}\right)^T.\boldsymbol{b}\mathrm{d}B_0\\
\boldsymbol{N}^{\mathrm{b}}_{\partial_{\xi_1}\boldsymbol{\kappa}} &= \int_{B_0}\rho_0\left(\boldsymbol{L}^{\lambda_1}_{\partial^2_{\xi_1}\boldsymbol{\kappa}}\right)^T.\boldsymbol{b}\mathrm{d}B_0\\
\boldsymbol{N}^{\mathrm{b}}_{\partial^2_{\xi_1}\boldsymbol{\kappa}} &= \int_{B_0}\rho_0\left(\boldsymbol{L}^{\lambda_1}_{\partial^3_{\xi_1}\boldsymbol{\kappa}}\right)^T.\boldsymbol{b}\mathrm{d}B_0\\
N^{\mathrm{b}}_p &= \int_{B_0}\rho_0\boldsymbol{L}^{\lambda_1}_{\partial_{\xi_1}p}.\boldsymbol{b}\mathrm{d}B_0\\
N^{\mathrm{b}}_{\partial_{\xi_1}p} &= \int_{B_0}\rho_0\boldsymbol{L}^{\lambda_1}_{\partial^2_{\xi_1}p}.\boldsymbol{b}\mathrm{d}B_0
\end{aligned} \tag{134}$$

A.3.4. Nodal internal force vector

$$\boldsymbol{f}^e_{\text{int}I} = \int_{\xi^e_{1a}}^{\xi^e_{1b}} \mathbb{B}_I^T \boldsymbol{B}_1^{eT} \boldsymbol{\mathcal{N}}^e_{\text{int}} \mathrm{d}\xi_1 = \left[\boldsymbol{f}^e_{\text{int}I1};\ \ \boldsymbol{f}^e_{\text{int}I2};\ \ \boldsymbol{f}^e_{\text{int}I3}\right]. \tag{135}$$

Here,

$$f^e_{\text{int}I1} = \int_{\xi^e_{1a}}^{\xi^e_{1b}} \left(\partial_{\xi_1} N_I \left(\boldsymbol{\mathcal{N}}^e_{\boldsymbol{\varepsilon}} + \hat{\boldsymbol{\kappa}}.\boldsymbol{\mathcal{N}}^e_{\partial_{\xi_1}\boldsymbol{\varepsilon}}\right) + \partial^2_{\xi_1} N_I \boldsymbol{\mathcal{N}}^e_{\partial_{\xi_1}\boldsymbol{\varepsilon}}\right)\mathrm{d}\xi_1;$$

$$\begin{aligned} f^e_{\text{int}I2} = \int_{\xi^e_{1a}}^{\xi^e_{1b}} & \left(N_I\left(-\partial_{\xi_1}\hat{\boldsymbol{\varphi}}.\boldsymbol{\mathcal{N}}^e_{\boldsymbol{\varepsilon}} - \left(\partial^2_{\xi_1}\hat{\boldsymbol{\varphi}} + \partial_{\xi_1}\hat{\boldsymbol{\varphi}}.\hat{\boldsymbol{\kappa}}\right).\boldsymbol{\mathcal{N}}^e_{\partial_{\xi_1}\boldsymbol{\varepsilon}}\right)\right. \\ & +\partial_{\xi_1} N_I.\left(\boldsymbol{\mathcal{N}}^e_{\boldsymbol{\kappa}} - \partial_{\xi_1}\hat{\boldsymbol{\varphi}}.\boldsymbol{\mathcal{N}}^e_{\partial_{\xi_1}\boldsymbol{\varepsilon}} + \hat{\boldsymbol{\kappa}}.\boldsymbol{\mathcal{N}}^e_{\partial_{\xi_1}\boldsymbol{\kappa}} + \left(\hat{\boldsymbol{\kappa}}.\hat{\boldsymbol{\kappa}} + \partial_{\xi_1}\hat{\boldsymbol{\kappa}}\right).\boldsymbol{\mathcal{N}}^e_{\partial^2_{\xi_1}\boldsymbol{\kappa}}\right. \\ & \left.+\left(\hat{\boldsymbol{\kappa}}.\partial_{\xi_1}\hat{\boldsymbol{\kappa}} + 2\partial_{\xi_1}\hat{\boldsymbol{\kappa}}.\hat{\boldsymbol{\kappa}} + \partial^2_{\xi_1}\hat{\boldsymbol{\kappa}} + \hat{\boldsymbol{\kappa}}.\hat{\boldsymbol{\kappa}}.\hat{\boldsymbol{\kappa}}\right).\boldsymbol{\mathcal{N}}^e_{\partial^3_{\xi_1}\boldsymbol{\kappa}}\right) \\ & + \partial^2_{\xi_1} N_I\left(\boldsymbol{\mathcal{N}}^e_{\partial_{\xi_1}\boldsymbol{\kappa}} + 2\hat{\boldsymbol{\kappa}}.\boldsymbol{\mathcal{N}}^e_{\partial^2_{\xi_1}\boldsymbol{\kappa}} + 3\left(\hat{\boldsymbol{\kappa}}.\hat{\boldsymbol{\kappa}} + \partial_{\xi_1}\hat{\boldsymbol{\kappa}}\right).\boldsymbol{\mathcal{N}}^e_{\partial^3_{\xi_1}\boldsymbol{\kappa}}\right) \\ & \left.+\partial^3_{\xi_1} N_I\left(\boldsymbol{\mathcal{N}}^e_{\partial^2_{\xi_1}\boldsymbol{\kappa}} + 3\hat{\boldsymbol{\kappa}}.\boldsymbol{\mathcal{N}}^e_{\partial^3_{\xi_1}\boldsymbol{\kappa}}\right) + \partial^4_{\xi_1} N_I.\boldsymbol{\mathcal{N}}^e_{\partial^3_{\xi_1}\boldsymbol{\kappa}}\right)\mathrm{d}\xi_1. \end{aligned}$$

$$f^e_{\text{int}I3} = \int_{\xi^e_{1a}}^{\xi^e_{1b}} \left(N_I.N^e_p + \partial_{\xi_1} N_I.N^e_{\partial_{\xi_1}p} + \partial^2_{\xi_1} N_I.N^e_{\partial^2_{\xi_1}p}\right)\mathrm{d}\xi_1.$$

A.3.5. Nodal external force vector

$$\begin{aligned} \boldsymbol{f}^e_{\text{ext}I}(x) &= \int_{\xi^e_{1a}}^{\xi^e_{1b}} \mathbb{B}_I^T \boldsymbol{B}_3 \boldsymbol{\mathcal{N}}^e_{\text{ext}}(x)\mathrm{d}\xi_1 = \left[\boldsymbol{f}^e_{\text{ext}I1};\ \ \boldsymbol{f}^e_{\text{ext}I2};\ \ \boldsymbol{f}^e_{\text{ext}I3}\right] \\ &= \int_{\xi^e_{1a}}^{\xi^e_{1b}} \begin{bmatrix} N_I.\boldsymbol{N}^e_{\boldsymbol{\varphi}}(x) + \partial_{\xi_1} N_I.\boldsymbol{N}^e_{\boldsymbol{\varepsilon}}(x) \\ \left(N_I.\left(\boldsymbol{N}^e_{\boldsymbol{\alpha}}(x) - \partial_{\xi_1}\hat{\boldsymbol{\varphi}}.\boldsymbol{N}^e_{\boldsymbol{\varepsilon}}(x)\right) + \partial^2_{\xi_1} N_I.\boldsymbol{N}^e_{\partial^2_{\xi_1}\boldsymbol{\kappa}}(x)\right. \\ \left.+\partial_{\xi_1} N_I.\left(\boldsymbol{N}^e_{\boldsymbol{\kappa}}(x) + \hat{\boldsymbol{\kappa}}.\boldsymbol{N}^e_{\partial_{\xi_1}\boldsymbol{\kappa}}(x) + \left(\hat{\boldsymbol{\kappa}}.\hat{\boldsymbol{\kappa}} + \partial_{\xi_1}\hat{\boldsymbol{\kappa}}\right).\boldsymbol{N}^e_{\partial^2_{\xi_1}\boldsymbol{\kappa}}(x)\right)\right. \\ N_I.N^e_p(x) + \partial_{\xi_1} N_I.N^e_{\partial_{\xi_1}p}(x) \end{bmatrix}\mathrm{d}\xi_1 \end{aligned} \tag{136}$$

A.4. Constitutive law

Define: $\tilde{\lambda} = 2G + \lambda$.

$$\overline{\mathbb{C}}_{11} = \begin{bmatrix} \tilde{\lambda} & 0 & 0 \\ 0 & G & 0 \\ 0 & 0 & G \end{bmatrix};\quad \overline{\mathbb{C}}_{12} = \begin{bmatrix} 0 & \lambda & 0 \\ G & 0 & 0 \\ 0 & 0 & 0 \end{bmatrix};\quad \overline{\mathbb{C}}_{13} = \begin{bmatrix} 0 & 0 & \lambda \\ 0 & 0 & 0 \\ G & 0 & 0 \end{bmatrix};$$

$$\overline{\mathbb{C}}_{21} = \begin{bmatrix} 0 & G & 0 \\ \lambda & 0 & 0 \\ 0 & 0 & 0 \end{bmatrix};\quad \overline{\mathbb{C}}_{22} = \begin{bmatrix} G & 0 & 0 \\ 0 & \tilde{\lambda} & 0 \\ 0 & 0 & G \end{bmatrix};\quad \overline{\mathbb{C}}_{23} = \begin{bmatrix} 0 & 0 & 0 \\ 0 & 0 & \lambda \\ 0 & G & 0 \end{bmatrix};$$

$$\overline{\mathbb{C}}_{31} = \begin{bmatrix} 0 & 0 & G \\ 0 & 0 & 0 \\ \lambda & 0 & 0 \end{bmatrix};\quad \overline{\mathbb{C}}_{32} = \begin{bmatrix} 0 & 0 & 0 \\ 0 & 0 & G \\ 0 & \lambda & 0 \end{bmatrix};\quad \overline{\mathbb{C}}_{33} = \begin{bmatrix} G & 0 & 0 \\ 0 & G & 0 \\ 0 & 0 & \tilde{\lambda} \end{bmatrix}. \tag{137}$$

The reduced force vectors are related to the mid-curve strains as:

$$\begin{aligned}
&\overline{\boldsymbol{\mathcal{N}}}_{\boldsymbol{\varepsilon}} = \overline{\mathbb{C}}_{11}.\overline{\boldsymbol{\varepsilon}} + \overline{\mathbb{C}}_{12}.\partial_{\xi_1}\overline{\boldsymbol{\varepsilon}} + \overline{\mathbb{C}}_{13}.\overline{\boldsymbol{\kappa}} + \overline{\mathbb{C}}_{14}.\partial_{\xi_1}\overline{\boldsymbol{\kappa}} + \overline{\mathbb{C}}_{15}.\partial^2_{\xi_1}\overline{\boldsymbol{\kappa}} + \overline{\mathbb{C}}_{16}.\partial^3_{\xi_1}\overline{\boldsymbol{\kappa}} + p.\overline{\mathbb{C}}_{17} + \partial_{\xi_1} p.\overline{\mathbb{C}}_{18} + \partial^2_{\xi_1} p.\overline{\mathbb{C}}_{19};\\
&\overline{\boldsymbol{\mathcal{N}}}_{\partial_{\xi_1}\boldsymbol{\varepsilon}} = \overline{\mathbb{C}}_{21}.\overline{\boldsymbol{\varepsilon}} + \overline{\mathbb{C}}_{22}.\partial_{\xi_1}\overline{\boldsymbol{\varepsilon}} + \overline{\mathbb{C}}_{23}.\overline{\boldsymbol{\kappa}} + \overline{\mathbb{C}}_{24}.\partial_{\xi_1}\overline{\boldsymbol{\kappa}} + \overline{\mathbb{C}}_{25}.\partial^2_{\xi_1}\overline{\boldsymbol{\kappa}} + \overline{\mathbb{C}}_{26}.\partial^3_{\xi_1}\overline{\boldsymbol{\kappa}} + p.\overline{\mathbb{C}}_{27} + \partial_{\xi_1} p.\overline{\mathbb{C}}_{28} + \partial^2_{\xi_1} p.\overline{\mathbb{C}}_{29};\\
&\overline{\boldsymbol{\mathcal{N}}}_{\boldsymbol{\kappa}} = \overline{\mathbb{C}}_{31}.\overline{\boldsymbol{\varepsilon}} + \overline{\mathbb{C}}_{32}.\partial_{\xi_1}\overline{\boldsymbol{\varepsilon}} + \overline{\mathbb{C}}_{33}.\overline{\boldsymbol{\kappa}} + \overline{\mathbb{C}}_{34}.\partial_{\xi_1}\overline{\boldsymbol{\kappa}} + \overline{\mathbb{C}}_{35}.\partial^2_{\xi_1}\overline{\boldsymbol{\kappa}} + \overline{\mathbb{C}}_{36}.\partial^3_{\xi_1}\overline{\boldsymbol{\kappa}} + p.\overline{\mathbb{C}}_{37} + \partial_{\xi_1} p.\overline{\mathbb{C}}_{38} + \partial^2_{\xi_1} p.\overline{\mathbb{C}}_{39};\\
&\overline{\boldsymbol{\mathcal{N}}}_{\partial_{\xi_1}\boldsymbol{\kappa}} = \overline{\mathbb{C}}_{41}.\overline{\boldsymbol{\varepsilon}} + \overline{\mathbb{C}}_{42}.\partial_{\xi_1}\overline{\boldsymbol{\varepsilon}} + \overline{\mathbb{C}}_{43}.\overline{\boldsymbol{\kappa}} + \overline{\mathbb{C}}_{44}.\partial_{\xi_1}\overline{\boldsymbol{\kappa}} + \overline{\mathbb{C}}_{45}.\partial^2_{\xi_1}\overline{\boldsymbol{\kappa}} + \overline{\mathbb{C}}_{46}.\partial^3_{\xi_1}\overline{\boldsymbol{\kappa}} + p.\overline{\mathbb{C}}_{47} + \partial_{\xi_1} p.\overline{\mathbb{C}}_{48} + \partial^2_{\xi_1} p.\overline{\mathbb{C}}_{49};\\
&\overline{\boldsymbol{\mathcal{N}}}_{\partial_{\xi_1}\boldsymbol{\kappa}} = \overline{\mathbb{C}}_{51}.\overline{\boldsymbol{\varepsilon}} + \overline{\mathbb{C}}_{52}.\partial_{\xi_1}\overline{\boldsymbol{\varepsilon}} + \overline{\mathbb{C}}_{53}.\overline{\boldsymbol{\kappa}} + \overline{\mathbb{C}}_{54}.\partial_{\xi_1}\overline{\boldsymbol{\kappa}} + \overline{\mathbb{C}}_{55}.\partial^2_{\xi_1}\overline{\boldsymbol{\kappa}} + \overline{\mathbb{C}}_{56}.\partial^3_{\xi_1}\overline{\boldsymbol{\kappa}} + p.\overline{\mathbb{C}}_{57} + \partial_{\xi_1} p.\overline{\mathbb{C}}_{58} + \partial^2_{\xi_1} p.\overline{\mathbb{C}}_{59};\\
&\overline{\boldsymbol{\mathcal{N}}}_{\partial^2_{\xi_1}\boldsymbol{\kappa}} = \overline{\mathbb{C}}_{61}.\overline{\boldsymbol{\varepsilon}} + \overline{\mathbb{C}}_{62}.\partial_{\xi_1}\overline{\boldsymbol{\varepsilon}} + \overline{\mathbb{C}}_{63}.\overline{\boldsymbol{\kappa}} + \overline{\mathbb{C}}_{64}.\partial_{\xi_1}\overline{\boldsymbol{\kappa}} + \overline{\mathbb{C}}_{65}.\partial^2_{\xi_1}\overline{\boldsymbol{\kappa}} + \overline{\mathbb{C}}_{66}.\partial^3_{\xi_1}\overline{\boldsymbol{\kappa}} + p.\overline{\mathbb{C}}_{67} + \partial_{\xi_1} p.\overline{\mathbb{C}}_{68} + \partial^2_{\xi_1} p.\overline{\mathbb{C}}_{69};\\
&\overline{\boldsymbol{\mathcal{N}}}_{p} = \overline{\mathbb{C}}_{71}.\overline{\boldsymbol{\varepsilon}} + \overline{\mathbb{C}}_{72}.\partial_{\xi_1}\overline{\boldsymbol{\varepsilon}} + \overline{\mathbb{C}}_{73}.\overline{\boldsymbol{\kappa}} + \overline{\mathbb{C}}_{74}.\partial_{\xi_1}\overline{\boldsymbol{\kappa}} + \overline{\mathbb{C}}_{75}.\partial^2_{\xi_1}\overline{\boldsymbol{\kappa}} + \overline{\mathbb{C}}_{76}.\partial^3_{\xi_1}\overline{\boldsymbol{\kappa}} + p.\overline{\mathbb{C}}_{77} + \partial_{\xi_1} p.\overline{\mathbb{C}}_{78} + \partial^2_{\xi_1} p.\overline{\mathbb{C}}_{79};\\
&\overline{\boldsymbol{\mathcal{N}}}_{\partial_{\xi_1} p} = \overline{\mathbb{C}}_{81}.\overline{\boldsymbol{\varepsilon}} + \overline{\mathbb{C}}_{82}.\partial_{\xi_1}\overline{\boldsymbol{\varepsilon}} + \overline{\mathbb{C}}_{83}.\overline{\boldsymbol{\kappa}} + \overline{\mathbb{C}}_{84}.\partial_{\xi_1}\overline{\boldsymbol{\kappa}} + \overline{\mathbb{C}}_{85}.\partial^2_{\xi_1}\overline{\boldsymbol{\kappa}} + \overline{\mathbb{C}}_{86}.\partial^3_{\xi_1}\overline{\boldsymbol{\kappa}} + p.\overline{\mathbb{C}}_{87} + \partial_{\xi_1} p.\overline{\mathbb{C}}_{88} + \partial^2_{\xi_1} p.\overline{\mathbb{C}}_{89};\\
&\overline{\boldsymbol{\mathcal{N}}}_{\partial^2_{\xi_1} p} = \overline{\mathbb{C}}_{91}.\overline{\boldsymbol{\varepsilon}} + \overline{\mathbb{C}}_{92}.\partial_{\xi_1}\overline{\boldsymbol{\varepsilon}} + \overline{\mathbb{C}}_{93}.\overline{\boldsymbol{\kappa}} + \overline{\mathbb{C}}_{94}.\partial_{\xi_1}\overline{\boldsymbol{\kappa}} + \overline{\mathbb{C}}_{95}.\partial^2_{\xi_1}\overline{\boldsymbol{\kappa}} + \overline{\mathbb{C}}_{96}.\partial^3_{\xi_1}\overline{\boldsymbol{\kappa}} + p.\overline{\mathbb{C}}_{97} + \partial_{\xi_1} p.\overline{\mathbb{C}}_{98} + \partial^2_{\xi_1} p.\overline{\mathbb{C}}_{99}.
\end{aligned} \tag{138}$$

Appendix B. Supplementary data

Supplementary data associated with this article can be found, in the online version, at https://doi.org/10.1016/j.ijsolstr.2020.06.002.

References

Altenbach, H., Bîrsan, M., Eremeyev, V.A., 2012. On a thermodynamic theory of rods with two temperature fields. Acta Mechanica 223 (8), 1583–1596.

Antman, S.S., 1974. Kirchhoff's problem for nonlinearly elastic rods. Quarterly of Applied Mathematics 32 (3), 221–240.

Antman, S.S., Jordan, K.B., 1975. Qualitative aspects of the spatial deformation of non-linearly elastic rods. Proceedings of the Royal Society of Edinburgh: Section A Mathematics, 73, 85–105. .

Argyris, J., 1982. An excursion into large rotations. Computer Methods in Applied Mechanics and Engineering 32 (1–3), 85–155.

Argyris, J., Symeonidis, S., 1980a. Nonlinear finite element analysis of elastic systems under nonconservative loading-natural formulation. Part I. quasistatic problems. Computer Methods in Applied Mechanics and Engineering 26 (1), 75–123.

Argyris, J., Symeonidis, S., 1980b. Nonlinear finite element analysis of elastic systems under nonconservative loading-natural formulation. Part ii. dynamic problems. Computer Methods in Applied Mechanics and Engineering 28 (2), 241–258.

Arora, A., Kumar, A., Steinmann, P., 2019. A computational approach to obtain nonlinearly elastic constitutive relations of special cosserat rods. Computer Methods in Applied Mechanics and Engineering.

Borkovic, A., Kovacevic, S., Radenkovic, G., Milovanovic, S., Guzijan-Dilber, M., 2018. Rotation-free isogeometric analysis of an arbitrarily curved plane bernoulli–euler beam. Computer Methods in Applied Mechanics and Engineering 334, 238–267.

Boyer, F., De Nayer, G., Leroyer, A., Visonneau, M., 2011. Geometrically exact kirchhoff beam theory: application to cable dynamics. Journal of Computational and Nonlinear Dynamics 6 (4). .

Brown, E., Burgoyne, C., 1994. Nonuniform elastic torsion and flexure of members with asymmetric cross-section. International Journal of Mechanical Sciences 36 (1), 39–48.

Burgoyne, C., Brown, E., 1994. Nonuniform elastic torsion. International Journal of Mechanical Sciences 36 (1), 23–38.

Cardona, A., Géradin, M., 1988. A beam finite element non-linear theory with finite rotations. International Journal for Numerical Methods in Engineering 26 (11), 2403–2438.

Carrera, E., Zozulya, V.V., 2019. Carrera unified formulation (cuf) for the micropolar beams: analytical solutions. Mechanics of Advanced Materials and Structures, 1–25.

Chadha, M., Todd, M.D., 2019. An improved shape reconstruction methodology for long rod like structures using cosserat kinematics-including the poisson's effect. In: Nonlinear Dynamics, Volume 1, Proceedings of the 34th IMAC, A Conference and Exposition on Structural Dynamics 2016, Springer, pp. 237–246. .

Chadha, M., Todd, M.D., 2017a. An introductory treatise on reduced balance laws of cosserat beams. International Journal of Solids and Structures 126, 54–73.
Chadha, M., Todd, M.D., 2017b. A generalized approach for reconstructing the three-dimensional shape of slender structures including the effects of curvature, shear, torsion, and elongation. Journal of Applied Mechanics 84, (4) 041003.
Chadha, M., Todd, M.D., 2017c. A displacement reconstruction strategy for long, slender structures from limited strain measurements and its application to underground pipeline monitoring. In: International Conference on Experimental Vibration Analysis for Civil Engineering Structures. Springer, pp. 317–327.
Chadha, M., Todd, M.D., 2019. On the material and material-adapted approaches to curve framing with applications in path estimation, shape reconstruction, and computer graphics. Computers & Structures 218, 60–81.
Chadha, M., Todd, M.D., 2019. A comprehensive kinematic model of single-manifold cosserat beam structures with application to a finite strain measurement model for strain gauges. International Journal of Solids and Structures 159, 58–76.
Chadha, M., Todd, M.D., 2019a. On the derivatives of curvature of framed space curve and their time-updating scheme. Applied Mathematics Letters.
Chadha, M., Todd, M.D., 2019. On the derivatives of curvature of framed space curve and their time-updating scheme: extended version with matlab code. arXiv of Differential Geometry:1907.11271. .
Cohen, H., 1966. A non-linear theory of elastic directed curves. International Journal of Engineering Science 4 (5), 511–524.
Cosserat, E., Cosserat, F., 1909. Théorie des corps déformables, A. Hermann et fils. .
Crisfield, M.A., 1990. A consistent co-rotational formulation for non-linear, three-dimensional, beam-elements. Computer Methods in Applied Mechanics and Engineering 81 (2), 131–150.
Crisfield, M.A., Jelenic, G., 1999. Objectivity of strain measures in the geometrically exact three-dimensional beam theory and its finite-element implementation. Proceedings of the Royal Society of London. Series A: Mathematical, Physical and Engineering Sciences 455 (1983), 1125–1147. .
Darboux, G., 1984. Leçons sur la théorie générale des surfaces. .
Demoures, F., Gay-Balmaz, F., Kobilarov, M., Ratiu, T.S., 2014. Multisymplectic lie group variational integrator for a geometrically exact beam in r^3. Communications in Nonlinear Science and Numerical Simulation 19 (10), 3492–3512.
Duhem, P., 1893. Le potentiel thermodynamique et la pression hydrostatique. Annales scientifiques de l'École Normale Supérieure 10, 183–230.
Ericksen, J., Truesdell, C., 1957. Exact theory of stress and strain in rods and shells. Archive for Rational Mechanics and Analysis 1 (1), 295–323.
Euler, L., Truesdell, C.A., 1960. The rational mechanics of flexible or elastic bodies, 1638–1788. Verlag nicht ermittelbar.
Greco, L., Cuomo, M., 2013. B-spline interpolation of kirchhoff-love space rods. Computer Methods in Applied Mechanics and Engineering 256, 251–269.
Green, A., Naghdi, P., 1979. On thermal effects in the theory of rods. International Journal of Solids and Structures 15 (11), 829–853.
Green, A.E., Naghdi, P., Wenner, M., 1974a. On the theory of rods. i. derivations from the three-dimensional equations. Proceedings of the Royal Society of London 337 (1611), 451–483.
Green, A., Naghdi, P., Wenner, M., 1974b. On theory of rods ii: Derivations by direct approach. Proceedings of Royal Society, London A 337, 485–507.
Hay, G., 1942. The finite displacement of thin rods. Transactions of the American Mathematical Society 51 (1), 65–102.
Hodges, D.H., 2006. Nonlinear Composite Beam Theory, American Institute of Aeronautics and Astronautics..
Hughes, T.J., 2012. The finite element method: linear static and dynamic finite element analysis. Courier Corporation.
Ibrahimbegović, A., 1995. On finite element implementation of geometrically nonlinear reissner's beam theory: three-dimensional curved beam elements. Computer Methods in Applied Mechanics and Engineering 122 (1–2), 11–26.
Ibrahimbegović, A., Frey, F., Kožar, I., 1995. Computational aspects of vector-like parametrization of three-dimensional finite rotations. International Journal for Numerical Methods in Engineering 38 (21), 3653–3673.
Iura, M., Atluri, S., 1988a. On a consistent theory, and variational formulation of finitely stretched and rotated 3-d space-curved beams. Computational Mechanics 4 (2), 73–88.
Iura, M., Atluri, S., 1988b. Dynamic analysis of finitely stretched and rotated three-dimensional space-curved beams. Computers and Structures 29 (5), 875–889.
Kapania, R., Li, J., 2003. A formulation and implementation of geometrically exact curved beam elements incorporating finite strains and finite rotations. Computational Mechanics 30 (5–6), 444–459.
Klapper, I., 1996. Biological applications of the dynamics of twisted elastic rods. Journal of Computational Physics 125 (2), 325–337.
Lang, H., Linn, J., Arnold, M., 2011. Multi-body dynamics simulation of geometrically exact cosserat rods. Multibody System Dynamics 25 (3), 285–312.
Li, W., Ma, H., Gao, W., 2017. Geometrically exact curved beam element using internal force field defined in deformed configuration. International Journal of Non-Linear Mechanics 89, 116–126.
Love, A.E.H., 2013. A Treatise on the Mathematical Theory of Elasticity. Cambridge University Press.
Manning, R.S., Maddocks, J.H., Kahn, J.D., 1996. A continuum rod model of sequence-dependent dna structure. The Journal of Chemical Physics 105 (13), 5626–5646.
Marsden, J.E., Hughes, T.J., 1994. Mathematical foundations of elasticity. Courier Corporation.
Mata, P., Oller, S., Barbat, A., 2007. Static analysis of beam structures under nonlinear geometric and constitutive behavior. Computer Methods in Applied Mechanics and Engineering 196 (45–48), 4458–4478.
Mata, P., Oller, S., Barbat, A., 2008. Dynamic analysis of beam structures considering geometric and constitutive nonlinearity. Computer Methods in Applied Mechanics and Engineering 197 (6–8), 857–878.
McRobie, F., Lasenby, J., 1999. Simo–vu quoc rods using clifford algebra. International Journal for Numerical Methods in Engineering 45 (4), 377–398.
Meier, C., Grill, M.J., Wall, W.A., Popp, A., 2018. Geometrically exact beam elements and smooth contact schemes for the modeling of fiber-based materials and structures. International Journal of Solids and Structures 154, 124–146.
Meier, C., Popp, A., Wall, W.A., 2019. Geometrically exact finite element formulations for slender beams: Kirchhoff–love theory versus simo–reissner theory. Archives of Computational Methods in Engineering 26 (1), 163–243.
Pimenta, P.M., Campello, E.M.B., Wriggers, P., 2008. An exact conserving algorithm for nonlinear dynamics with rotational dofs and general hyperelasticity. Part 1: Rods. Computational Mechanics 42.
Reissner, E., 1972. On one-dimensional finite-strain beam theory: the plane problem. Zeitschrift für angewandte Mathematik und Physik ZAMP 23 (5), 795–804.
Reissner, E., 1973. On one-dimensional large-displacement finite-strain beam theory. Studies in Applied Mathematics 52 (2), 87–95.
Reissner, E., 1981. On finite deformations of space-curved beams. Zeitschrift für angewandte Mathematik und Physik ZAMP 32 (6), 734–744.
Romero, I., Armero, F., 2002. An objective finite element approximation of the kinematics of geometrically exact rods and its use in the formulation of an energy–momentum conserving scheme in dynamics. International Journal for Numerical Methods in Engineering 54 (12), 1683–1716.
Sander, O., 2010. Geodesic finite elements for cosserat rods. International Journal for Numerical Methods in Engineering 82 (13), 1645–1670.
Simo, J.C., 1985. A finite strain beam formulation. the three-dimensional dynamic problem. Part I. Computer Methods in Applied Mechanics and Engineering 49 (1), 55–70.
Simo, J., Hughes, T., 1986. On the variational foundations of assumed strain methods. Journal of Applied Mechanics 53 (1), 51–54.
Simo, J.C., Vu-Quoc, L., 1986. A three-dimensional finite-strain rod model. Part II: Computational aspects. Computer Methods in Applied Mechanics and Engineering 58 (1), 79–116.
Simo, J., Vu-Quoc, L., 1987. The role of non-linear theories in transient dynamic analysis of flexible structures. Journal of Sound and Vibration 119 (3), 487–508.
Simo, J.C., Vu-Quoc, L., 1988. On the dynamics in space of rods undergoing large motions – a geometrically exact approach. Computer Methods in Applied Mechanics and Engineering 66 (2), 125–161.
Simo, J.C., Vu-Quoc, L., 1991. A geometrically-exact rod model incorporating shear and torsion-warping deformation. International Journal of Solids and Structures 27 (3), 371–393.
Simo, J.C., Tarnow, N., Doblare, M., 1995. Non-linear dynamics of three-dimensional rods: exact energy and momentum conserving algorithms. International Journal for Numerical Methods in Engineering 38 (9), 1431–1473.
Sokolnikoff, I.S., 1956. Mathematical Theory of Elasticity. McGraw-Hill book company.
Sokolov, I., Krylov, S., Harari, I., 2015. Extension of non-linear beam models with deformable cross sections. Computational Mechanics 56 (6), 999–1021.
Sonneville, V., Cardona, A., Brüls, O., 2014. Geometrically exact beam finite element formulated on the special euclidean group se (3). Computer Methods in Applied Mechanics and Engineering 268, 451–474.
Todd, M.D., Stull, C.J., Dickerson, M., 2013. A local material basis solution approach to reconstructing the three-dimensional displacement of rod-like structures from strain measurements. Journal of Applied Mechanics 80, (4) 041028.
Travers, A., Thompson, J., 2004. An introduction to the mechanics of dna. Philosophical Transactions of the Royal Society of London A: Mathematical, Physical and Engineering Sciences 362 (1820), 1265–1279.
Vu-Quoc, L., 1986. Dynamics of flexible structures performing large overall motions: a geometrically-nonlinear approach. Electronics Research Laboratory, College of Engineering, University of California at Berkeley. .
Vu-Quoc, L., Simo, J.C., 1987. Dynamics of earth-orbiting flexible satellites with multibody components. Journal of Guidance, Control, and Dynamics 10 (6), 549–558.
Whitman, A.B., DeSilva, C.N., 1969. A dynamical theory of elastic directed curves. Zeitschrift für angewandte Mathematik und Physik ZAMP 20 (2), 200–212.
Yang, Y.-B., Yau, J.-D., Leu, L.-J., 2003. Recent developments in geometrically nonlinear and postbuckling analysis of framed structures. Applied Mechanics Reviews 56 (4), 431–449.
Yiu, F., 2005. A geometrically exact thin-walled beam theory considering in-plane cross-section distortion. PhD thesis, Cornell University..
Zupan, D., Saje, M., 2003. Finite-element formulation of geometrically exact three-dimensional beam theories based on interpolation of strain measures. Computer Methods in Applied Mechanics and Engineering 192 (49–50), 5209–5248.
Zupan, E., Zupan, D., 2018. On conservation of energy and kinematic compatibility in dynamics of nonlinear velocity-based three-dimensional beams. Nonlinear Dynamics, 1–16. .